CZECH TECHNICAL UNIVERSITY IN PRAGUE

FACULTY OF CIVIL ENGINEERING

Department of Steel and Timber structures

COMPRESSED STEEL FIBRE-REINFORCED CONCRETE SLAB IN JOINT OF STEEL-CONCRETE COMPOSITE FRAME STRUCTURE

DOCTORAL THESIS

Ing. Petr Červenka

Doctoral study programme: Civil Engineering

Branch of study: Building Structures

Supervisor: doc. Dr. Ing. Jakub Dolejš, IWE

Prague, 2023

Abstract

This thesis deals with a steel fibre-reinforced concrete (SFRC) slab in compression as a composite steel-concrete frame joint component. Based on the results of an experiment with a realistic-sized steel-concrete specimen, a numerical model has been validated in Atena Science. Based on a parametric study with these models, an analytical relationship was derived for the resistance and stiffness of the steel fibre-reinforced concrete slab in compression. In contrast to the standard procedure given in Annex C of EN 1998-1:2004 (Eurocode 8), the new procedure is designed for a steel fibre-reinforced concrete slab and takes into account the favourable state of stress in the concrete slab in the joint area.

Keywords: steel fibre-reinforced concrete; composite steel-concrete frame joint; slab in compression; effective width; earthquake; FEM

Abstrakt

Tato disertační práce se zabývá deskou z betonu vyztuženého ocelovými vlákny (drátkobetonu) v tlaku jako komponentou spřaženého ocelobetonového rámu. Na základě výsledků experimentu s ocelobetonovou konstrukcí reálných rozměrů byl v programu Atena Science validován numerický model. Na základě parametrické studie s těmito modely byl odvozen analytický vztah pro výpočet únosnosti a tuhosti ocelovými vlákny vyztužené betonové desky v tlaku. Na rozdíl od normového postupu uvedeného v příloze C normy EN 1998-1:2004 (Eurokód 8) je nový postup navržen pro betonovou desku vyztuženou ocelovými vlákny a zohledňuje příznivý stav napjatosti v betonové desce v oblasti styčníku.

Klíčová slova: beton vyztužený ocelovými vlákny; spřažený ocelobetonový rámový styčník; deska v tlaku; účinná šířka; zemětřesení; MKP

Declaration

Prohlášení

Aspirant: Ing. Petr Červenka

Title of doctoral thesis: Compressed steel fibre-reinforced concrete slab in joint of steel-concrete composite frame structure

Název disertační práce: Tlačená betonová deska s rozptýlenou výztuží ve styčníku spřažené ocelobetonové rámové konstrukce

I declare I wrote the submitted thesis on my own under the supervision of doc. Dr. Ing. Jakub Dolejš, IWE.

Literature and other sources are stated in the list of references.

This thesis arose in relation to the solution of projects: SGS15/137/OHK1/2T/11, SGS17/124/OHK1/2T/11, SGS19/150/OHK1/3T/11, TA ČR ZETA 1 (STA02017TJ010) - TJ01000045.

Prohlašuji, že jsem předloženou disertační práci vypracoval samostatně pod vedením školitele doc. Dr. Ing. Jakub Dolejš, IWE.

Použitou literaturu a další zdroje uvádím v seznamu použité literatury.

Tato disertační práce vznikla v souvislosti s řešením projektů: SGS15/137/OHK1/2T/11, SGS17/124/OHK1/2T/11, SGS19/150/OHK1/3T/11, TA ČR ZETA 1 (STA02017TJ010) - TJ01000045.

In Prague on / V Praze dne 28.02.2023

Signature / Podpis

Acknowledgements

This work was carried out at the Department of Steel and Timber Structures, Czech technical university in Prague in 2016 - 2023.

I would like to thank especially my supervisor doc. Jakub Dolejs for his professional guidance and support during the preparation of this thesis. I would also like to thank other people not named here from the department and outside the department for their valuable advice and help.

The experiment was carried out at the University Centre for Energy Efficient Buildings in Bustehrad.

This work was supported by grants SGS15/137/OHK1/2T/11, SGS17/124/OHK1/2T/11, SGS19/150/OHK1/3T/11, and TA CR ZETA 1 (STA02017TJ010) - TJ01000045.

I thank my family members for their support during my studies.

https://doi.org/10.14311/dis.fsv.2023.013

Poděkování

Práce vznikla na Katedře ocelových a dřevěných konstrukcí Českého vysokého učení technického v Praze v letech 2016 – 2023.

Děkuji zejména svému školiteli doc. Jakubu Dolejšovi za odborné vedení a podporu při vzniku této práce. Děkuji dalším zde nejmenovaným lidem z katedry i mimo ní za cenné rady a pomoc.

Experiment byl uskutečněn v Univerzitním centru energeticky efektivních budov v Buštěhradě.

Práce byla vytvořena za finanční podpory grantů SGS15/137/OHK1/2T/11, SGS17/124/OHK1/2T/11, SGS19/150/OHK1/3T/11, TA ČR ZETA 1 (STA02017TJ010) - TJ01000045.

Děkuji členům své rodiny za podporu během studia.

Content

Nomenclature

Symbols and abbreviations used in Section 1.

F_t	force in the reinforcement or tensile resistance of the reinforcement
F_{tq}	tensile force in the transverse reinforcement
M_{Ed}	design value of the bending moment
M	bending moment
N	normal force
q_{serv}	uniformly distributed load on the ceilings
$M_{Ed,G}$	design value of bending moment from gravity load
$M_{Ed,E}$	design value of bending moment from lateral loading
b_e	effective slab width on each side of the web
l_0	distance between zero moment points from the horizontal load
l_0^-	distance between zero moment points from the horizontal load for a hogging moment
l_0^+	distance between zero moment points from the horizontal load for a sagging moment
L	span of the beam
L_1	span of the beam
b_{eff}	effective width of the slab
b_1	half the axial distance of the beams
F_{Rd}	design value of the resistance
h_c	column cross-section height
b_c	column cross-section width
l_b	anchorage length of the reinforcement
A_T	area of the transverse reinforcement
θ	angle of inclination of the concrete struts
μ	coefficient of the ratio of applied moments
M_{left}	bending moment on the left connection of the joint

M_{righ}	bending moment on the right connection of the joint
δ	additional angle of the concrete struts
e_L	distance of the centre of gravity of the longitudinal reinforcement to the centre of gravity of the column section
e_T	distance of the centre of gravity of the transverse reinforcement to the face of the column section
F_{left}	tensile normal force in the concrete slab on the left side of the joint
F_{righ}	tensile normal force in the concrete slab on the right side of the joint
A_{SL}	area of the longitudinal reinforcement
t_{slab}	thickness of the concrete slab
f_{cd}	design value of the compressive strength of the concrete
f_{sdL}	design value of the yield strength of the longitudinal reinforcement
A_{ST}	area of the transverse reinforcement
f_{sdT}	design yield strength of the transverse reinforcement
t	end-plate thickness
d	bolt diameter
f_{ub}	ultimate strength of the bolt steel
f_y	yield strength of the steel
$M_{Rd,pl}$	plastic bending resisting moment
$M_{Rd,c}$	design value of the moment of resistance of the column
$M_{Rd,b}$	design value of the moment of resistance of the beam
$\Delta_{plastic}$	plastic displacement
$\theta_{plastic}$	plastic rotation
ϕ_M	connection rotation
ϕ_V	column web panel rotation in shear
F_{R1}	resistance of mechanism 1
F_{R2}	resistance of mechanism 2
e	column flange thickness
b_o	concrete strut width
v	reduction factor of the concrete in shear according to EN 1992-1-1 [14]

f_{strut}	compressive strength of the concrete strut
f_{ck}	characteristic compressive strength of the concrete
F_{cd}	design value of the axial resistance of the concrete strut
F_c	design value of the resistance of the concrete strut parallel to the beam
l_1	minimum length of the reinforcement
A_s	reinforcement area or area of longitudinal reinforcement
ρ_s	reinforcement ratio
f_{sd}	design value of the yield strength of reinforcement steel
$b_{eff,conn}$	effective width of the slab in compression in the joint
z	thickness of the compressed concrete slab or lever arm of the internal forces
k_{sc}	coefficient of stiffness of the concrete slab component in compression
E_c	Young's modulus of elasticity of concrete
E_a	elastic Young's modulus for steel
F_{R3}	resistance of mechanism 3
F_{stud}	resistance of one shear connector
n	number of connectors in half of the effective width of the slab
V	shear force
F_{SC}	force in the effective width of the slab for the sagging moment
F_{St}	force in the effective width of the slab for the hogging moment
d_{eff}	concrete slab thickness
f'_c	strength of the concrete slab in front of the column flange
γ	shear deformation of the column web panel
u_1, u_2	horizontal displacement of the bottom flanges of the beams
u_3, u_4	horizontal displacement on the top surface of the concrete slab
θ_1, θ_2	rotation of the steel connections
l_1, h_1	dimensions of the hole in the concrete slab in the column location

Symbols and abbreviations used in Sections 3 - 7.

SFRC	steel fibre-reinforced concrete
FRC	fibre-reinforced concrete
FEM	finite element method
b_{eff}	effective width
h_c	height of the column cross-section
b_c	width of the column cross-section
$M+$	sagging bending moment
$M-$	hogging bending moment
VAR	population variance
f_y	yield strength of steel
f_u	ultimate tensile strength of steel
DIC	digital image correlation
exp.	experiment
inc	inclinometer(s)
sens	displacement sensor(s)
σ	normal stress
ε	strain
$\varepsilon_{loc,t}$	tensile localised strain
$\varepsilon_{loc,c}$	compressive localised strain
L_{ch}	characteristic length
L_t	crack band size
L_c	crush band size
f_t	tensile strength of the concrete
ε_1	maximum principal stress
RI_v	reinforcing index of fibres by volume
V_f	fibre volume fraction
L_f	fibre length
d_f	fibre diameter

SDEM	Simplified Diverse Embedment Model
CBFEM	Component-based Finite Element Method
E	Young's modulus of elasticity
HM	hardening modulus
d	concrete slab thickness
f_c	compressive strength of the concrete
V_f	fibre volume fraction
μ	friction coefficient
E_c	modulus of elasticity of SFRC
t_f	column flange thickness
t_w	column web thickness
n	model number
A_s	reinforcement area of the concrete slab
max.	maximum value
min.	minimum value
$F_{R,FEM}$	resistance of the concrete slab in compression calculated by FEM
$s_{ini,FEM}$	initial stiffness coefficient calculated by FEM
$s_{res,FEM}$	secant stiffness coefficient calculated by FEM
$t_{0.025}$	2.5 % upper quantile of the t-distribution
$F_{R,an}$	concrete slab resistance in compression calculated by the proposed analytical method
$s_{ini,an}$	coefficient of initial stiffness calculated by the proposed analytical method
$s_{res,an}$	coefficient of secant stiffness calculated by the proposed analytical method
$s_{ini,EC3}$	coefficient of initial stiffness calculated by the method given in EN 1993-1-8 [10]
$F_{R,EC8}$	concrete slab compression resistance calculated by the method given in EN 1998-1 [3]
$F_{R,BENN}$	concrete slab compression resistance calculated by Bennacer et al. [20]

List of figures

List of tables

1 State of the art

1.1 Introduction

This thesis focuses on describing the compressive behaviour of a concrete slab in composite steel-concrete frame joints.

The loading of the concrete slab in compression in the joint region occurs in the following situations:

1) when the unequal hogging moment loading (Fig. 1) is applied at the joint of the interior column, the difference of forces in the reinforcement (which is equal to F_{t2} subtracted from F_{t1} in Fig. 1) is transferred to the column, and the concrete slab in contact with the column flanges is subjected to compression from the side of the smaller hogging moment [1];

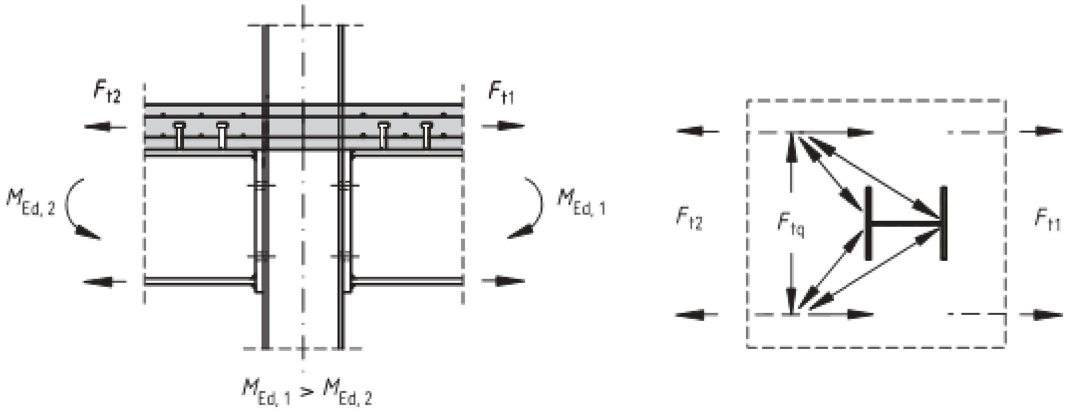

***Fig. 1**. Strut and tie model for the case when the joint is loaded by unequal hogging moments - F_t is the force in the reinforcement, M_{Ed} is the design value of bending moment, and F_{tq} is the tensile force in the transverse reinforcement [1].*

2) in an exceptional situation (e.g. bomb explosions, motor vehicle collision) in which the interior column is lost. The joint above the failed column is loaded by the interaction of the sagging moment and the normal force (Fig. 2b) before the beam begins to act as a catenary loaded only by the axial force (Fig. 2c) [2];

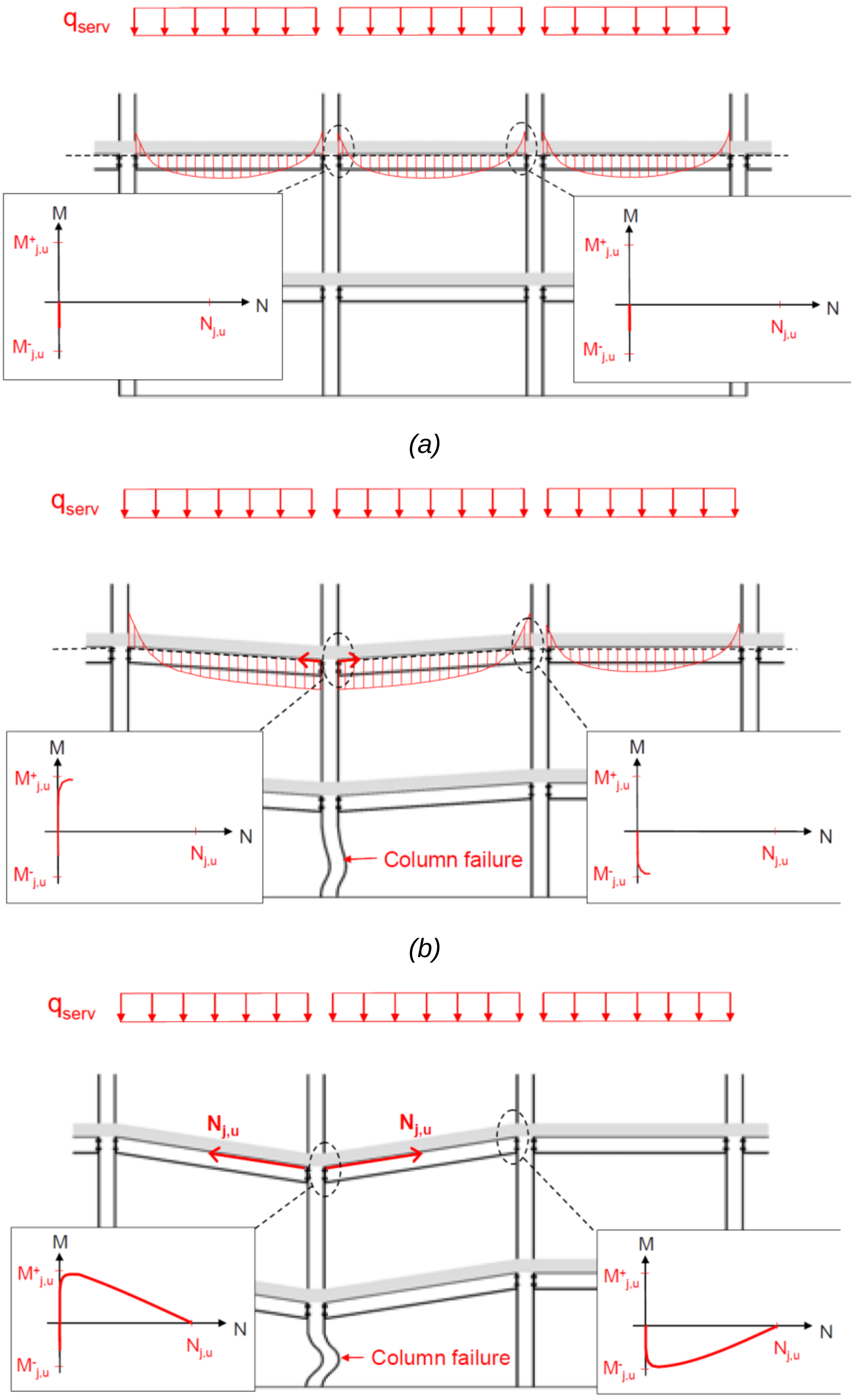

(a)

(b)

(c)

Fig. 2. *The behaviour of the frame in case of column loss: normal situation (a), column failure - joints above the failed column are subjected to a combination of sagging bending moment and tensile normal force (b), generation of membrane forces, beams above the failed column act as a catenary (c). The figures contain interaction diagrams of bending moment M and normal force N;* $M_{j,u}$ *is the moment of resistance of the joint,* $N_{j,u}$ *is the tensile resistance of the joint, and* q_{serv} *is the uniformly distributed load on the ceilings [2].*

3) under horizontal wind loading (Fig. 3);

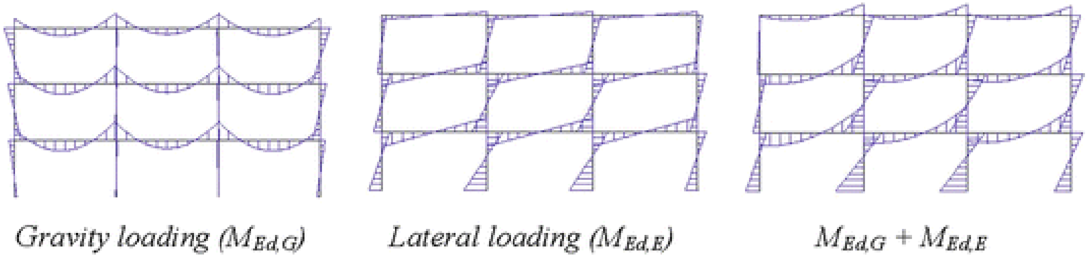

Fig. 3. *Effect of horizontal loading on an unbraced frame [4].*

4) under extraordinary seismic loading (Fig. 3). The forces acting on the beam in the effective width of the slab have to be carried by the joint. The values of the effective width of the concrete slab under horizontal seismic loading are given in EN 1998-1 [3] and are derived from moment diagrams on the beam, Fig. 4. The joint carries these loads primarily by two mechanisms as listed in Annex C of EN 1998-1 [3], Fig. 5. Mechanism 1 represents the direct action between the concrete slab and the column flange. Mechanism 2 is defined by the strut and tie model, where the concrete struts compress the column web and the far flange of the column at an angle of 45 °.

$$b_e^+ = \frac{\ell_o^+}{8} = 0{,}075\ \mathrm{L} \qquad\qquad b_e^- = \frac{\ell_o^-}{8} = 0{,}1\ \mathrm{L}$$

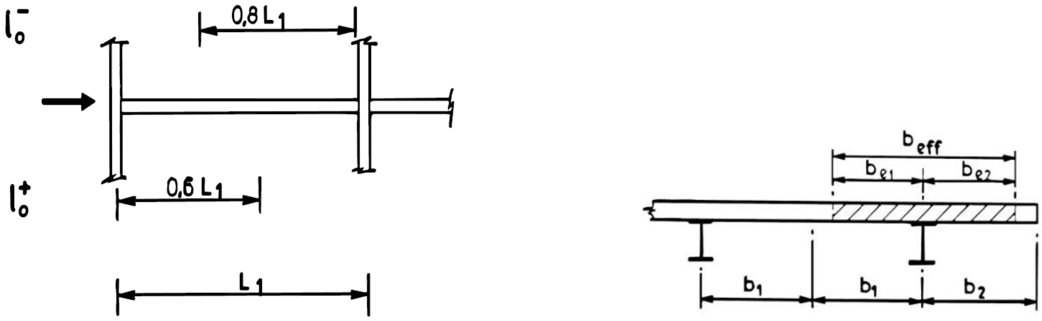

Fig. 4. *Derivation of the effective slab width on each side of the web* b_e *from the distribution of bending moments on the beam in the plastic state from the horizontal seismic loading (similar to EC4 [1], where it is given for vertical loads;* b_e *corresponds to the experimental results [5]), where* l_0 *is the distance between zero moment points from the horizontal load (*l_{0-} *for a hogging moment,* l_{0+} *for a sagging moment),* L_1 *and L is the span of the beam,* b_{eff} *is the effective width of the slab,* b_1 *is half the axial distance of the beams [5].*

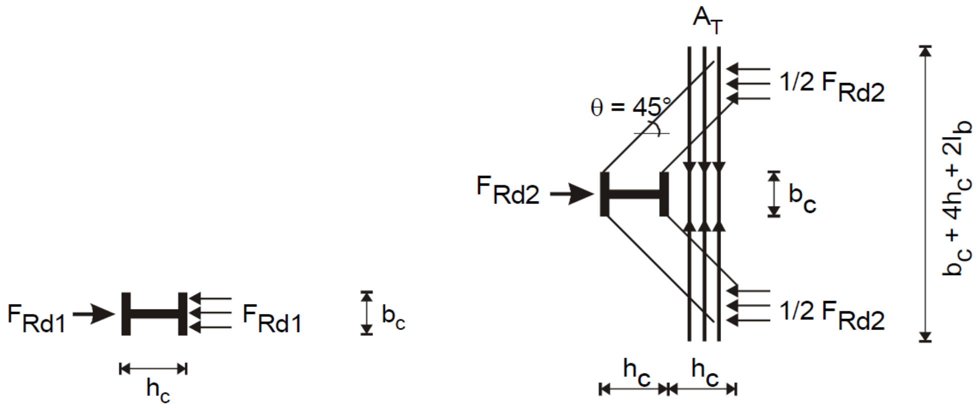

(a) *(b)*

Fig. 5. *Load transfer in concrete slab - F_{Rd1} is the resistance of mechanism 1 (a), F_{Rd2} is the resistance of mechanism 2 (b); h_c and b_c are the cross-sectional dimensions of the column, l_b is the anchorage length of the reinforcement and A_T is the area of the transverse reinforcement, θ is the angle of inclination of the concrete struts [5].*

1.2 Joint subjected to unequal hogging moments

1.2.1 Procedure according to COST C1 1996

When unequal hogging moments are applied in the interior column joint, the difference in forces in the reinforcement is carried by the column. The concrete slab in contact with the column flanges is subjected to compressive forces on the side of the smaller hogging moment (Fig. 1). In this chapter the relationships given in COST C1 1996 [6] and ENV 1994-1-1 [7] are presented. The relationships are used to calculate the area of longitudinal reinforcement limited by the possible brittle failure of the slab in compression and also the minimum area of transverse reinforcement to carry the transverse tensile forces in the joint (force F_{tq} in Fig. 1). In these relationships, only mechanism 1 from Annex C of EN 1998-1 [3] is considered. Mechanism 1 represents the compressive force acting in the concrete slab to column flange, Fig. 5.

Based on the ratio of the applied moments M_{left} and M_{right} in the interior joint, the coefficient μ is calculated (the sign convention of the moments for this relationship is shown in Fig. 1):

$$\mu = 1 - \frac{M_{left}}{M_{right}} \tag{1}$$

where $$M_{left} < M_{right} \tag{2}$$

The distance of the centres of gravity of the transverse and longitudinal reinforcement from the column cross-section (Fig. 6) must satisfy the following geometric conditions. From these distances, the additional angle of the concrete struts δ is obtained when applying mechanism 1 in the concrete slab (Fig. 7a):

$$\frac{e_L}{b_c} = 1 \div 1.5 \tag{3}$$

$$\frac{e_T}{e_L} = 1 \div 1.5 \tag{4}$$

$$tan\delta = \frac{\frac{e_T}{e_L} - 0.3}{0.7} \tag{5}$$

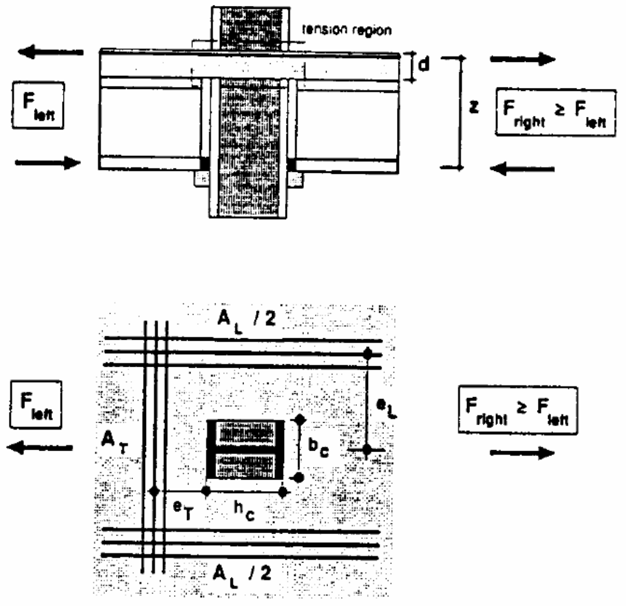

Fig. 6. *Distances of the centres of gravity of the transverse and longitudinal reinforcement from the column section [5].*

To prevent brittle failure of the concrete slab, the area of the longitudinal reinforcement A_{SL} is limited by the condition:

$$A_{SL} \leq \frac{0.94\, b_c\, t_{slab}}{\mu} \frac{f_{cd}}{f_{sdL}} \tag{6}$$

where b_c is the width of the column flange, t_{slab} is the thickness of the concrete slab, f_{cd} is the design value of the compressive strength of the concrete, f_{sdL} is the design value of the yield strength of the longitudinal reinforcement.

The area of the transverse reinforcement A_{ST} should satisfy the relationship:

$$A_{ST} \geq \frac{\mu}{2\, tan\delta} A_{SL} \frac{f_{sdL}}{f_{sdT}} \tag{7}$$

where f_{sdT} is the design value of the yield strength of the transverse reinforcement.

1.2.2 Extension of the relationships for extreme load cases by Plumier et al.

Plumier et al. [5] further applied the relationships to the case of maximum asymmetric vertical loading (one of the moments is equal to zero) and to a horizontally loaded structure where one of the bending moments of the interior joint is sagging and the other hogging.

In the extreme case (Fig. 7a) of a vertically loaded structure with $M_{left} = 0$ ($\mu = 1$):

$$A_{SL} \leq 0.94\, b_c\, t_{slab} \frac{f_{cd}}{f_{sdL}} \tag{8}$$

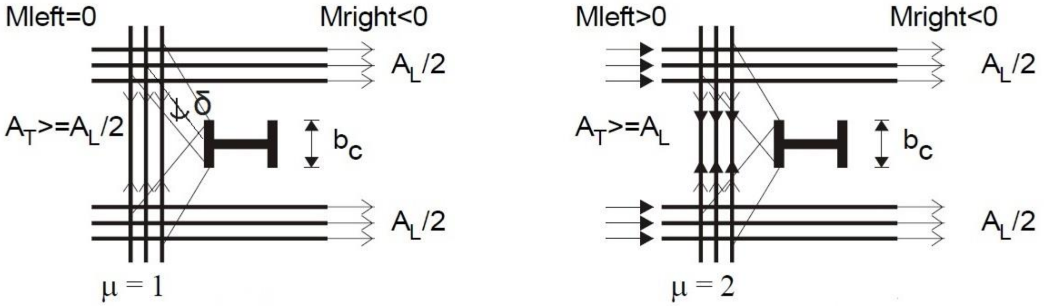

(a) *(b)*

Fig. 7. *Minimum area of transverse reinforcement (if δ = 45 °) under the action of mechanism 1 - in the extreme case of a vertically loaded structure (a), in the extreme case of a horizontally loaded structure (b) [5].*

For concrete struts with 45 ° inclination angle ($tan\delta = 1$):

$$A_{ST} \geq 0.5\, A_{SL} \frac{f_{sdL}}{f_{sdT}} \tag{9}$$

When applying the relationships to the horizontally loaded structure (Fig. 7b) in the case of $M_{left} = -M_{right}$ ($\mu = 2$):

$$A_{SL} \leq 0.47\, b_c\, t_{slab} \frac{f_{cd}}{f_{sdL}} \tag{10}$$

When the concrete struts are inclined with the angle of 45 ° ($\tan\delta = 1$):

$$A_{ST} \geq A_{SL} \frac{f_{sdL}}{f_{sdT}} \tag{11}$$

1.3 Joints subjected to seismic loading according to EN 1998-1, Annex C, and related documents

The subject of this chapter is Annex C of EN 1998-1 [3] and related documents, which deal with the joints subjected to seismic loading.

The joint should be designed to be ductile, allowing the absorption and dissipation of the motion energy under seismic loading. Therefore, the components that determine the collapse of the joint shall be ductile (Fig. 8) and shall be designed with the capacity design in accordance with Table 1 and Table 2.

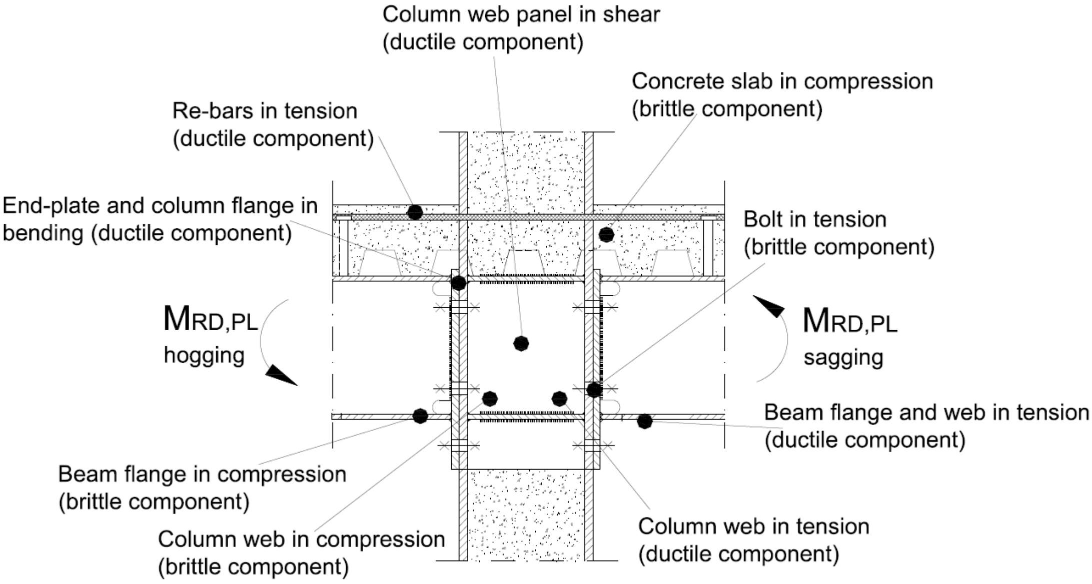

Fig. 8. *The ductile and brittle components of a steel-concrete joint [8].*

Table 1. *Capacity design of the joint subjected to the sagging moment, where $F_{Rd,1}$ is the resistance of the end-plate and column flange in bending (1), $F_{Rd,2}$ of the concrete slab in compression (2), $F_{Rd,3}$ of the column web panel in shear (3) [9].*

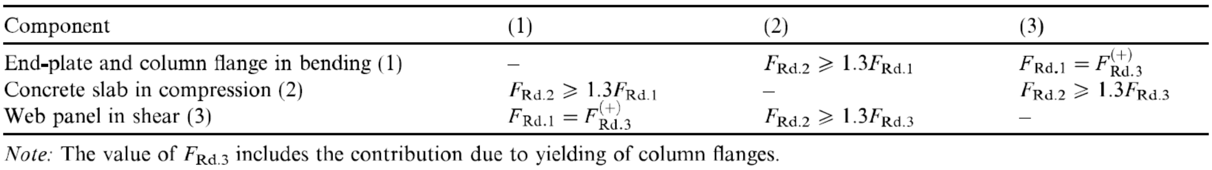

Component	(1)	(2)	(3)
End-plate and column flange in bending (1)	–	$F_{\mathrm{Rd.2}} \geqslant 1.3F_{\mathrm{Rd.1}}$	$F_{\mathrm{Rd.1}} = F^{(+)}_{\mathrm{Rd.3}}$
Concrete slab in compression (2)	$F_{\mathrm{Rd.2}} \geqslant 1.3F_{\mathrm{Rd.1}}$	–	$F_{\mathrm{Rd.2}} \geqslant 1.3F_{\mathrm{Rd.3}}$
Web panel in shear (3)	$F_{\mathrm{Rd.1}} = F^{(+)}_{\mathrm{Rd.3}}$	$F_{\mathrm{Rd.2}} \geqslant 1.3F_{\mathrm{Rd.3}}$	–

Note: The value of $F_{\mathrm{Rd.3}}$ includes the contribution due to yielding of column flanges.

Table 2. *Capacity design of the joint subjected to the hogging moment, where $F_{Rd,1}$ is the resistance of the longitudinal reinforcement and bolt row in tension (1), $F_{Rd,2}$ of the beam flange in compression (2), $F_{Rd,3}$ of the column web panel in shear (3) [9].*

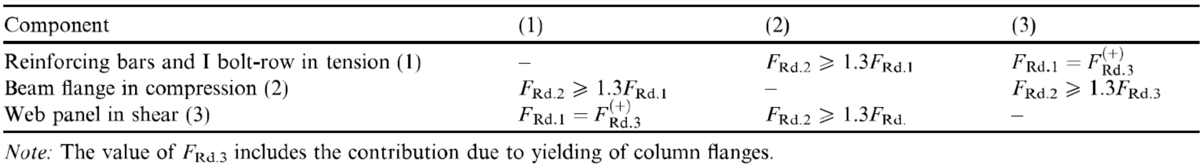

Component	(1)	(2)	(3)
Reinforcing bars and I bolt-row in tension (1)	–	$F_{\mathrm{Rd.2}} \geqslant 1.3F_{\mathrm{Rd.1}}$	$F_{\mathrm{Rd.1}} = F^{(+)}_{\mathrm{Rd.3}}$
Beam flange in compression (2)	$F_{\mathrm{Rd.2}} \geqslant 1.3F_{\mathrm{Rd.1}}$	–	$F_{\mathrm{Rd.2}} \geqslant 1.3F_{\mathrm{Rd.3}}$
Web panel in shear (3)	$F_{\mathrm{Rd.1}} = F^{(+)}_{\mathrm{Rd.3}}$	$F_{\mathrm{Rd.2}} \geqslant 1.3F_{\mathrm{Rd.}}$	–

Note: The value of $F_{\mathrm{Rd.3}}$ includes the contribution due to yielding of column flanges.

The design of the bolted end-plate connections should be made to avoid brittle failure of the bolts. The connection should satisfy the relationship:

$$t \leq 0.36\, d \sqrt{f_{ub}/f_y} \tag{12}$$

where t is the thickness of the end-plate or column flange, d is the diameter of the bolts, f_{ub} is the ultimate strength of the bolt steel, and f_y is the yield strength of the end-plate or column flange steel [10].

The maximum ductility of a structure is guaranteed when a global mechanism develops without the formation of an undesirable local or storey mechanism, Fig. 9. The condition for the formation of a global mechanism is the capacity design according to the relationship [3]:

$$\sum M_{Rd,c} \geq 1.3 \sum M_{Rd,b} \tag{13}$$

where $\Sigma M_{Rd,c}$ is the sum of the design values of the column resistance moments in the joint and $\Sigma M_{Rd,b}$ is the sum of the design values of the beam resistance moments of the corresponding joint. In the case of partial-strength joints, the moments of resistance of these joints are considered instead of the moments of resistance of the beams.

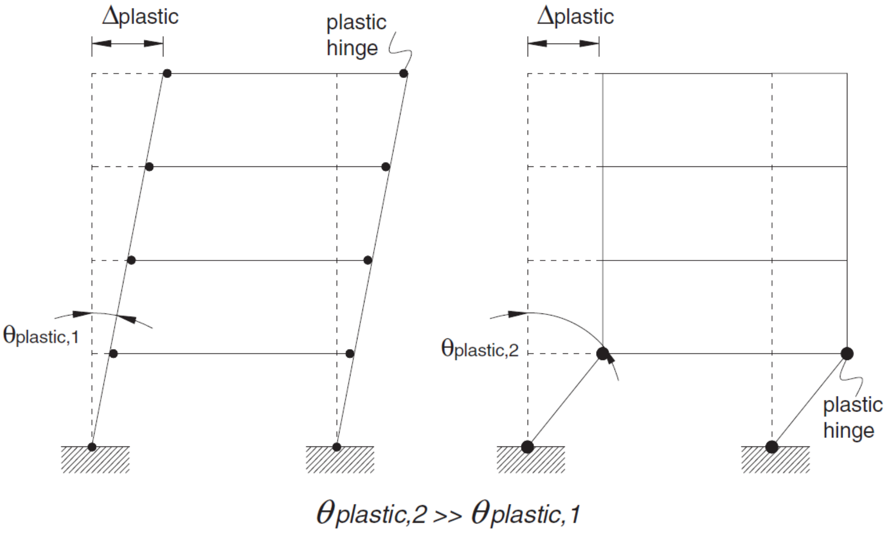

(a) *(b)*

Fig. 9. *The global mechanism when plastic hinges are formed at the ends of beams (a), the undesired storey mechanism when plastic hinges are formed in columns (b) [12].*

Another condition for the formation of the global mechanism is the achievement of the necessary rotation capacity of the joints. A minimum rotation of 35 mrad is required for the high ductility class and a minimum rotation of 25 mrad for the medium ductility class, with a maximum reduction of 20 % in resistance and stiffness under cyclic loading [3]. The rotation of the joint consists of the rotation of the connection and the rotation of the column web panel in shear, as shown in Fig. 10. A maximum contribution of 30 % of the column web rotation to the total plastic rotation is required [3].

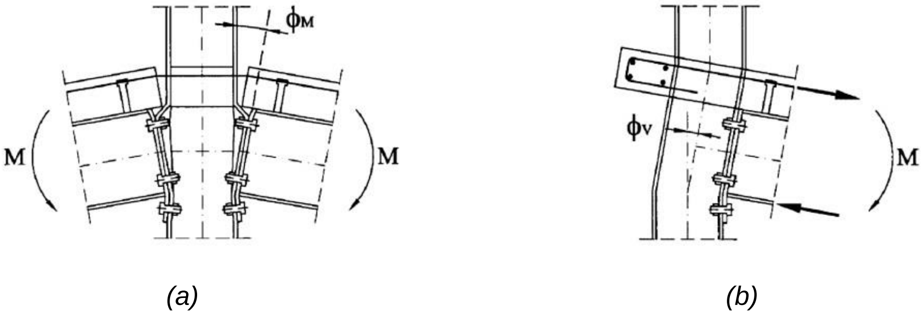

(a) (b)

Fig. 10. *The joint rotation: connection rotation ϕ_M (a), column web panel rotation in shear ϕ_V (b) [13].*

1.3.1 Concrete slab in compression in the joint region

The forces acting on the beam in the effective width of the concrete slab b_{eff} (Fig. 4) must be carried by the joint. The concrete slab transfers the sagging moment forces into the joint by two mechanisms (Fig. 11) [5], which are described in Annex C of EN 1998-1 [3]. The forces are also transferred by mechanism 3 in the case of a shear connection between the concrete slab and the transverse beam [3], Chapter 1.3.2. Mechanism 1 is represented by the direct compression of the concrete slab against the column flange. Mechanism 2 is defined by a strut and tie model where the concrete struts compress the column web and the more distant column flange at a 45 ° angle. The condition for the formation of mechanism 2 is a column cross-section with a “concave zones” or special connections [5].

1.3.1.1 A derivation of the relationships for EC8 according to Plumier et al.

The content of Annex C of EN 1998-1 [3] for an external joint under sagging moment loading is described in more detail in, e.g., Plumier et al. [5], which is the subject of this chapter.

If the inclination of the concrete struts is 45 ° under the action of mechanism 2:

$$b_o = (h_c - e)/\sqrt{2} \cong h_c/\sqrt{2} \tag{14}$$

where h_c and e are the cross-sectional dimensions of the column shown in Fig. 11; b_o is the width of this concrete strut.

The compressive strength of the concrete strut is

$$f_{strut} = \nu\, f_{cd} \tag{15}$$

where ν is the reduction factor of the concrete in shear according to EN 1992-1-1 [14], f_{cd} is the design value of the compressive strength of the concrete in units of MPa, where $$\nu = 0.7 - f_{ck} / 200 \geq 0.5 \tag{16}$$

For example, for concrete of class C20/25, this implies ν = 0.6, and hence:

$$F_{cd} = f_{strut}\, t_{slab}\, b_0 = 0.6\, f_{cd}\, t_{slab}\, h_c/\sqrt{2} \tag{17}$$

$$F_{c2} = F_{cd} \,/\, \sqrt{2} = 0.3\, f_{cd}\, t_{slab}\, h_c \tag{18}$$

$$F_{R2} = 2\, F_{c2} = 0.6\, f_{cd}\, t_{slab}\, h_c = 0.7\,(0.85\, f_{cd})\, t_{slab}\, h_c \tag{19}$$

$$F_{t2} = A_{s2}\, f_{sd} \tag{20}$$

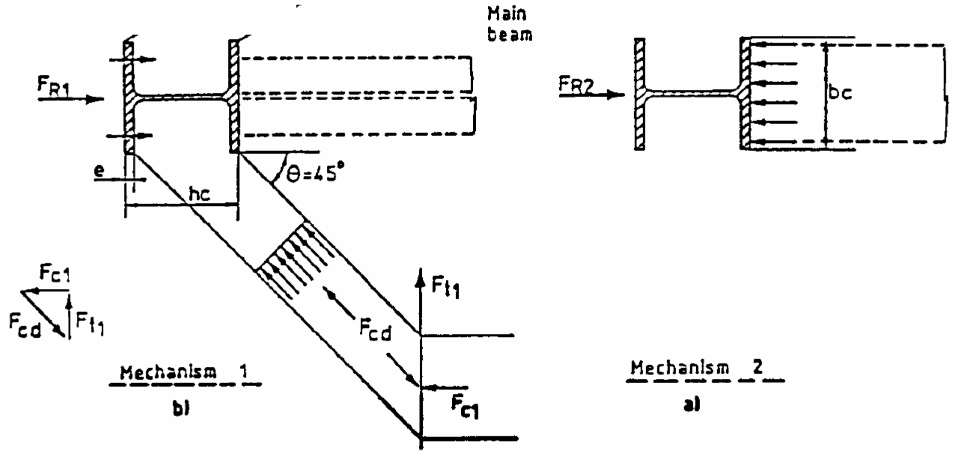

Fig. 11*. Mechanisms for the transfer of forces from the concrete slab to the column when the joint is subjected to a sagging moment, b_c and h_c are the column cross-sectional dimensions, F_{R1} and F_{R2} are the resistances of the mechanisms, F_{t1} is the transverse tensile force, θ is the angle of inclination of the concrete struts when applying mechanism 1 [5]. Note: Fig. 11 to Fig. 13 uses the "Plumier convention" of marking mechanisms 1 and 2 [5]. Since the other publications cited mark the mechanisms in reverse (including EC8), throughout this thesis the mechanisms are marked as is usual everywhere else, i.e. in reverse of the "Plumier convention" and in accordance with EC8 [3].*

As these forces are the equal

$$F_{t2} = F_{c2} \tag{21}$$

the area of transverse reinforcement for mechanism 2 must then satisfy the relationship

$$A_{s2} \geq 0.3\ t_{slab}\ h_c \frac{f_{cd}}{f_{sd}} \tag{22}$$

The transverse reinforcement is placed within the distance h_c from the face of the column (Fig. 12). Minimum reinforcement ratio:

$$\rho_{s2} = \frac{A_{s2}}{t_{slab}\ h_c} \geq 0.3\ \frac{f_{cd}}{f_{sd}} \tag{23}$$

The design value of the resistance of mechanism 1 is

$$F_{R1} = f_{cd}\ t_{slab}\ b_c \tag{24}$$

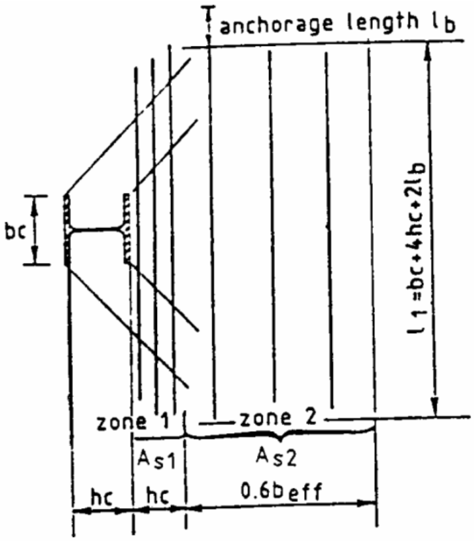

Fig. 12. *Transverse reinforcement to carrying transverse forces of mechanism 1 in zone 1 and mechanism 2 in zone 2; l_b is the anchorage length of the reinforcement, and l_1 is the minimum length of the reinforcement [5]. Note: Fig. 11 to Fig. 13 uses the "Plumier convention" of marking mechanisms 1 and 2 [5], see the caption to Fig. 11.*

The stress from the force F_{R1} is concentrated at the contact between the concrete slab and the column flange. This stress is spread over the effective width b_{eff} at a distance of the effective width b_{eff} from the face of the column flange (Fig. 13a). The resultant transverse tensile force F_{t1} is applied at approximately half the b_{eff} distance from the face of the column (Fig. 13b). The transverse reinforcement required to transfer the force F_{t1}:

$$F_{t1} = \frac{F_{R1}}{4}\,\frac{b_{eff} - b_c}{b_{eff}} = 0.21\, f_{cd}\, b_c\, t_{slab}\,\frac{0.15\,L - b_c}{0.15\,L} = A_{s1}\, f_{sd} \tag{25}$$

$$A_{s1} \geq 0.21\, t_{slab}\, b_c\,\frac{0.15\,L - b_c}{0.15\,L}\,\frac{f_{cd}}{f_{sd}} \tag{26}$$

The transverse reinforcement carrying the force F_{t1} is distributed over a length of $0.6b_{eff} = 0.09L$ to h_c from the face of the column (Fig. 12). The minimum reinforcement ratio is

$$\rho_{s1} = \frac{A_{s1}}{t_{slab}\, 0.09\, L} \geq 0.08\,\frac{f_{cd}}{f_{sd}} \tag{27}$$

with the first transverse bar at a maximum distance of 30 mm from the face of the column [3]. The transverse forces resulting from mechanisms 1 and 2 are usually carried by the reinforcement itself designed for permanent and service loads [5].

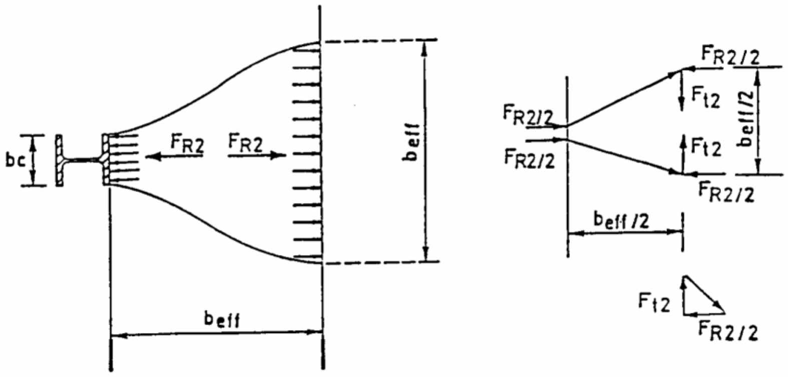

(a) *(b)*

***Fig. 13**. Forces in the concrete slab under the action of mechanism 2, b_{eff} is the effective width of the slab on the beam, and F_{t2} is the transverse tensile force [5]. Note: Fig. 11 to Fig. 13 uses the "Plumier convention" of marking mechanisms 1 and 2 [5], see the caption to Fig. 11.*

1.3.1.2 Interior joint

The interior joint of the composite frame is subjected to a sagging moment on one side and a hogging moment on the other side under seismic loading. The tensioned reinforcement on the hogging moment side contributes to the compressive stress of the concrete slab on the sagging moment side (Fig. 14) [9]. This reinforcement is anchored in the concrete slab behind the column on the sagging moment side and the reinforcement forces are transmitted to the column from the anchorage by concrete struts.

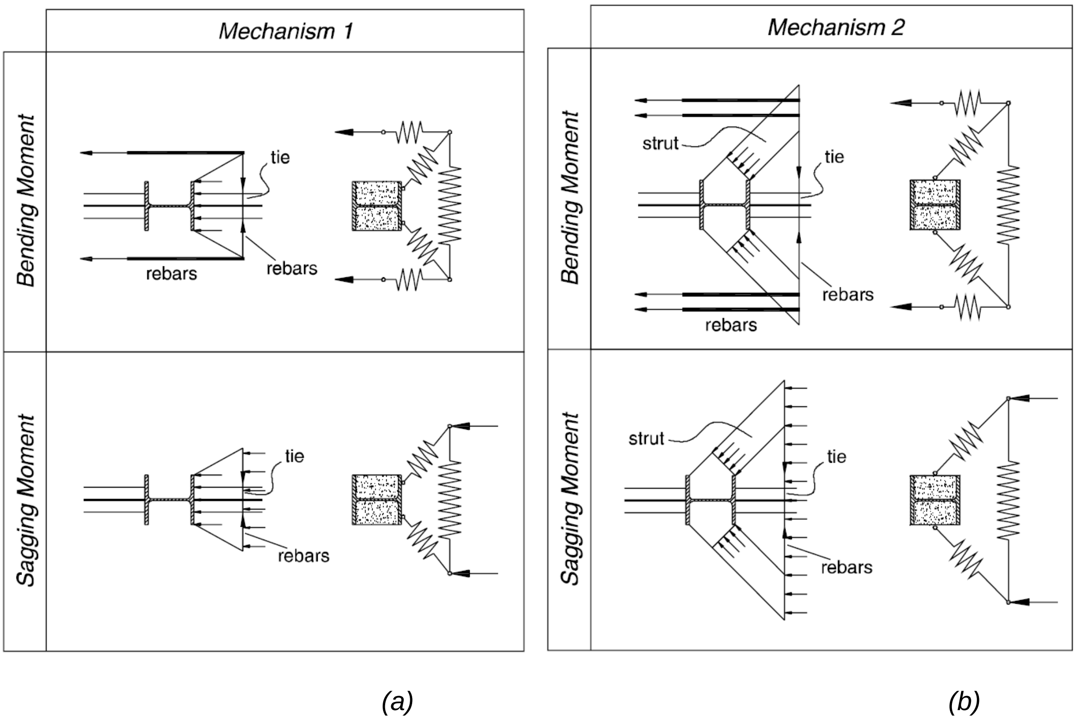

Fig. 14. *Mechanisms of force transfer from slab to a column in a seismic situation [9] for the sagging and hogging bending moment, which is denoted here as the "bending moment".*

The total resistance of mechanisms 1 and 2:

$$F_{Rd} = F_{R1} + F_{R2} = b_{eff,conn}\, t_{slab}\, 0.85\, f_{cd} \tag{28}$$

where

$$b_{eff,conn} = 0.7\, h_c + b_c \tag{29}$$

1.3.1.3 Effective slab thickness

More precisely, e.g., according to Liew et al. [15], instead of the total thickness of the concrete slab t_{slab}, the thickness of the compressed concrete slab can be considered, which is calculated from the equality of the resistances of the tensioned and compressed components in the joint. If the plastic neutral axis of the joint loaded with a sagging moment lies in the concrete slab (Fig. 15):

$$z = \frac{F_{R1} + F_{R2} + F_{R3}}{b_{eff,conn}\, 0.85\, f_{cd}} \le t_{slab} \tag{30}$$

where z is the thickness of the compressed concrete slab, $F_{R,i}$ are the forces in the tensioned bolt rows.

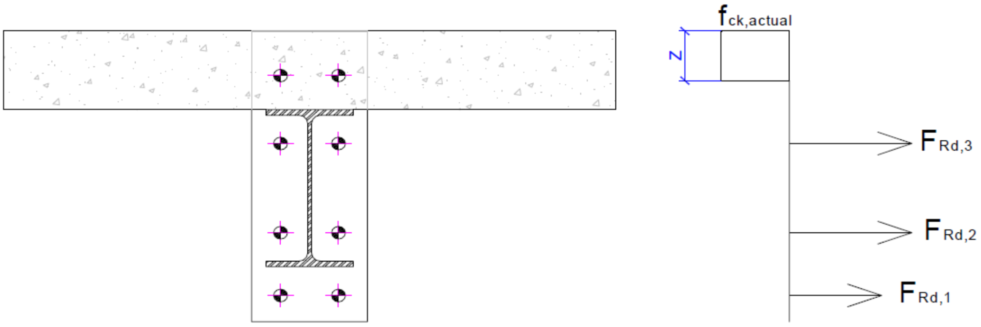

__Fig. 15.__ Distribution of forces in a joint loaded with a sagging moment [16].

1.3.1.4 Component stiffness

In terms of stiffness, this component can be considered as concrete in compression according to EN 1993-1-8 [10]:

$$k_{sc} = \frac{E_c \sqrt{b_{eff,conn}\, z}}{1.275\, E_a} \tag{31}$$

where k_{sc} is the coefficient of stiffness of the concrete slab component in compression, E_c is the modulus of elasticity of concrete and E_a is the elastic Young's modulus for steel.

1.3.2 Behaviour of a transverse beam under seismic loading according to Plumier et al.

The content of Annex C of EN 1998-1 [3] for a joint loaded by a sagging bending moment with a transverse beam is described in more detail, e.g. in Plumier et al. [5], which is the subject of this chapter.

When a joint is subjected to a sagging bending moment under seismic loading, the value of the effective slab width in the joint $b_{eff,conn}$ is usually less than the value of the effective slab width in the girder b_{eff} [5] (Fig. 4):

$$b_{eff,conn} \approx (0.7\ h_c + b_c) \approx 1.7\ b_c \approx 0.085\ L_1 \ < \ b_{eff} \approx 0.15\ L_1 \tag{32}$$

$$b_{eff,conn} \approx 0.5\ b_{eff} \qquad\qquad (\text{if } b_c \approx h_c;\ b_c \approx 0.05\ L_1) \tag{33}$$

Therefore, without a transverse beam connected to the concrete slab (Fig. 16), plastic hinges cannot be provided at the ends of the girders loaded with sagging moments, because the concrete slab in the joint region would be damaged by even a small plastic rotation [5]. The transverse beam in the joint connected to the concrete slab forms mechanism 3 whereby shear connectors transfer the normal stress from the effective width of the slab to this transverse beam. Shear, bending, and torsional stresses are then applied to the transverse beam (due to the small torsional stiffness of the I-sections, the calculation can be simplified to the bending and shear stresses of the upper flange of the beam) [5]. The procedure for calculating the resistance of Mechanism 3 is given in Annex C of EN 1998-1 [3] and is described in more detail in e.g. [5].

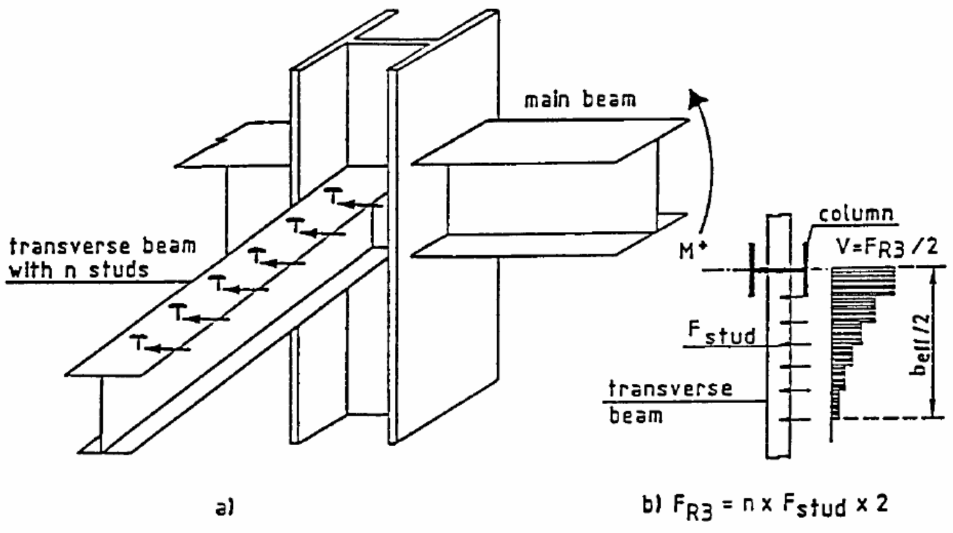

Fig. 16. *Mechanism 3 (a), diagram of the shear force in the slab effective width of the girder (i.e. the main beam) and calculation of the resistance of mechanism 3 (b) [5].*

In the case of an interior joint, the following ductility condition must be met to plasticize the beam bottom flange or slab reinforcement before brittle failure of the concrete slab [5], [3]:

$$1.2\ (F_{SC} + F_{St}) \leq F_{Rd1} + F_{Rd2} + F_{Rd3} \tag{34}$$

where
$$F_{Rd1} + F_{Rd2} + F_{Rd3} = (0.7\ h_c + b_c)\ d_{eff}\, f_{cd} + 2\, n\, F_{stud} \tag{35}$$

where F_{SC} is the force in the effective width of the slab for the sagging moment, F_{St} is the force in the effective width of the slab for the hogging moment, F_{Rd1} is the resistance of mechanism 1, F_{Rd2} is the resistance of mechanism 2, and F_{Rd3} is the resistance of mechanism 3. The resistance of mechanism 3 is considered as the resistance of the shear connection on the transverse beam in the effective width of the slab, n is the number of connectors in half of the effective width of the slab, F_{stud} is the shear resistance of one connector.

The simple sum of the resistances of mechanisms 1, 2, and 3 can be considered the total resistance of the concrete slab in the joint if the mechanism with the highest stiffness is sufficiently ductile. If the concrete slab fails in the compression of mechanism 1 before mechanism 3 is activated, then this simple sum is not valid. Thus, mechanism 3 can only transfer forces effectively if a large number of shear connectors are designed in the effective width of the beam slab b_{eff} (practically as close to the column as possible within approximately 500 mm of its axis according to [5]). Another condition is that the transverse beam and its connection to the column are sufficiently torsionally stiff. The I-section transverse beam itself usually does not have high torsional stiffness, so alternatively cantilever structures in the effective width connected to the column can be designed to transfer the stress directly from the slab to the column to avoid brittle failure of the concrete slab [5]. An example of such an arrangement is shown in Fig. 17 [8]. In Annex C of EN 1998-1 [3], this design arrangement contributes to the resistance of mechanism 1.

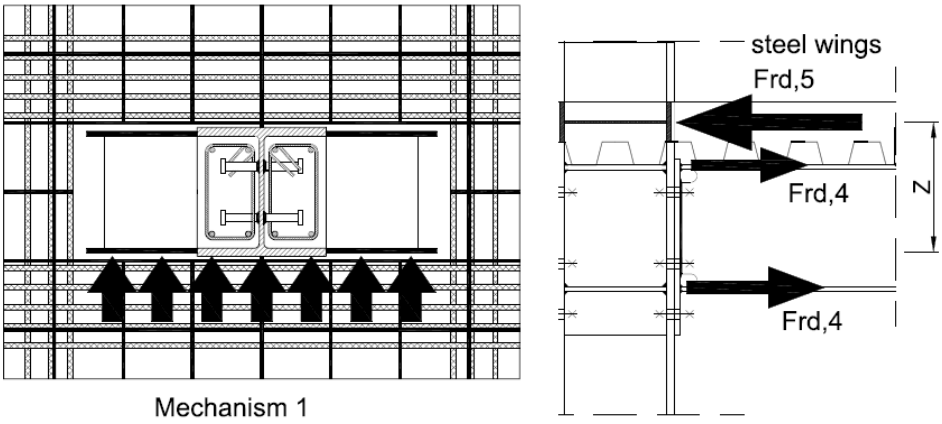

(a) *(b)*

Fig. 17. *Cantilever structure of steel I-section at the level of the concrete slab to increase the compressive resistance of the concrete slab in the joint: plan view (a), side view (b), where z is the lever arm of the internal forces, $F_{rd,4}$ is the forces in the tensioned part of the joint, $F_{rd,5}$ is the compressive reaction in the concrete slab at the level of the cantilever structure [8].*

1.4 Confinement effect acting on mechanism 1

In some publications, a higher resistance is given for mechanism 1 than in the standard relationship in Annex C of EN 1998-1 [3], because the effect of a favourable 3D stress state (confinement effect) on the resistance can be taken into account for this mechanism. The favourable stress state is due to a large amount of transverse reinforcement in front of the column flange (lateral and vertical restraint), the friction at the interface between the column flange and the concrete slab (vertical restraint) (Fig. 18) [5], and the top flange of the beam supporting the concrete slab [17].

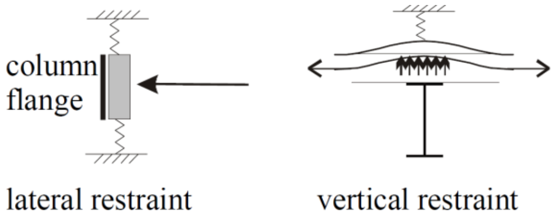

(a) *(b)*

Fig. 18. *The lateral and vertical restraints providing the favourable stress state in the concrete slab in front of the column flange [5]. The left part of figure (a) shows the plan view and the right figure part (b) shows the steel-concrete beam cross-section at the joint.*

Du Plessis et al. in [17] determined a relationship for calculating the resistance of a concrete slab in a composite frame joint based on a set of experiments:

$$f'_c = 1.3\ (\ 0.85\ f_c) \tag{36}$$

where f_c is the cylinder compressive strength of the concrete, f'_c is the strength of the concrete slab in front of the column flange, and the coefficient 1.3 takes into account the favourable stress state in the joint area. The relationship was determined based on the lower limit of the ratios of the experimentally determined joint resistance moments to the analytically calculated joint resistance moments using the actual strengths of the structural elements. For most specimens, the concrete slab in compression determined the resistance moment. Mechanism 2 is not considered in this relationship for calculating the resistance of a concrete slab because only one flange of the column was in contact with the concrete slab during the experiments.

Kato et al. [18] derived a different relationship based on experiments:

$$f'_c = 1.8\ f_c \tag{37}$$

which is valid only for a column with I-cross-section. Thus, this relationship takes into account the effect of mechanism 2 and also the favourable stress state. According to the authors, the effect of the transverse beam on the effective width can be neglected due to its low torsional stiffness [19].

Based on a validated numerical model [5], Plumier et al. derived that the concrete strength for mechanism 1 can be considered multiplied by 1.3 and the ultimate compressive strain of concrete can be multiplied by 1.9 due to confinement.

Bennacer et al. [20] performed a parametric study based on experimentally validated numerical models of a concrete slab of the exterior joint. The parametric study was carried out for several column cross-sections (I - III, Fig. 19), the steel reinforcement ratios (0.25 - 0.7 %), etc. They calculated the stress from mechanism 1 in the concrete slab near the column flange for different cases of concrete slab geometry and column cross-section. These values ranged from 1.28 to 1.34 times the strength of the concrete along this flange. To simplify the analytical relationship, the value was rounded to 1.3. One of the results of their parametric study is shown in Fig. 20, which shows the stress versus distance from the slab *Y*-axis. The normal stress distribution is plotted at several distances from the column (Fig. 21). Concrete with a cylinder strength equal to 30 MPa was considered and the column flange width was 200 mm. Only half of the concrete slab is shown in this figure, the plotted stress is parallel to the *y*-axis (Fig. 19).

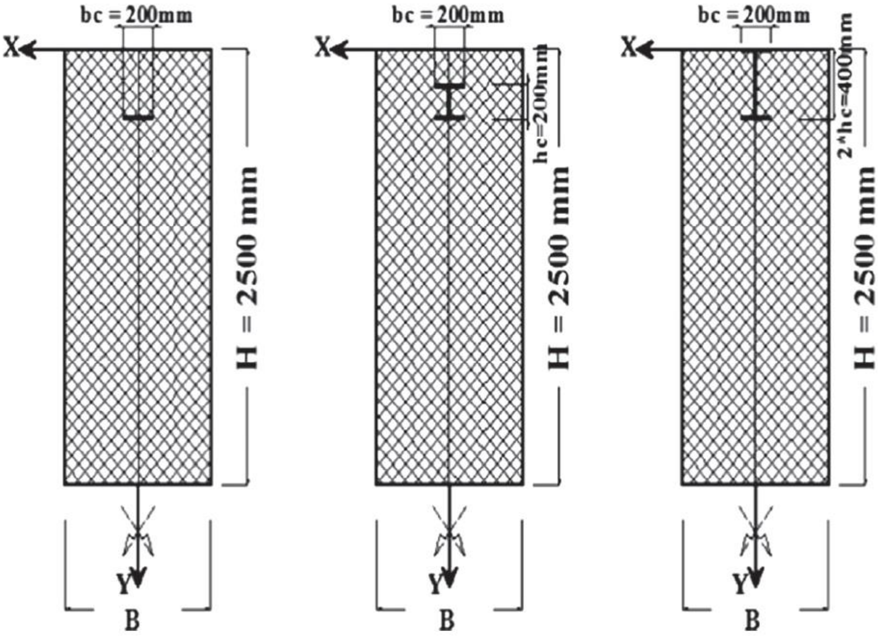

(a) Column type I . (b) Column type II. (c) Column type III.

Fig. 19. *Types of column cross-sections used in the parametric study [20].*

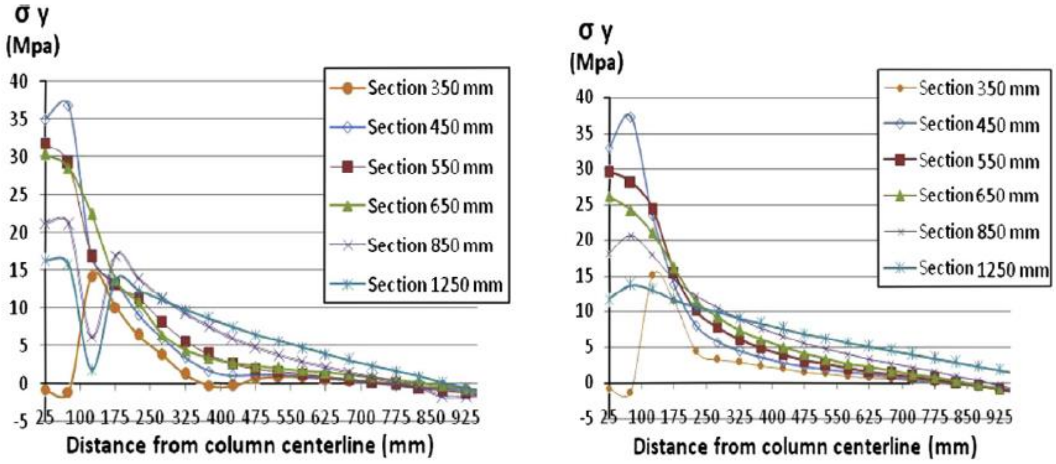

(a) Specimen (II/2/0.25%).

(b) Specimen (II/2/0.5%).

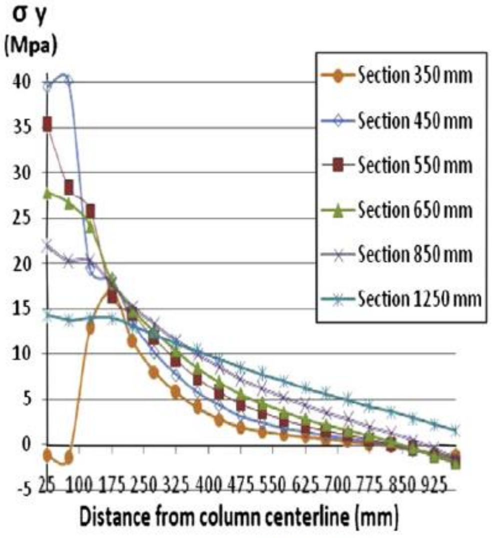

(c) Specimen (III/2/0.7 %).

Fig. 20. *Normal stress distribution in concrete slab under the action of mechanism 1 for three different specimens [20].*

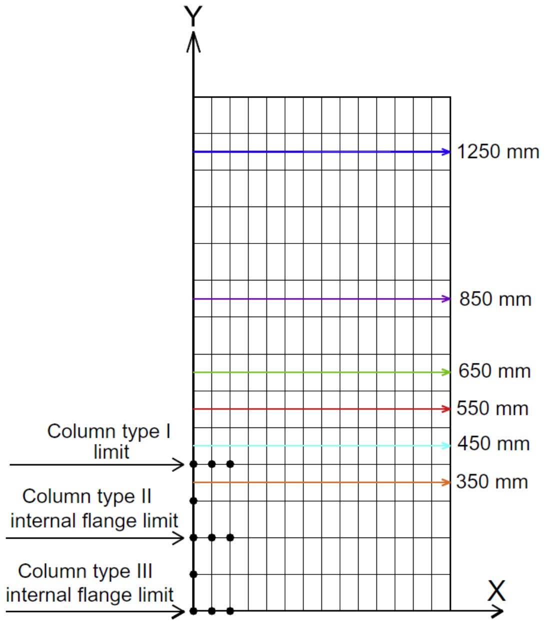

Fig. 21. *The plan view of half of the concrete slab with investigated places of the concrete slab. The y-coordinates marking these places are plotted. The column flange width is 200 mm [20].*

Following the recommendations in [22], Macrae et al. [21] described that the resistance of mechanism 1 can be further increased by a structural arrangement (vertical restraint in Fig. 18), namely 1) a steel plate on the top surface of the slab mechanically connected to the concrete slab by threaded rods, 2) a reinforcement cage in the concrete slab in front of the column flanges together with the design of a solid concrete slab in the joint area (Fig. 22) recommended in other literature up to 150 mm from the face of the column [23], [24].

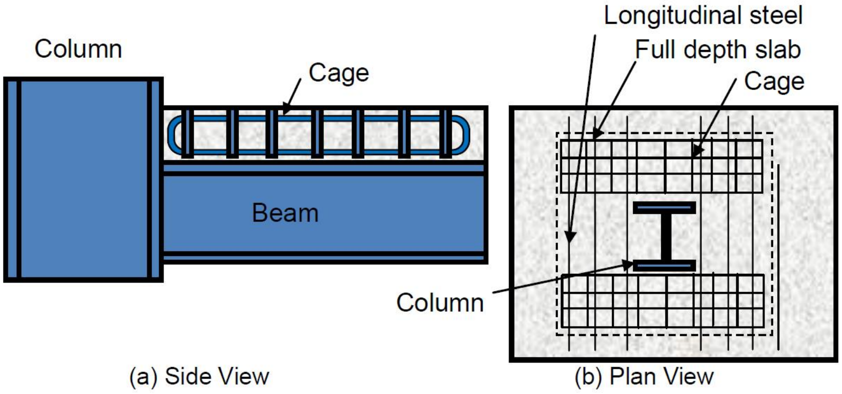

Fig. 22. *Reinforcement cage in concrete slab - side view (a), plan view (b) [21].*

1.5 Inclination of concrete struts of mechanism 2

The standard procedure given in Annex C of EN 1998 - 1 [3] considers a 45 ° inclination angle for concrete struts (Fig. 11), but there are different approaches.

Bennacer et al. [20] verified the 30 ° angle on a validated numerical model. The value of the inclination angle of the minimum principal stress from the *Y*-axis versus the distance from the *Y*-axis is plotted in Fig. 23. The graphs show the results in slab cross-sections (some of the investigated cross-sections are shown in Fig. 21). The main cross-sections examined were located at distances of 350 mm and 450 mm from the edge of the slab, i.e. behind the column flange and in front of the column flange. At a distance of 100 to 200 mm from the *Y*-axis of the slab, the measured angles for all models were approximately 30 °.

The authors then established a relationship to calculate the effective width of the concrete slab in compression in the joint area of the composite frame, taking into account the 30 ° angle of inclination of the concrete struts. This value was independently confirmed by the results of another investigation [25].

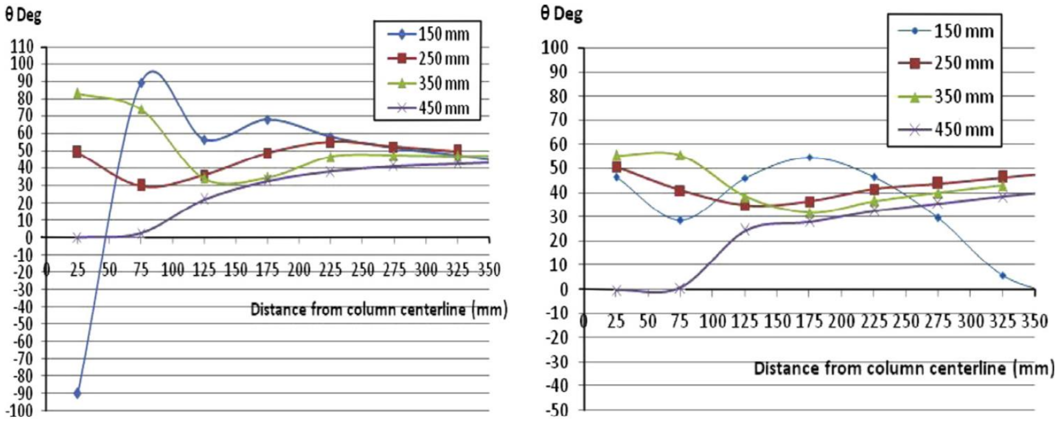

(a) Inclination of specimen (II/2/0.5 %). (b) Inclination of specimen (III/2/0.7 %).

Fig. 23. *The direction of minimum principal stress (inclination from the Y-axis) in each investigated cross-section for two different models (the specification of the models is explained in Section 1.4) [20].*

In an experiment with a composite joint subjected to cyclic loading, Civjan et al. [26] measured the strain distribution on the top surface of the concrete slab near the column flange, as shown in Fig. 24. According to the orientation of the cracks in the concrete slab at the joint (Fig. 25), the authors concluded that the value of the inclination angle of the concrete struts is between 15 ° and 30 °.

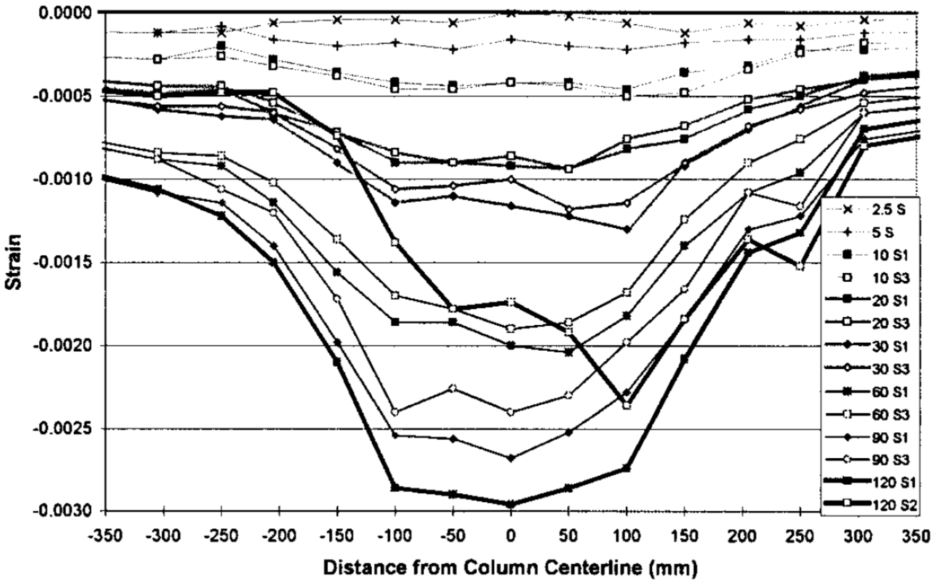

Fig. 24. *Strain distribution (-) on the concrete slab near the column flange, which was 330 mm wide [26].*

Fig. 25. *Photograph of the top surface of the concrete slab at the joint after testing [26].*

1.6 Effect of column encasement on the resistance of mechanism 2

If a steel-concrete column consisting of steel I-section is used in the composite frame and the column is fully or partially encased at the level of the concrete slab before casting the concrete slab, the shear resistance of mechanism 2 at the interface of the different aged concretes shall be assessed. The frictional connection created by the aggregate interlock is usually insufficient and mechanism 2 is not applied in the concrete slab [27]. When designing such a structure, the influence of mechanism 2 can be conservatively neglected.

The activation of mechanism 2 when using such a steel-concrete column can be achieved by adding reinforcement or extended stirrups to the steel-concrete column at the level of the concrete slab (Fig. 26) [28], which connect the two structural elements and allow the formation of concrete struts. The above design solution has been experimentally verified [29], [8]. Fig. 27 shows the dependence of the applied horizontal force on the storey displacement of a steel-concrete column during testing of an interior steel-concrete composite joint loaded monotonically on one side with a sagging moment and on the other side with a hogging moment. For specimen *CJ1* without these stirrups in the concrete slab region, a sudden decrease in the applied force is observed when the concrete slab fails in compression. While in specimen *CJ4* with extended stirrups, this sudden decrease in applied force was almost eliminated [8].

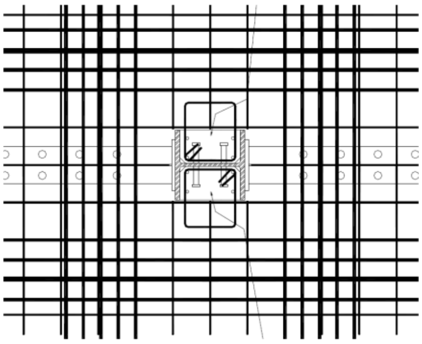

Fig. 26. *Structural solution for the activation of mechanism 2 - extended stirrups of a steel-concrete composite column at the level of the concrete slab [28].*

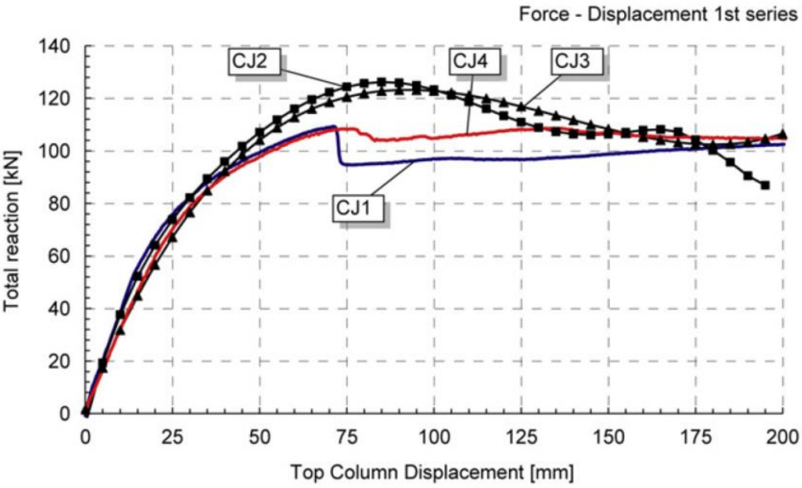

Fig. 27. *Experimental results of specimen CJ1 without extended stirrups and specimen CJ4 with extended stirrups at concrete slab level [8].*

1.7 Concrete slab failure due to shear deformation of the column web panel

Failure of the concrete slab in compression in a composite frame joint can also occur due to shear deformation of the column web panel (Fig. 28). The column web panel in shear often determines the resistance of the joint at highly unequal moments, and its deformation leads to premature failure of the concrete slab in compression.

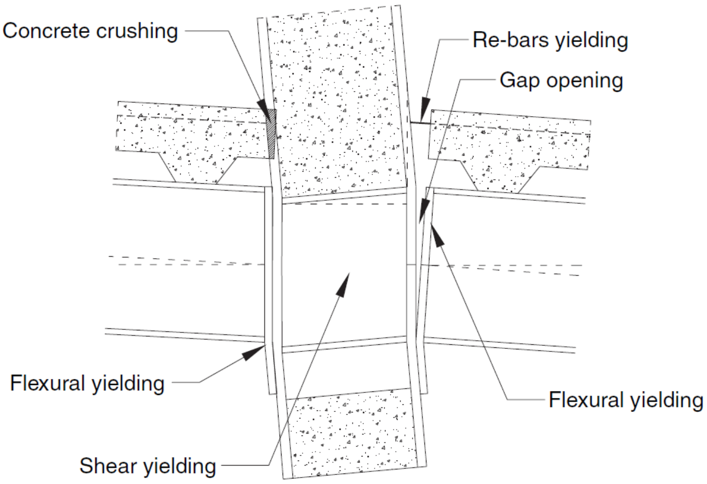

Fig. 28. *Failure of the slab in compression by shear deformation of the column web panel [30].*

Based on experiments, an advanced component model for this type of failure has been verified [30]. Fig. 29 shows the interior joint created by this component model, which contains the following components: concrete slab in compression (1), column web panel in shear (2), T-stub in compression on sagging moment side (3) and hogging moment side (7), T-stub in tension on sagging moment side (4) and hogging moment side (8), concrete slab and reinforcement in tension (5), connectors in longitudinal shear on sagging moment side (6) and hogging moment side (9); shear deformation of the column web panel (γ), horizontal displacement of the bottom flanges of the beams (u_1, u_2), horizontal displacement on the top surface of the concrete slab (u_3, u_4), rotation of the steel connections (θ_1, θ_2). In the model, the column web panel in shear at the concrete slab level was considered infinitely stiff. The concrete slab in compression was modelled in multiple layers along the slab height for the following reasons: 1) to more accurately distribute the non-uniform compression from the deformed column web panel in shear; 2) to determine the portion of the concrete slab where a favourable stress state can be considered and where not (the portion of the slab cross-section above the reinforcement). From the results of the parametric study of this advanced model with an interior joint loaded with unequal moments, it is clear that increasing the thickness of the concrete slab from 95 mm to 150 mm will not prevent the failure of the concrete slab due to the large deformation of the column web panel in shear, and the failure of the slab will occur in both cases at the same rotation (Fig. 30, Fig. 31).

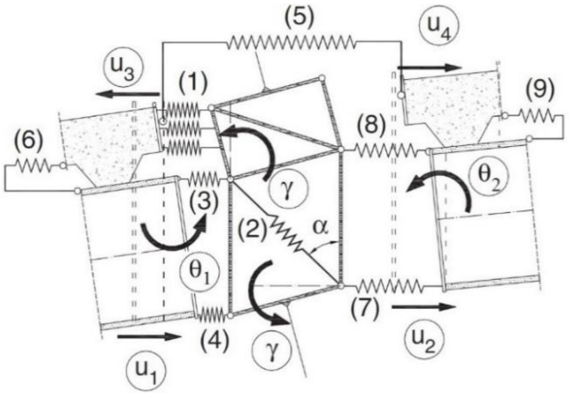

Fig. 29. *Advanced component model [30].*

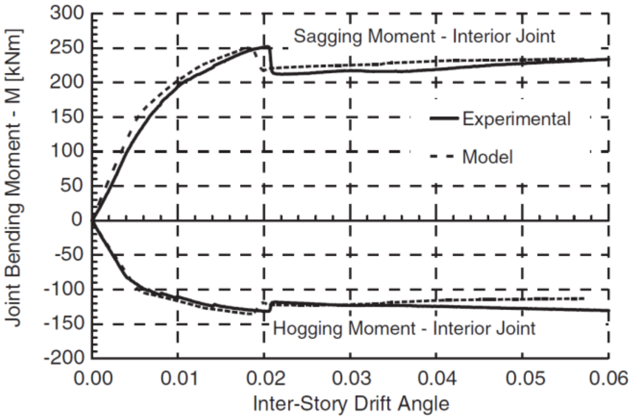

Fig. 30. *Graph of the moment versus rotation of the interior joint with a 95 mm thick concrete slab - experimental results and results of the component model [30].*

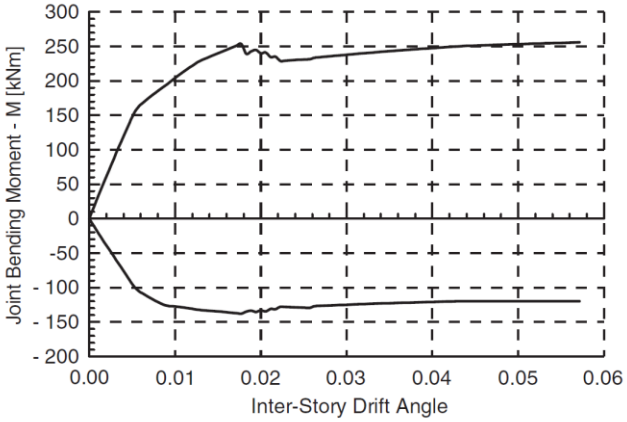

Fig. 31*. Moment versus rotation diagram of an interior joint with a 150 mm thick concrete slab - results of the parametric study [30].*

In [31] (described in more detail in [16]), experiments with exterior joints were carried out with the aforementioned concrete slab thicknesses of 95 mm and 150 mm. However, when using a 150 mm thick slab, the sudden drop in applied load was eliminated (Fig. 32). In these experiments, extended stirrups (see Section 1.6) were used at the level of the concrete slab to effectively connect the steel-concrete column and the concrete slab. The use of stirrups resulted in a more favourable behaviour of the slab compared to the parametric study [30] described in the previous paragraph, in which extended stirrups were not used for the steel-concrete columns, and therefore the effect of mechanism 2 on the resistance of the concrete slab was negligible and was not considered (conservatively) in the component model [30].

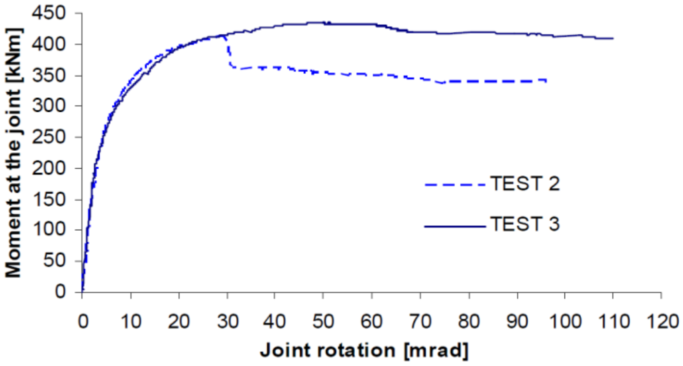

***Fig. 32.** Graph of the moment versus rotation of the exterior joint with 95 mm thick concrete slab (TEST 2) and 150 mm thick concrete slab (TEST 3) [16].*

1.8 Mechanism 4 acting in concrete slab

In the case of a concrete slab isolated from the column, the forces in the concrete slab at the interior joint of the composite frame are transferred by mechanism 4 [32], shown in Fig. 33. The normal stress in the concrete slab when a sagging moment is applied in the joint or the normal stress in the longitudinal reinforcement when a hogging moment is applied in the joint are distributed beyond this joint to the shear connectors of the beam using a strut and tie model acting in the concrete slab and transverse reinforcement.

The resistance of this mechanism is more significant under a hogging moment load. In the case of a sagging bending moment, the behaviour of the steel-concrete joint is close to that of the steel joint [32].

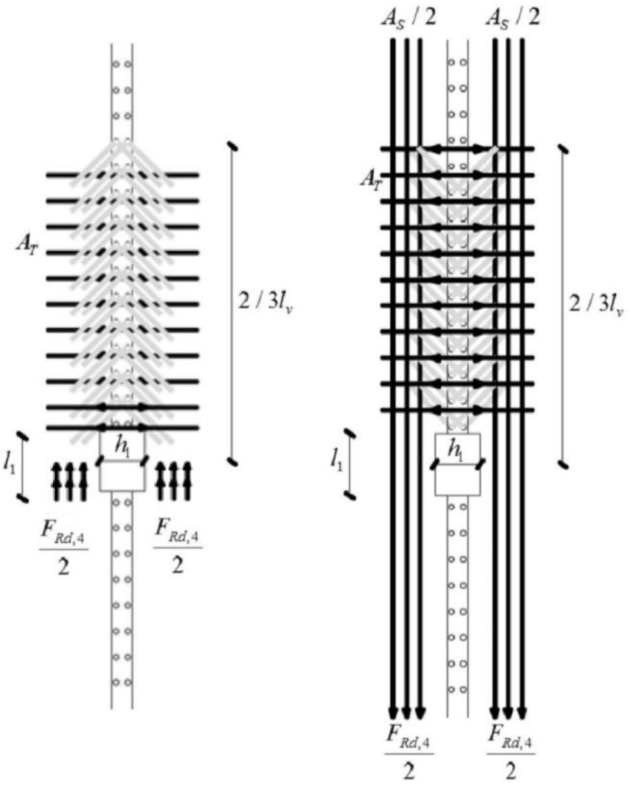

(a) *(b)*

Fig. 33. *Mechanism 4 – for a sagging moment (a), for a hogging moment (b); $F_{Rd,4}$ is the resistance of mechanism 4, A_S is the area of longitudinal reinforcement, A_T is the area of transverse reinforcement, l_1 and h_1 are the dimensions of the hole in the concrete slab in column location [32].*

Therefore, the gap (e.g., due to shrinkage) between the concrete slab and the column significantly affects the contribution of the concrete slab in compression to the moment of resistance of the joint [17]. It can be assumed that mechanism 4 will also act in the case of an unisolated concrete slab from the column after the concrete slab fails in compression due to the failure of mechanisms 1 and 2.

1.9 Comparison of joint behaviour under cyclic and monotonic loading

The joint is subjected to cyclic loading under seismic action. According to the experimental results shown in Fig. 34 [33], it can be concluded that the behaviour of the steel-concrete composite frame joint under monotonic and cyclic loading does not differ much. The maximum deviation between the diagrams was less than 12 %. The curve under cyclic loading was generated based on the peak moment values obtained in each cycle.

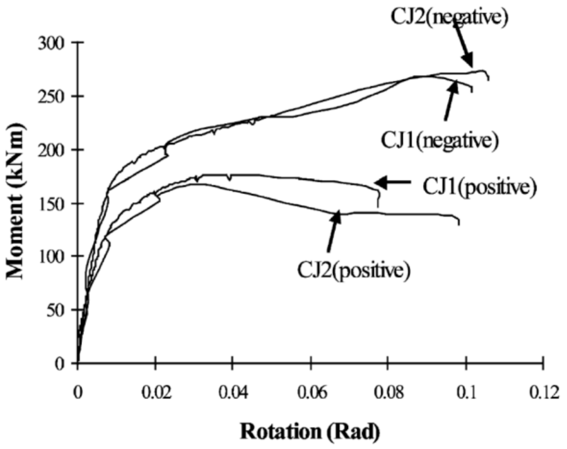

Fig. 34. *Moment vs. rotation dependence for an interior steel-concrete composite joint under monotonic (CJ1) and cyclic loading (CJ2) [33].*

Similar conclusions can be derived from test results reported in another paper [29], where four comparisons are made between monotonic and cyclic tests of interior joints. One of the comparisons is shown in Fig. 35 as an example. For all joints, the column web panel in shear (without the supplementary web plate) together with the concrete slab in compression determined the overall resistance of the joints. The other three comparisons show even better agreement than in Fig. 35.

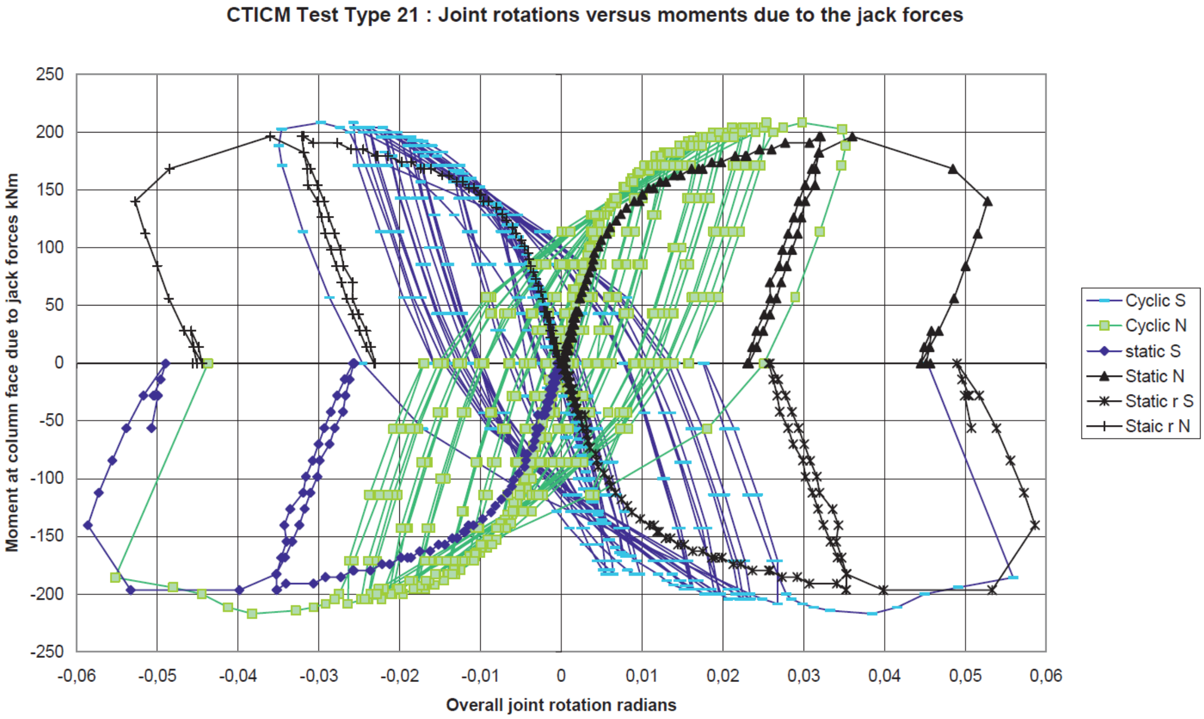

Fig. 35. *Dependence of moment on rotation for an interior steel-concrete composite joint under monotonic and cyclic loading [29]. For illustrative comparison, the monotonic load curves are also shown in adjacent quadrants of the graph.*

2 Research objectives and methods of this thesis

This thesis aims to derive an analytical relationship for calculating the resistance and stiffness of a concrete slab in compression in the area of the interior joint of a composite frame with a fibre-reinforced concrete slab, in contrast to previous investigations which have only considered a conventional reinforced concrete slab. The addition of fibres mainly changes the tensile properties of the concrete. Tensile strength and compressive strength are increased and the shape of the softening branch in tension is also affected. The effect of lateral tension (cracking) on compressive strength is reduced. Along with fibre reinforcement, steel reinforcement bars of the concrete slab are also considered.

The procedure is as follows:

1) experiment on a realistic-sized structure of an interior joint of the composite frame using fibre-reinforced concrete for the slab;
2) validation of the numerical model in Atena based on the experiment;
3) parametric study with these models;
4) derivation of the analytical relationship for calculating the resistance and stiffness of the fibre-reinforced concrete slab in compression in the joint.

3 Experiment study

An experiment was carried out with a composite steel-concrete frame joint of realistic dimensions. The scheme of the experiment is shown in Fig. 36. The joint was loaded with both a sagging bending moment on one side of the joint and a hogging moment on the other side. The joint's overall behaviour was investigated, particularly the strain distribution on the concrete slab in front of the column (mechanism 1) and next to the column (mechanism 2).

3.1 Preparation of experiment

3.1.1 Basic geometry

According to the laboratory conditions and the usual position of the zero moment points on the continuous beam under vertical load, a cantilever length of 2 m was chosen. The width of the concrete slab of 1.4 m was chosen after a preliminary analysis of the normal stress distribution in the concrete slab in the engineer FEM program Scia Engineer [34] and also according to Annex C of EN 1998-1 [3], which gives the geometric requirements for the development of struts and tie by mechanism 2 in the concrete slab in the joint area. Taking into account the normal height of the storey, a column height of 3.4 m was chosen for the specimen. The column is supported rigidly, primarily to ensure the overall torsional stability of the structure.

3.1.2 Rigid frame test structure

The basic scheme of the rigid test frame is also shown in Fig. 36. The steel-concrete composite cantilever, subjected to a sagging bending moment, is secured against lateral buckling by side supports. Between the girders of the frame, which are composed of two high welded U-profiles, it was necessary to insert an HEB 400 profile element to support the upper end of the specimen column. The specimen was subjected to significantly unequal moments during the experiment, hence a large horizontal force was generated in the test girders and significant bending moments in the frame joints. The columns were doubled in the plane of the frame to: 1) reduce the bending stresses on the columns, which consist of welded I-sections bent around a minor axis; 2) reduce the floor deformation of the frame. To ensure the out-of-plane stability of the frame, one of the four columns was additionally doubled by another column also in the transverse direction by connecting them with the short beam. The test frame, including the anchorage to the concrete slab of the test hall, was assessed by elastic calculation for the maximum forces developed by the hydraulic jacks.

There were two hydraulic jacks in total, the first applied tension and the second applied compression. The maximum force applied by these hydraulic jacks is 100 kN in tension and 400 kN in compression. The end of the steel-concrete cantilever was connected to the hydraulic jack by a pin connection with a longitudinal hole to allow for the horizontal displacement caused by the rotation of the cantilever.

The test configuration is shown in Fig. 36: steel-concrete composite joint (1), steel test frame columns (2), steel test frame girders (3), beam inserted between the steel test frame girders to support the column (4), transverse beam to provide out-of-plane stability of test frame (5), hydraulic jack producing tensile force on the hogging bending moment side (6), hydraulic jack producing compressive force on the sagging bending moment side (7), pin joint (8), sliding lateral support for the end of the cantilever subjected to the sagging bending moment (9).

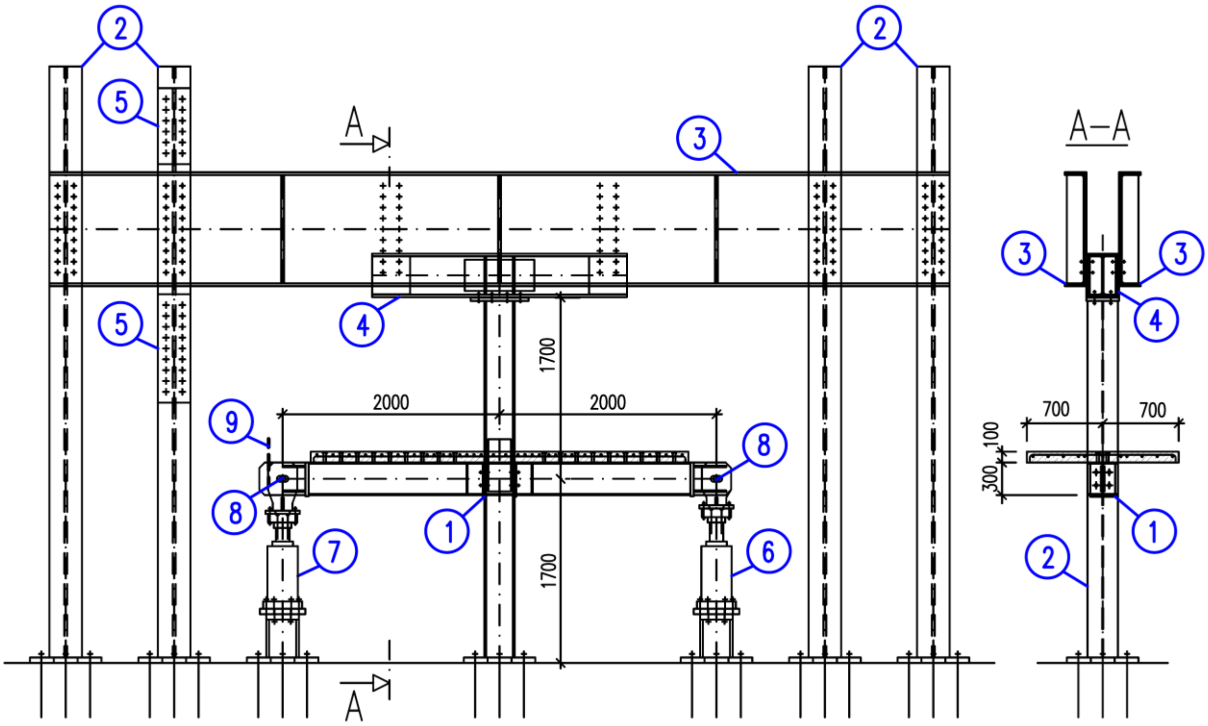

Fig. 36. *The test set-up.*

3.1.3 Design of the steel-concrete composite joint

The design of the joint was carried out so that the side of the joint loaded with a hogging bending moment is more resistant than the side of the joint loaded with a sagging bending moment. The concrete slab in compression was designed to be the weakest component determining the resistance of the entire joint. The other components were intentionally oversized compared to this component. The component method implemented in COP AM 2.1.2 [35] was used for the design of the joint, Fig. 37. The designed joint is shown in Fig. 38.

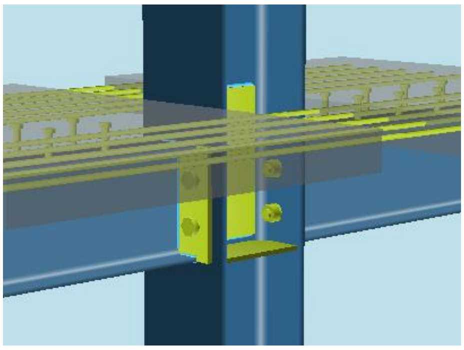

Fig. 37. *Rough visualization of the steel-concrete composite joint in COP AM 2.1.2 [35].*

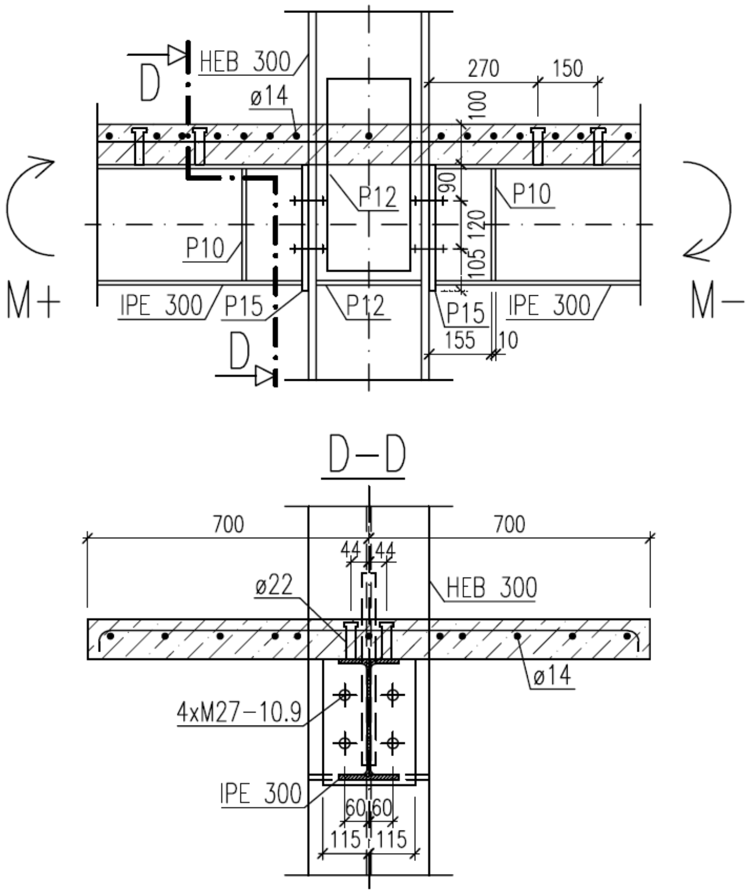

Fig. 38. *The joint details.*

The nominal strength class of the concrete slab was C25/30, of the steel elements S355, of the reinforcement B500B (ribbed bars). The actual properties were determined by tests, Chapter 3.2.

A thickness of the concrete slab was 100 mm. The concrete slab was further reinforced with TriTreg 50-1 steel fibres in the amount of 80 kg/m^3.

The compressive resistance of the concrete slab in the joint was calculated according to the relationship for normal concrete given in Annex C of EN 1998-1 [3]. Similarly, the stiffness of this component was calculated according to EN 1993-1-8 [10]. The calculation showed that the slab in compression in the joint would fail already with an elastic distribution of forces in the joint. However, it was assumed that the actual strength of the concrete would be higher than the nominal strength, so the steel components of the joint were designed ductile to be capable of plastic force distribution with subsequent failure of the concrete slab in compression.

The column profile was chosen to be HEB 300 and the beam profile was chosen to be IPE 300.

The column web panel in shear was stiffened on both sides with supplementary plates not to be a critical component when reversed moments are applied in the joint. The column was also equipped with stiffeners at the level of the lower flange of the beams.

The resistance of mechanism 1 in the concrete slab, calculated according to the standard procedure for ordinary concrete, was less than the resistance of the column web in transverse compression. Local buckling of the column web at the level of the concrete slab near the stiffeners was neglected.

The equivalent t-stub in tension according to EN 1993-1-8 [10] for the steel connection was designed to allow tensile failure mode 1) or 2), not a failure of the bolts (failure mode 3).

The shear connection between the concrete slab and the steel beam was provided by headed studs that were placed in two rows on each beam. The design of the full connection was carried out plastically. The design principles for the arrangement of the studs on the beam were followed.

To achieve the desired rotational capacity of the joint: 1) the end-plate was designed only for the height of the beam; 2) the distance of the first studs from the column flange was chosen to be almost twice the axial distance of the studs on the beam.

The area of longitudinal reinforcement of the concrete slab was chosen large enough to allow the concrete slab in compression to control the moment of resistance of the joint. Only the nearest four members of the longitudinal reinforcement were conservatively considered in the calculation. On the other hand, the reinforcement area was limited by the compressive resistance of the beam flange. To reduce the possibility of the beam flange buckling in compression, the beams near the joint were also stiffened, Fig. 38.

The design of the transverse reinforcement in the concrete slab was carried out according to EN 1992-1-1 [14] for the tension caused by the longitudinal shear force in the shear connection. The design of the transverse reinforcement in the joint area was carried out according to EN 1998-1 [3] Annex C for the transverse tension from the action of mechanisms 1) and 2) in the concrete slab.

According to a preliminary analytical calculation, the displacements induced by the hydraulic jacks should have been up to 50 mm and the forces up to 80 kN. The preliminary calculation took into account the nominal strengths and stiffness of the materials, the deformation of the entire test frame, the initial or secant stiffness of all connections, the equivalent stiffness of the composite structure, etc.

3.2 Material properties

The tests of fibre-reinforced concrete were carried out with a total of 15 specimens, Fig. 39. The mechanical properties found are shown in Table 3 and were determined 98 days after casting when the experiment was performed on the steel-concrete composite joint. Each parameter was determined using three tests. The average cubic strength of the concrete was 61.8 MPa, which when multiplied by Zhu's coefficient of 0.738 [36] gives a cylindrical strength of 45.6 MPa. According to the results obtained, the fibre-reinforced concrete can be classified as L1.6/1.1. The results of the four-point bending test with a 150 mm x 150 mm x 700 mm specimen are shown in Fig. 39.

Coupon tests were also carried out with steel specimens and with steel reinforcement. The material parameters found are given in Table 4.

Fig. 39. *SFRC test specimens.*

Table 3. *Mechanical properties of SFRC determined from tests.*

Average material properties	(MPa)	VAR[1]
Modulus of elasticity	35 800	287
Cubic compressive strength (150 mm x 150 mm x 150 mm)	61.8	4.6
Splitting tensile strength (150 mm x 150 mm x 150 mm)	5.8	0.3
Flexural tensile strength (100 mm x 100 mm x 400 mm)	8.2	0.0
Flexural tensile strength (150 mm x 150 mm x 700 mm)	5.4	0.7

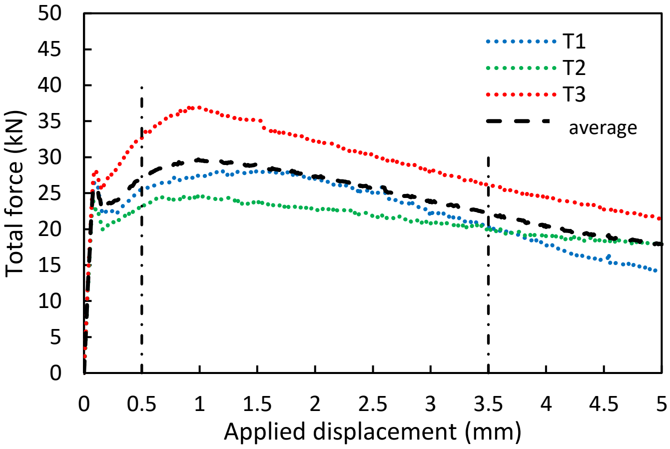

Fig. 40. *Graph of the relationship between the force and the applied displacement of the concrete beam (150x150x700 mm) during the four-point bending test.*

Table 4. *Mechanical properties of steel members determined from coupon tests.*

	HEB		IPE		rebars	stiffeners[2]
	web	flange	web	flange		
f_y (MPa)	428	415	395	444	625	375
f_u (MPa)	565	554	503	543	668	535

3.3 Instrumentations for the measurement

The strain distribution in the concrete slab in compression in front of the column on the top surface of the slab was recorded using HBM-1-LY41-50/120 strain gauges, Fig. 41. Strain gauges were also placed at the bottom surface of the slab, but their measured data are unusable due to the higher actual strength of the concrete - shifted neutral axis to the slab

---

[1] Population Variance

[2] column web stiffeners

caused tensile cracking at the bottom surface of the slab. The strain gauges were placed on the slab in a total of 7 cross-sections marked from 0 to 6. In cross-sections 6, 4 and 2, the strain from the transverse forces of the two mechanisms and the longitudinal forces in the concrete slab was recorded. In cross-section 1, the strain from both mechanisms was measured and there were strain gauge rosettes to evaluate the minimum principal strains and their direction in mechanism 2. Similarly, in cross-sections 3 and 5, the longitudinal strain from both mechanisms was measured.

The digital image correlation (DIC) method was also used to record the strain of the concrete slab under the action of mechanism 2 on an area of approximately 30 cm x 30 cm next to the column.

Strain gauges were also placed on the reinforcement bars of the concrete slab, Fig. 41. On the longitudinal reinforcement in the hogging bending moment region and on the transverse reinforcement in the sagging bending moment region to evaluate the transverse tensile strain from Mechanisms 1 and 2.

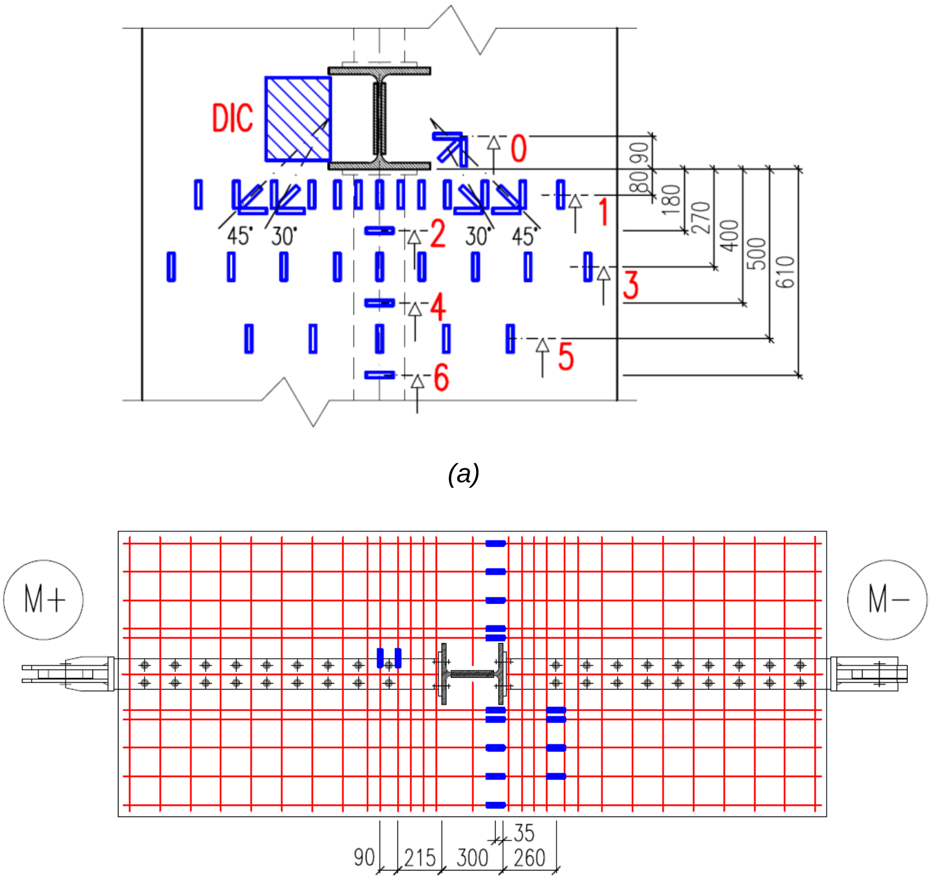

(a)

(b)

Fig. 41. *Strain gauges on the top surface of the concrete slab and monitoring of strain using the DIC method (a), strain gauges on reinforcement bars (b).*

Inclinometers and displacement sensors were placed on the joint to independently evaluate the dependence of the bending moment on the rotations of the joint, connections and column panel according to [37], Fig. 42. Five displacement sensors for the evaluation of panel distortion were connected to a separate structure. Furthermore, the displacement sensors recorded: 1) the slips between the concrete slab and the top flange of the steel cantilevers at their ends; 2) the horizontal displacements at the column support at its ends. Hydraulic jacks recorded the applied displacements and forces.

The HBM-1-LY11-6/120 strain gauges were placed on the steel part of the joint (Fig. 43) on these selected components: beam flanges in tension and compression, end-plate and column flange in bending, column panel in shear (strain gauge rosette), beam web in tension.

Fig. 44 to Fig. 49 show photos of the steel test frame with the specimen of the composite joint before casting, before the experiment, and during the experiment, along with the instrumentations for the measurement.

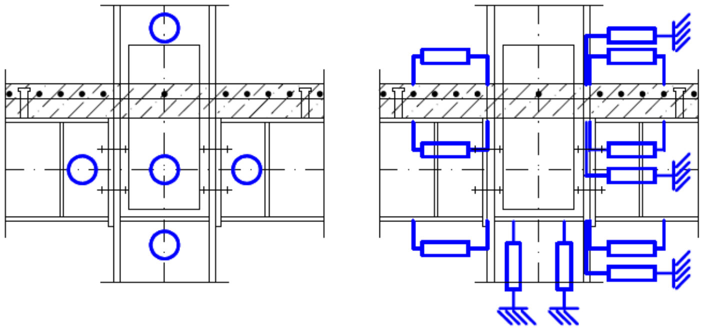

(a) *(b)*

Fig. 42. *Inclinometers (a) and displacement sensors (b) on the joint.*

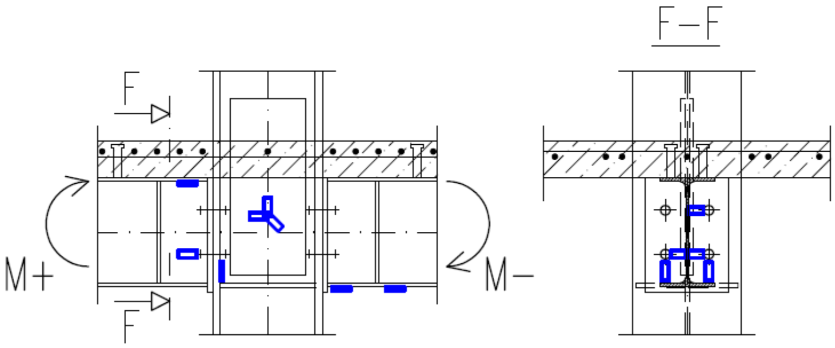

Fig. 43. *Strain gauges on the steel components of the joint.*

(a) *(b)*

(c) *(d)*

Fig. 44. *Photo of the reinforcement of the concrete slab (a,b,c) and the steel test frame with the specimen before casting (d).*

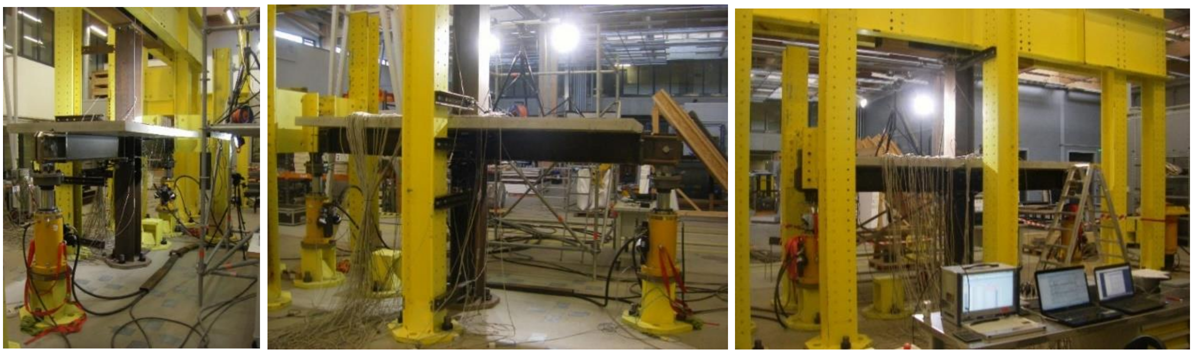

(a) *(b)* *(c)*

Fig. 45. *Steel specimen before the experiment (a) and during the experiment (b c).*

Fig. 46. *Photos of both sides of the steel-concrete composite joint.*

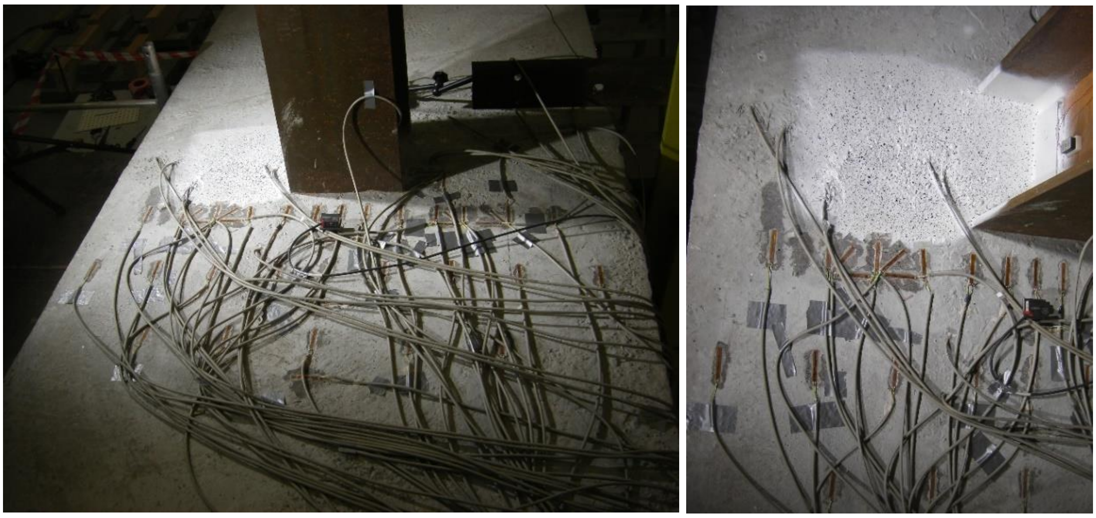

Fig. 47. *Photographs of the top surface of the concrete slab with strain gauges and the surface of the slab prepared for DIC measurement.*

(a) *(b)*

Fig. 48. *Photographs of the ends of steel-concrete composite cantilevers with the displacement sensors for slip measurement - on the sagging moment side with lateral restraint of the cantilever (a), on the hogging moment side (b).*

(a) (b)

(c) (d) (e)

(f) (g) (h)

Fig. 49. *The separate structure with displacement sensors to evaluate horizontal column displacements and column web panel distortion.*

3.4 Results of the experiment

The hydraulic jacks used in the test were displacement controlled. Previously, a gradual displacement was applied up to 60 mm on the sagging bending moment side (the first part of the test, i.e. the 1st cycle). Subsequently, the structure was unloaded and re-loaded up to a displacement of 105 mm (the second part of the test, i.e. the 2nd cycle), Fig. 50. The loading speeds were 1 mm/s and 1.25 mm/s for the first part of the test, for the sagging and the hogging bending moment side, respectively. For the second part, the speed was 10 mm/s.

The hydraulic jack inducing the load on the hogging bending moment side was only able to apply a maximum force of 100 kN, which results in a bending moment of 185 kNm. The distance from the point of load applied by the hydraulic jack to the face of the column flange is considered as the lever arm of the force.

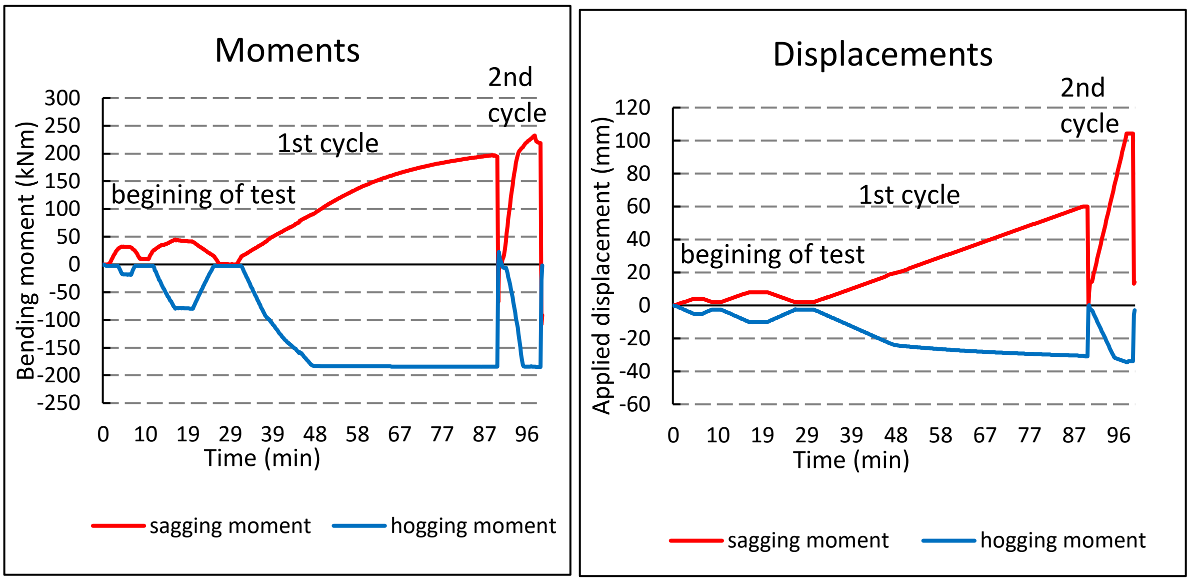

(a) *(b)*

Fig. 50. *Hydraulic jacks – forces (a), applied displacements (b) vs time from the beginning of the experimental test.*

A diagram of the dependence of bending moments on the rotation of the joint is shown in Fig. 51 for the case of the rotations measured by the inclinometers and also by the displacement sensors for both parts of the experiment ("1" is for the first part of the test and "2" for the second part of the test; “M+” means a sagging bending moment and “M-“ means a hogging bending moment). The most important effect on the measured rotation was the rotation of the connection. On the other hand, the column panel rotation was negligible (less than 8 % of the joint rotation). The measured values of the joint rotation were higher for the displacement sensors by 20 % and 23 % compared to the values measured by the inclinometers, on the sagging and hogging bending moment side, respectively.

During the experiment, plasticization of the beam end-plate occurred on the sagging moment side (at approximately +140 kNm of sagging bending moment) and cracks appeared at the bottom surface of the concrete slab at this connection (at approximately +60 kNm and -160 kNm of sagging and hogging bending moment, respectively). On the upper surface of the slab, the crushed concrete slab was in contact with the column flange on the sagging moment side (the crushed or sheared part of the slab was approximately 1 cm deep, 3 cm wide and was along the entire column flange). The failures described are shown in Fig. 52, Fig. 53, and Fig. 54. The weakest part of the connection was the end-plate in bending instead of the concrete slab in compression, as the actual strength of the concrete slab was approximately twice the nominal strength.

The slip versus bending moment diagram and the bending moment versus column web panel rotation diagram are shown in Fig. 74.

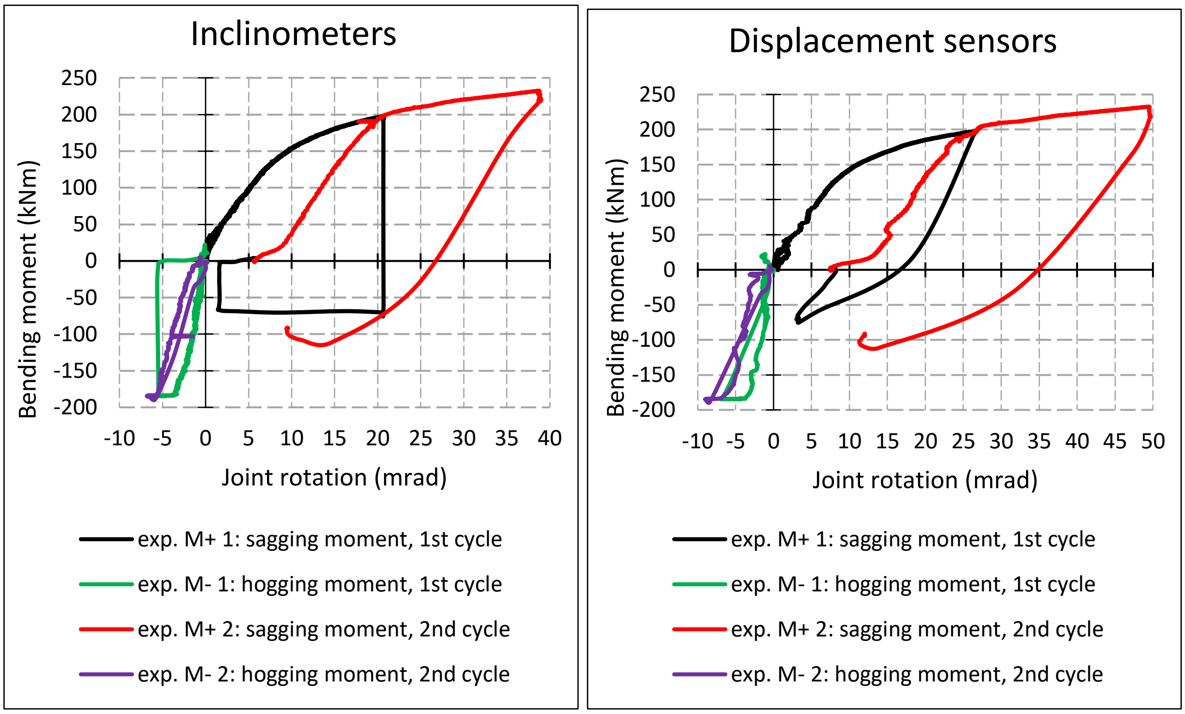

(a) *(b)*

Fig. 51. *Graph of the moment versus joint rotation measured by inclinometers (a) and displacement sensors (b).*

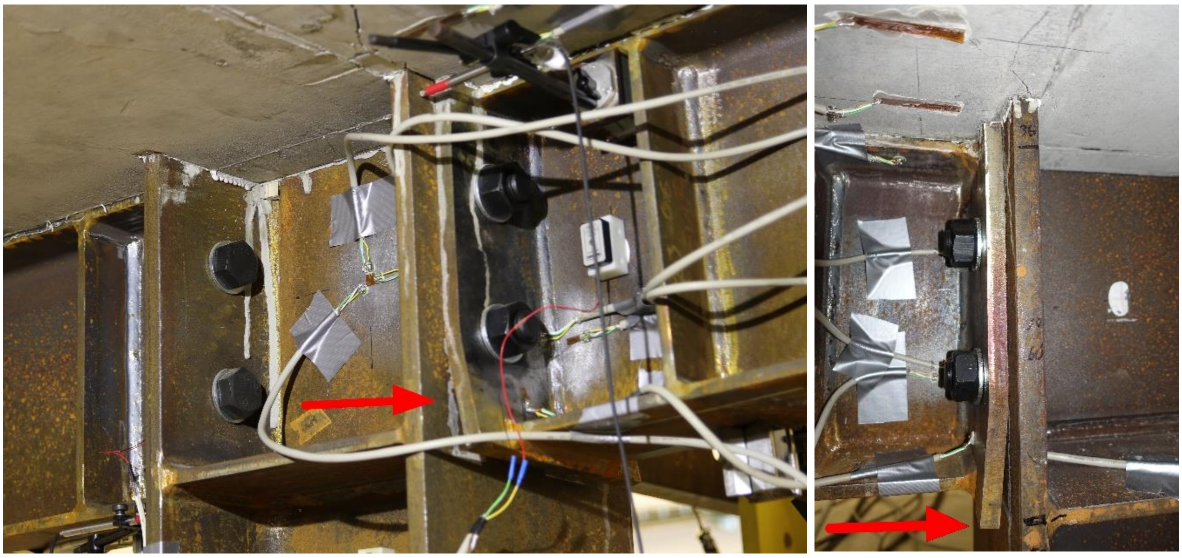

(a) *(b)*

Fig. 52. *Plasticized end-plate loaded by sagging bending moment during the experiment (a) and after the experiment (b).*

Fig. 53. *Crushing the concrete slab in front of the column by a sagging bending moment.*

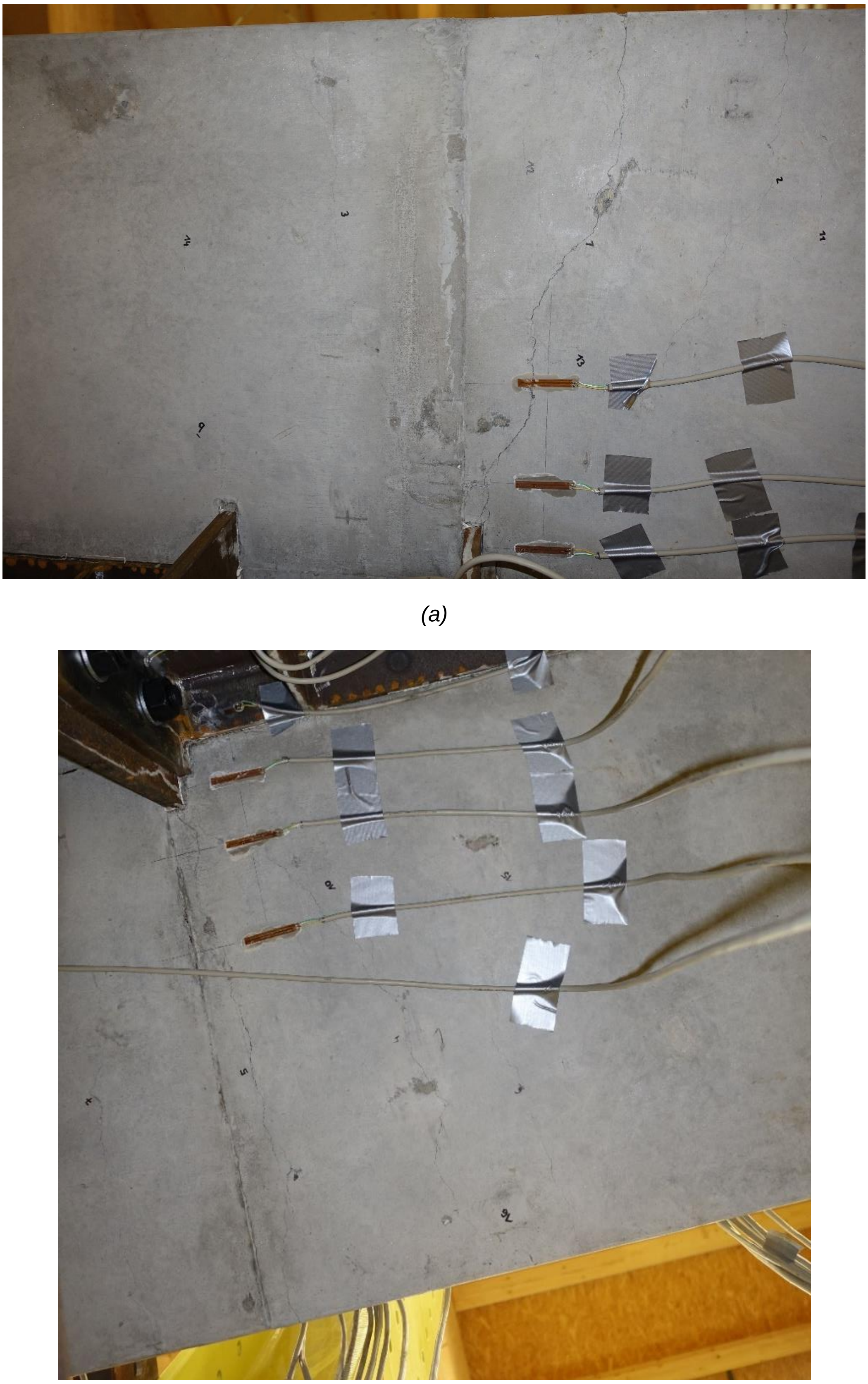

(a)

(b)

Fig. 54. *Cracks at the sagging moment connection on the bottom surface of the concrete slab to the left (a) and right (b) of the slab axis in Fig. 56.*

3.4.1 The strain distribution in the concrete slab

Fig. 56 shows the distribution of the normal strain in different sections of the slab at a distance of 80 mm, 270 mm and 500 mm from the face of the column. In the sections at a distance of 80 mm and 270 mm from the column, the action of both mechanism 1 and mechanism 2 can be seen. Mechanism 2 is manifested by struts which gradually approach the axis of symmetry.

To the left of the axis of symmetry of the slab, there are higher values of the strain due to the manufacturing imperfections of the shape of the column cross-section. The flanges of the column were not accurately perpendicular to the column web, which resulted in horizontal shifting of the ends of the cantilevers (this was particularly significant for the cantilever loaded with a sagging moment), Fig. 55. The dimensions of the imperfect cross-section of the column are described in Annex C.

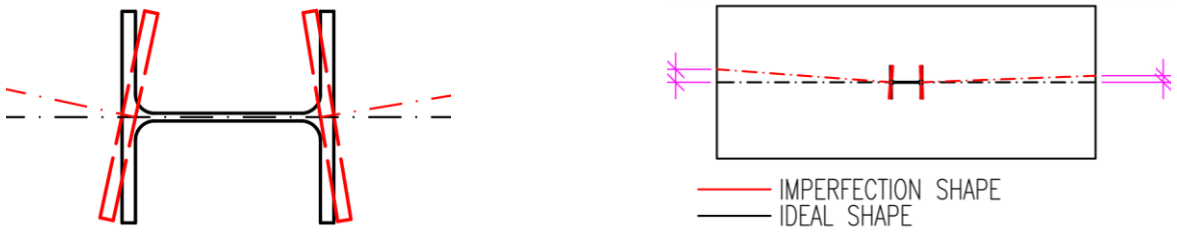

(a) (b)

Fig. 55. *The manufacturing imperfections of the column cross-section shape (a), horizontal shifting of the axes and ends of the cantilevers and the legend (b).*

After the local crushing of the concrete slab in front of the column, in the section at a distance of 80 mm from the column, the strain in front of the column in mechanism 1 decreased and subsequently, the strain in the struts of mechanism 2 increased.

The strain of the concrete slab in front of the column exceeded the ultimate compressive strain (2.6 ‰ for SRFC according to [38], 2.3 ‰ for ordinary concrete according to EN 1992-1-1 [14]), but after the test, there were no signs of failure at the locations of the strain gauges.

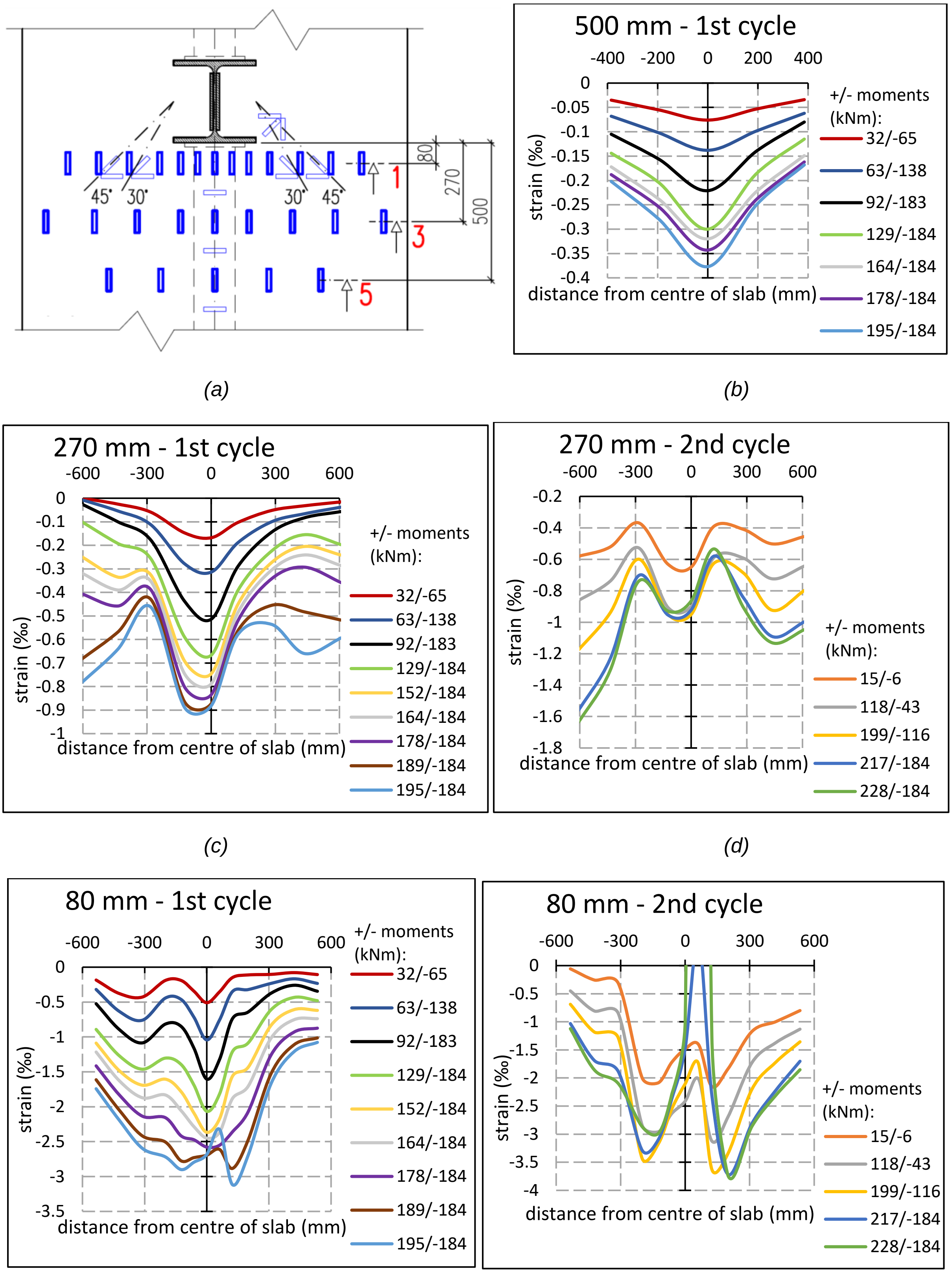

(a) *(b)*

(c) *(d)*

(e) *(f)*

Fig. 56. *The strain distribution in the upper surface of the concrete slab in different cross-sections in front of the face of the column in the sagging bending moment side during the first and second cycles.*

The DIC method was used to record the value of the principal strain and its direction at the point next to the column where the concrete strut from mechanism 2 acts, Fig. 57. The figures are from the second cycle of the experiment when the hogging moment was 184 kNm and the sagging moment was 215 kNm. The measured value of the minimum principal strain exceeded the ultimate compressive strain. The distribution of cracks, which were barely visually apparent after the experiment, can be seen in the maximum principal strain plot. The cameras were not placed perpendicular to the slab surface, but graphically it was estimated that the cracks in the concrete struts have an inclination of approximately 40 ° from the longitudinal axis of the concrete slab.

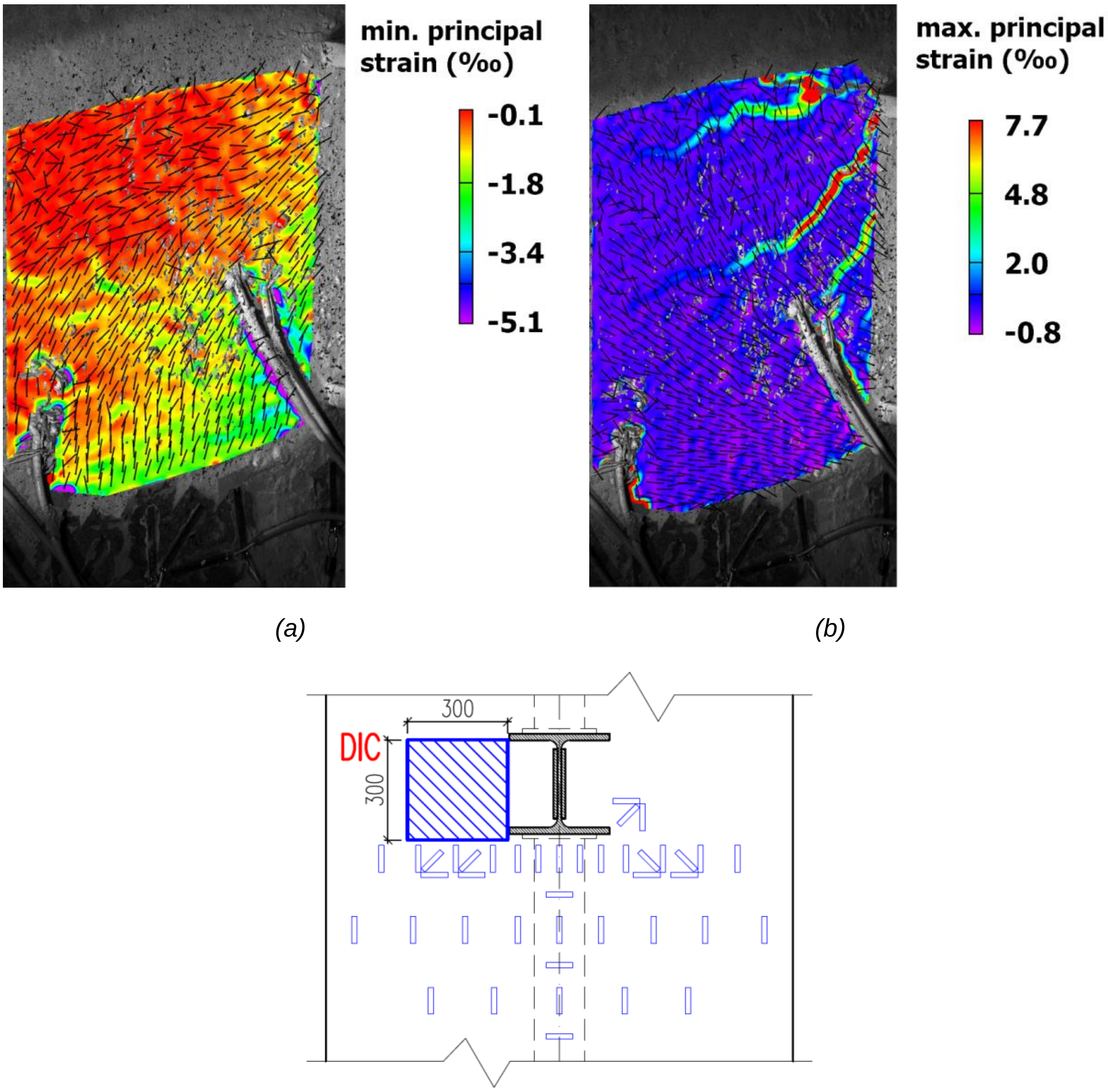

(a) *(b)*

(c)

Fig. 57. *Drawing of the minimum (a) and maximum (b) principal strain next to the column and its direction using the DIC method [39], investigated area of the concrete slab (c).*

3.4.2 The strain distribution in the steel reinforcement

The strain distribution of the longitudinal reinforcement at the connection on the hogging moment side is shown in Fig. 58. On the left side, there are higher values of strain again due to the previously described manufacturing imperfections of the specimen. At a constant moment of 184 kNm and increasing sagging bending moment, the reinforcement strain near the column increases, which may be due to the fact that the forces of mechanism 2 are transferred by the longitudinal reinforcement on the hogging moment side back to mechanism 1 on the sagging bending moment side.

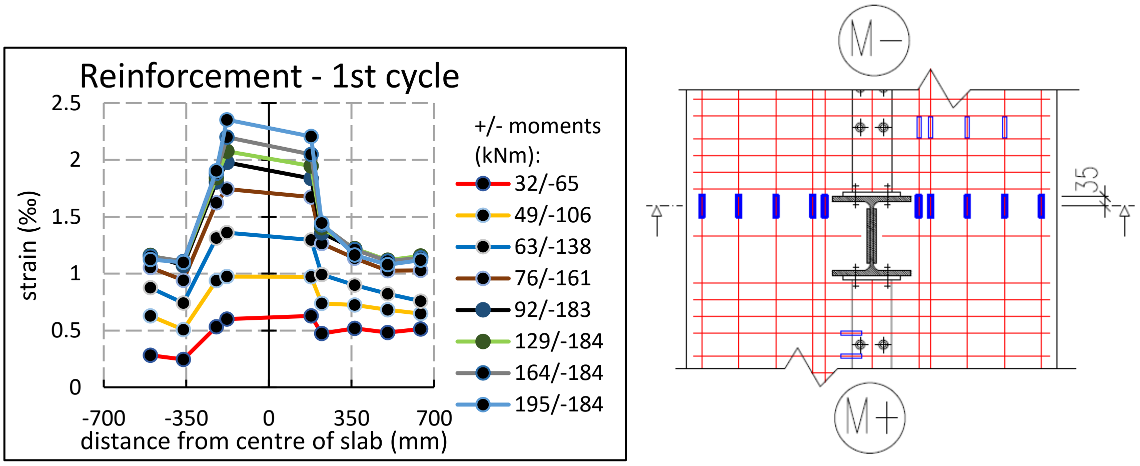

(a) (b)

Fig. 58. *Strain distribution in the steel reinforcement subjected to the hogging bending moment in the 1st cycle (a), investigated cross-section (b).*

4 Numerical study

A numerical nonlinear material model was developed in Atena Studio [40], version 5.6.1. Based on the experimental results, the model was validated. The Newton-Raphson method was chosen to solve the nonlinear system. A parametric study was developed to derive an analytical relationship for calculating the resistance and stiffness of the compressed concrete slab.

Atena is a finite element method-based program which is mainly used for nonlinear analysis of concrete reinforced structures. Atena uses the so-called GiD program (version 12.0.10) [41] as a pre-processor to model the structure, to specify boundary conditions, materials, etc.

4.1 Material model

4.1.1 Material model for SFRC

The CC3DnonLinCementious2User model was used, which is Atena's most sophisticated material model. It also allows the user to specify most of the material parameters in the general form [42]. Among other things, user-defined tensile and compressive functions can be entered. The *y*-value of the tensile and compressive function divided by the tensile and compressive strength of the concrete, respectively, is entered into the program. The value *x* represents the plastic deformation.

The localization strain ε_{loc} (i.e. the localization onset) is the strain after which the material usually softens. The constitutive law of stress and strain is valid up to the value of the localization strain. After the tensile localization strain $\varepsilon_{loc,t}$ is exceeded, tensile softening occurs and the stress is calculated based on the crack band approach [43]. Similarly, after exceeding the compressive localization strain $\varepsilon_{loc,c}$, concrete crushing occurs and the stress is calculated similarly [44]. Thus, once the localization strain is exceeded, the tension and compression functions valid for the characteristic length L_{ch} are adjusted to be valid for the actual length (L_t or L_c), which is determined by the geometry of the finite element used and the direction of the principal stress [45]. Fig. 59 [46] gives an example of a tensile function with the localization strain $\varepsilon_{loc,t}$ marked, where the tensile characteristic length $L_{ch,t}$ and the actual length L_t are given by the direction of the principal stress and the size of the mesh, σ is the tensile stress, f_t is the tensile strength of the concrete, and ε_1 is the maximum principal stress.

The user-defined properties of the CC3DnonLinCementious2User material model are as follows: tensile and compressive stress-strain law, tensile and compressive strength, characteristic size in tension and compression, localization onset in compression, Young's modulus, Poisson's ratio, aggregate size to activate aggregate interlock, fixed or rotated crack model, shear stiffness function, reduction in compressive strength due to cracking (lateral tension), Eccentricity parameter determining the shape of the failure surface Menetrey-Willam [47] for concrete crushing in triaxial compression, the direction of plastic flow, geometric nonlinearity (linear, nonlinear), idealization (plane strain, plane stress, 3D or axisymmetric).

4.1.1.1 SFRC material model for validation

The mechanical properties of the SFRC slab are shown in Table 3. The tensile strength was calculated from the splitting tensile strength according to [14].

From the results of three four-point bending tests with beams of dimensions 150 × 150 × 700 mm (Table 3; graph of force versus displacement in Fig. 40) the tension function was determined using the inverse analysis described in [42], Fig. 59. This procedure allows the tension function to be determined without uniaxial tensile tests, which are usually very complicated. First, a beam loaded with a four-point bending is modelled in Atena. Known material parameters are set into the program. The results of the load-displacement diagram are compared with the result of the experiment. If the diagrams are significantly different, the shape of the softening branch of the tension function is adjusted according to [42] and the calculation is performed again. This is done until the results are acceptable. The tensile characteristic size $L_{ch,t}$ is a material parameter and was chosen according to the size of the finite element mesh of the above calibration model loaded with four-point bending [42].

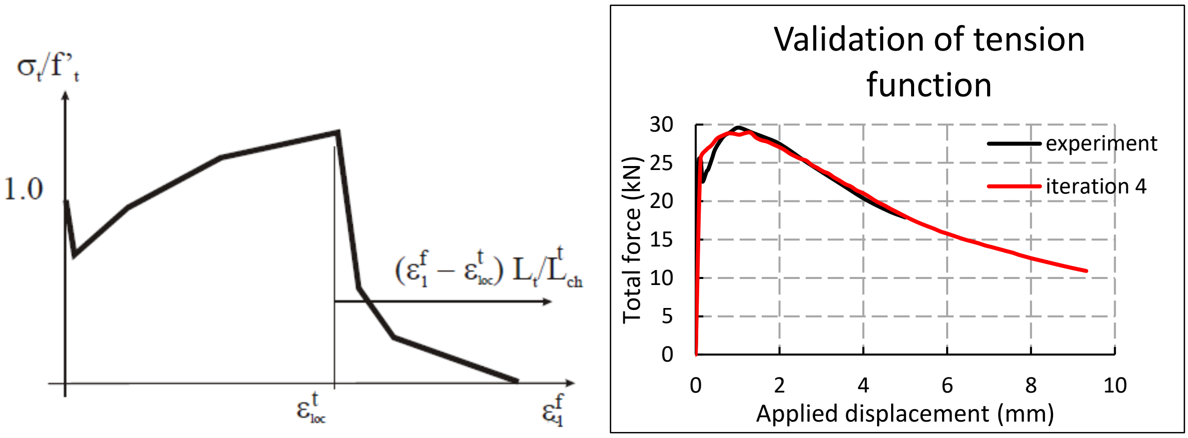

(a) *(b)*

Fig. 59. *Example of tension function [46] (a), load–displacement diagram of four-point bending test with SFRC beam (b).*

The maximum aggregate size used in the concrete was 16 mm and was entered into the program to activate the aggregate interlock.

The compressive function was determined using the procedure described in [38], Fig. 60. It depends mainly on the fibre volume fraction, fibre length, and fibre diameter. The compressive characteristic size was chosen to be 150 mm based on the usual diameter of the specimens in cylinder compressive strength tests. This is consistent with [48], which considers the minimum dimension of the calibration specimen as the localization limit.

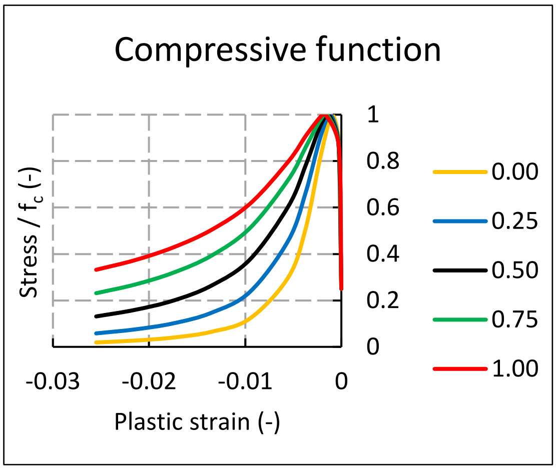

Fig. 60. *Compression function for different reinforcing index of fibres by volume $RI_{V.}$*

The so-called “fixed crack model” [49], [50] was chosen because the calculation was non-convergent when the “rotated crack model” [51], [52] was set up.

A shear stiffness function was considered according to [53] as a function of the steel reinforcement ratio, Fig. 61.

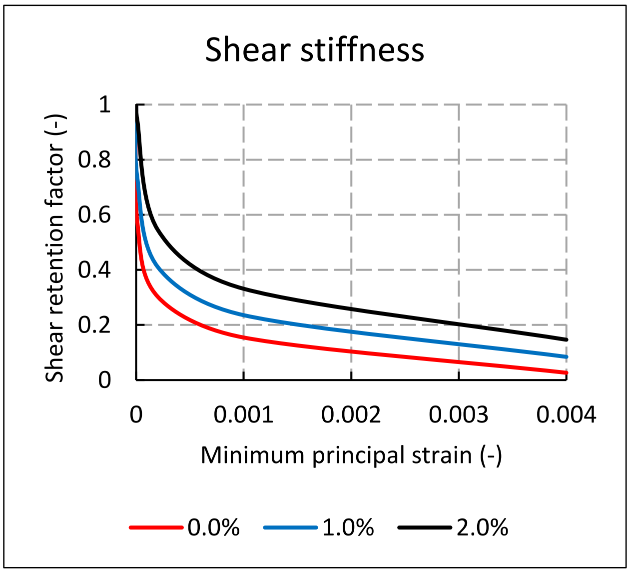

Fig. 61. *Shear stiffness function for different reinforcement ratios.*

A reduction of compressive strength due to cracking (lateral tension) was deactivated with the value of the function set to a constant of 1.0 as recommended based on the experience of the programme developers with fibre-reinforced concrete [42].

Atena uses the biaxial stress failure criterion according to [54].

An eccentricity parameter determines the shape of the Menetrey-Willam failure surface [47] for concrete crushing under triaxial stress. The shape of the surface is sharp-edged (0.5) or circular around the hydrostatic axis (1.0). The value of eccentricity can be determined depending on the ratio of the biaxial compressive strength to the compressive strength of the concrete according to [55]. The value of the biaxial compressive strength was determined using the procedure given in [56] and depends mainly on the fibre orientation factor (considered with 0.5), the length efficiency factor (considered with 0.5), the fibre volume fraction, the length and diameter of fibres, the compressive and tensile strength of the concrete. Since [55] only contains eccentricity values for the ratio of biaxial compressive strength to compressive strength up to a value of 1.2, for higher values of this ratio the eccentricity was determined by extrapolation.

A parameter “direction of plastic flow Beta” indicates the change in volume during concrete crushing. This parameter can significantly influence the development of the confinement effect [57]. A value of 0.5 was chosen to represent the expansivity. According to [57], a value of 0.5-0.9 usually gives the best results and a value of 0 tends to be conservative (no volume change). However, for a value greater than 0.5, the calculation took several times longer and the results did not differ much.

The function of the tensile strength reduction factor due to transverse compression was chosen to be linear according to [46], Fig. 62. Other types of function have a hyperbolic shape, but “type b” was non-convergent, and "type a" resulted in only slightly less resistance by 1 – 2 %.

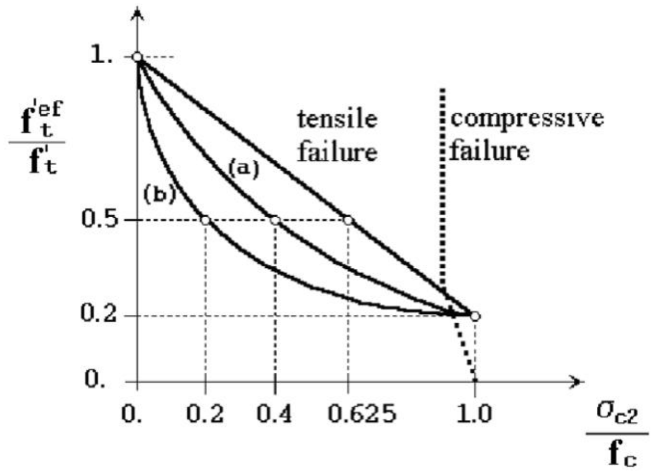

***Fig. 62.** The function of the tension strength reduction factor due the transversal compression [46].*

A parameter “geometric nonlinearity” was chosen to be “linear” (the geometric nonlinear effect is based on the shape of the deformed structure from the last step, not the last iteration) and the idealization was chosen to be 3D.

The other concrete parameters were left at their default values in Atena as they did not affect the final behaviour of the structure according to the sensitivity analysis.

4.1.1.2 SFRC material models for parametric study

Among other things, the material properties of the concrete slab were varied for the parametric study.

The compressive strength of concrete without fibres and the reinforcing index were chosen as the initial material value for the parametric study. The other material parameters of the concrete were calculated based on these two selected parameters. The reinforcing index of fibres by volume RI_v [38] is defined as $RI_v = V_f \,.\, L_f / d_f$, where V_f is the fibre volume fraction, L_f is the fibre length, and d_f is the fibre diameter.

The increase of concrete compressive strength depending on reinforcing index was calculated using the procedure described in [38].

The splitting tensile strength of fibre-reinforced concrete was calculated from the compressive strength of fibre-reinforced concrete using the procedure given in [58]. The tensile strength was further calculated from the splitting tensile strength according to [14].

Young's modulus of elasticity was calculated from the compressive strength of fibre-reinforced concrete using the formula given in [14] since this material parameter is negligibly affected by the addition of fibres according to [59].

The tensile function (Fig. 63) was determined by the so-called Simplified diverse embedment model (SDEM) procedure presented in [60] and also in [61], [62]. It takes into account the fibre mechanical anchorage and frictional bond. It depends mainly on the volume fraction of fibres, the length and diameter of fibres, the compressive and tensile strength of concrete, the fibre orientation factor (conservatively considered with a value of 0.5, which is valid for structures whose dimensions are much larger than the length of fibres [60]), and the distance between the end hooks of fibres. The tension function determined by an iterative procedure with the four-point bending loaded beam model in Atena (1 % fibre volume fraction, the reinforcing index of fibres by volume $RI_v = 0.5$) and calculated by SDEM are in good agreement with each other, Fig. 63. By varying the ratio of fibre length to diameter while keeping the fibre reinforcing index constant, the SDEM procedure provides a slightly different graph of the tensile function (as opposed to the compressive function). However, according to the sensitivity analysis, this does not at all affect the resistance and stiffness of the concrete slab in compression in the joint.

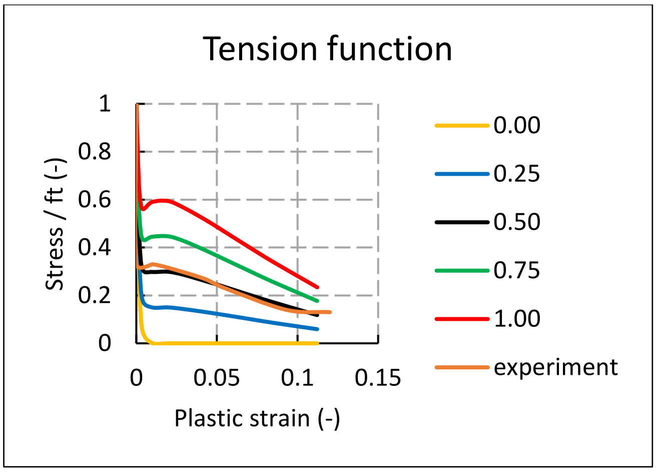

Fig. 63. *Tensile function (b) for different reinforcing index of fibres by volume RI_v (fibre length to diameter ratio is 50).*

For concrete without fibres, the reduction of compressive strength due to cracking (lateral tension) was determined according to [63], Fig. 64. Further described, e.g., in [64].

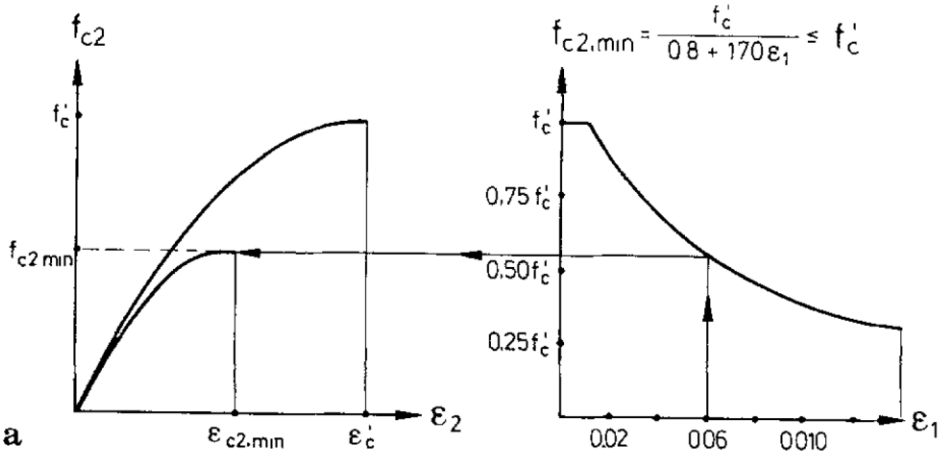

Fig. 64. *The reduction of compressive strength due to lateral tension strain [64].*

Other material parameters of the concrete were determined in the same way as described in the previous section 4.1.1.1.

4.1.2 Material model for reinforcement bars

The CCReinforcement material model was used. The reinforcement was modelled in discrete form as truss elements [46], not in a smeared form. Uniaxial stress is assumed. Based on the coupon test, a multilinear stress-strain diagram with a total of five branches was used, Fig. 65. The reinforcement was activated in both tension and compression.

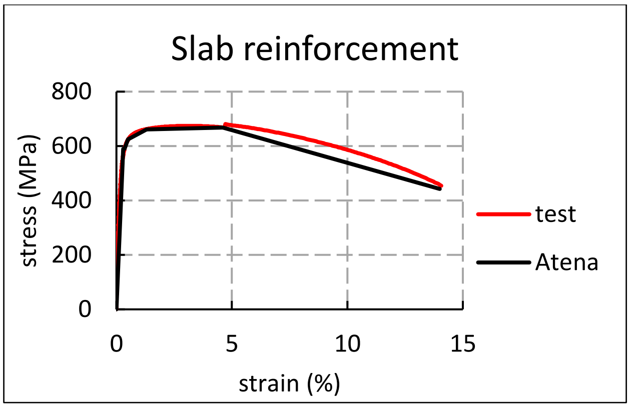

Fig. 65. *Coupon test on reinforcement bars and diagram set into the FEM program.*

The bond-slip law of the reinforcement was defined based on the CEB-FIP model code 1990 [65] (Fig. 66), no anchorage was considered at the ends of the reinforcement bars.

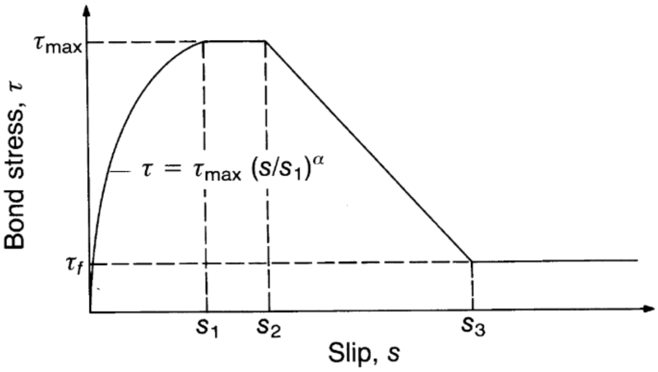

Fig. 66. *Bond-slip law according to CEB-FIP model code 1990 [65].*

4.1.3 Material model for steel members

ATENA is a program designed primarily for the nonlinear analysis of reinforced concrete structures [57]. Therefore, the material model for steel called CC3DBiLinearSteelVonMises uses the Von Mises plasticity condition with only the bilinear stress-strain law with hardening. The failure of an element can be determined by exceeding the ultimate strain value by the principal plastic strain, regardless of the stress. Thus, the bilinear stress-strain law with hardening was determined for the steel elements based on coupon tests and the hardening was determined conservatively based on the ultimate strain and ultimate strength determined by coupon tests, Fig. 67.

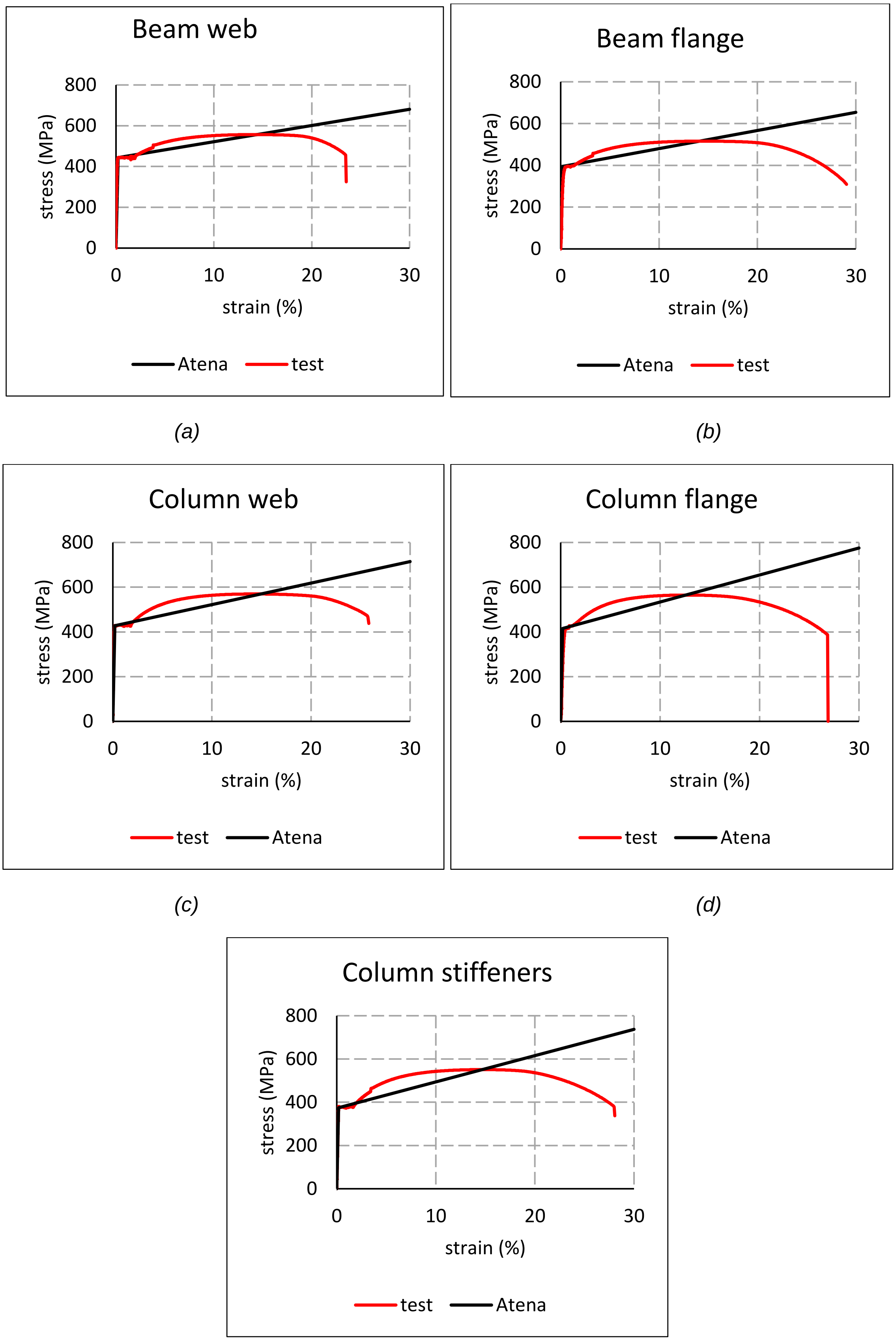

(a) *(b)*

(c) *(d)*

(e)

Fig. 67. *Coupon tests on steel joint components and diagrams set into FEM program.*

4.1.4 Material model for interface

The contact area between the concrete slab and the steel column was modelled using the so-called interface (material model CC3Dinterface). This requires specification of normal and tangential stiffness, cohesion (i.e. shear strength), friction coefficient, and tensile strength. The steel structure used in the experiment was not coated, so the friction coefficient was considered by a value of 0.4 in the model. To ensure numerical stability [57], the shear and cohesion strengths were set to non-zero values, namely 0.01 MPa and 0.02 MPa, respectively. The normal stiffness was considered as Young's modulus of elasticity of the concrete divided by the size of the adjacent finite element of the slab (9.32E+05 MN/m^3). The shear stiffness was calculated in a similar manner using the shear modulus. According to [57], the stiffness calculated in this way is the minimum stiffness of the interface. The maximum stiffness is then 1000 times this value, but the calculation did not converge when this value was set. The recommended value is 10 times this value, but the calculation took longer, required almost four times as many iterations, and the resulting resistance and compressive stiffness of the concrete slab were the same. Since this was a contact between surfaces with an incompatible finite element mesh, it was necessary to connect the contact volume to the adjacent surface from one side using Master and Slave conditions [57].

The interface was also modelled in the contact area between the top flange of the beams and the concrete slab. This interface simulates a shear connection using headed studs. Its tangential stiffness (0.325E+05 MN/m^3) was chosen so that the slip in the model matches the slip observed in the experiment. The normal stiffness was set to the same value. The cohesion, friction coefficient, and tensile strength were chosen high enough to avoid contact failure.

4.2 Validation of steel concrete composite joint model

The model corresponds to the tested joint with the same dimensions, cross-sectional dimensions, and reinforcement profiles, material properties determined by tests, the same method of support and loading, etc., Fig. 68. This model has been validated based on the experimental results.

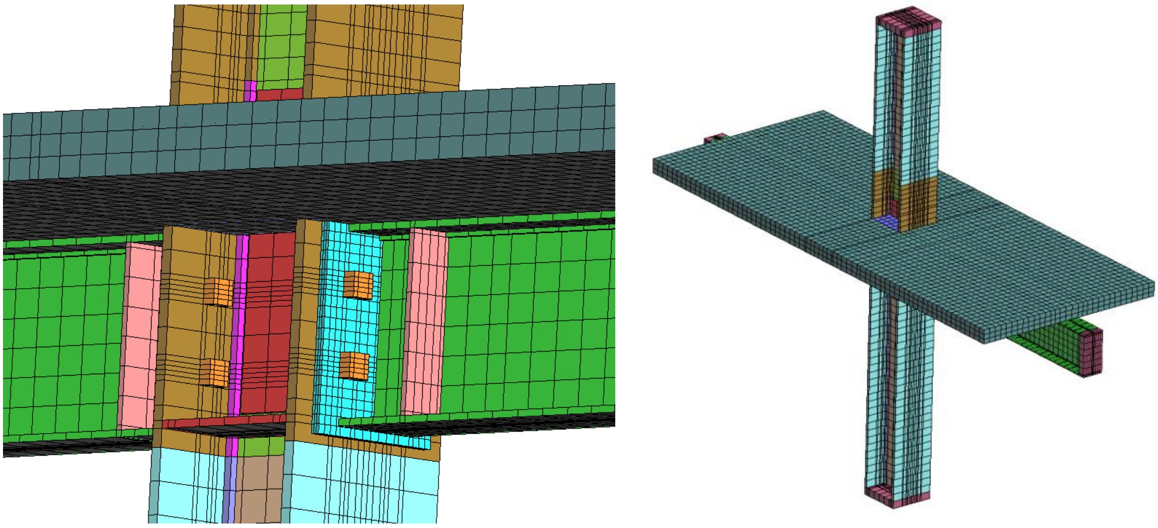

Fig. 68. *Model of steel-concrete composite joint validated by experiment [40].*

According to the sensitivity analysis, the self-weight of the structure had no significant effect on the behaviour of the model (bending moment-rotation of the joint diagram, strain distribution on the concrete slab, etc.) and was therefore neglected in the final model.

The load history was divided into several intervals in which the displacements were applied in sequential steps. In the first interval, the displacements were applied with smaller increments to obtain the initial stiffness of the joint. On the other hand, in the last interval, when the concrete slab and steel elements were plasticised, the displacements were applied with several times larger increments than in the first interval to save calculation time. The displacements were applied according to the actual load history used in the experiment.

The finite element mesh was created using so-called hexahedral elements. The mesh size was optimised to be from 33 to 50 mm for the concrete slab and from 5 to 30 mm for the steel elements.

4.2.1 End-plate and bolts

Detailed modelling of an end-plate concerning the actual bolt behaviour, including consideration of the prying effect, is quite complex and this research is not primarily focused on the bending behaviour of the end-plate. Atena is a software mainly designed for the nonlinear analysis of reinforced concrete structures. For these reasons, some simplifications were made in the modelling of the end-plate with the bolts.

The bolts and bolt heads were modelled with a square cross-section corresponding to the actual cross-section of the M27 bolts in the thread used in the experiment. This made it easier to create a finite element mesh using hexahedral elements. The bolt heads are rigidly connected to the face of the end-plate and the face of the column flange. However, the bolts are separated from the end-plate and column flange in holes.

In the case of a connection loaded with a sagging bending moment, there is free contact between the end-plate and the column flange and the prying effect of the bolts is neglected. For a connection loaded with a hogging moment, the column flange and end-plate are connected at the level of the bottom flange of the beam on an area corresponding to the area of the beam flange to transfer the compressive reaction from the bending. The connection is made on the so-called “master and slave” principle. Because the compressive reaction from the bending moment load is carried only by the bottom flange of the beam without the contribution of the beam web, the bottom flange in the joint area is therefore set with a higher yield strength of 600 MPa to avoid unrealistic plastification (according to coupon test, the column flange has a yield strength of 444 MPa). In the remaining area between this end-plate and the column flange, there is a free contact. Therefore, the prying effect is also neglected here.

The end-plate was validated based on the results of additional numerical analysis in Idea Statica [66], a program based on the Component-based Finite Element Method (CBFEM). For this beam-column joint with an end-plate, the program provides very accurate results. However, the disadvantage of this program is that it uses a stress-strain diagram for steel with only a bilinear curve without hardening. Therefore, hardening was not considered in the validation of the contact beam in Atena, but hardening is accounted for in the final model (the hardening of the end-plate steel is approximately the same as the hardening of the other elements determined by coupon tests). The assessment in Idea Statica was carried out without material partial factors.

The material parameters of the end-plate steel and the bolt head steel were chosen so that the behaviour of the Atena model of the steel contact member would match that of the Idea Statica model.

The hogging moment loaded connection was validated based on the hogging moment loaded joint model in Idea Statica, Fig. 69 and Fig. 70. In Idea Statica, the model was modelled for fine and coarse finite element mesh variants (10 mm and 38 mm). In both cases, the results were almost the same. The resulting material properties of the end-plate are on the hogging moment side: Young's modulus E = 125 000 MPa, yield strength f_y = 300 MPa, hardening modulus HM = 400 MPa. The material properties of the bolt heads are: Young's modulus E = 90 000 MPa, yield strength f_y = 100 MPa, hardening modulus HM = 0 MPa. The reduced material properties of the bolt heads compensate for the idealised model in Atena where the bolt head is rigidly connected to the end-plate.

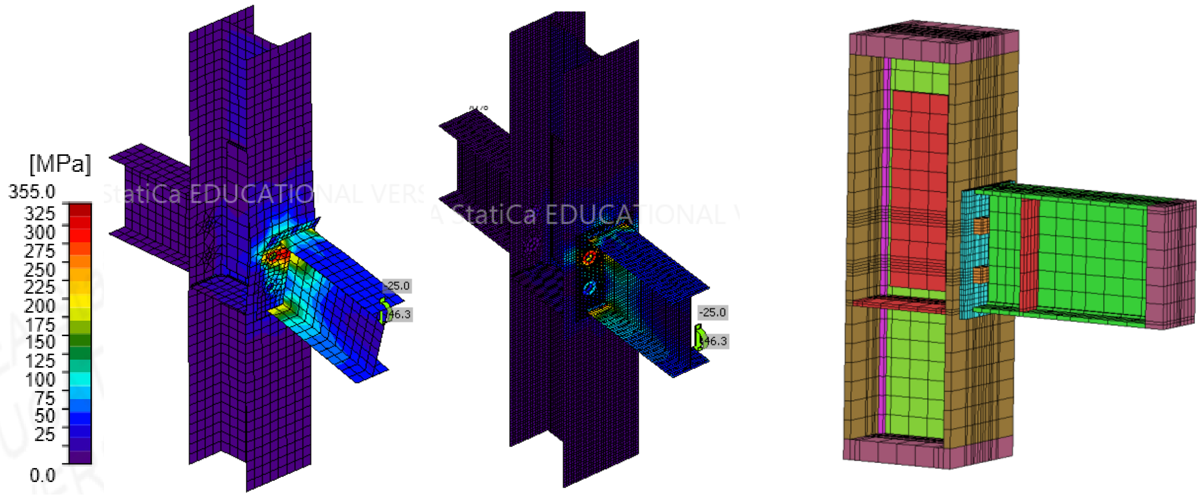

(a) (b) (c)

Fig. 69. *Steel joint loaded with hogging bending moment with coarse mesh (a) and fine mesh (b) in Idea Statica [66], Von Mises stress plotted. Model of a steel joint in Atena (c).*

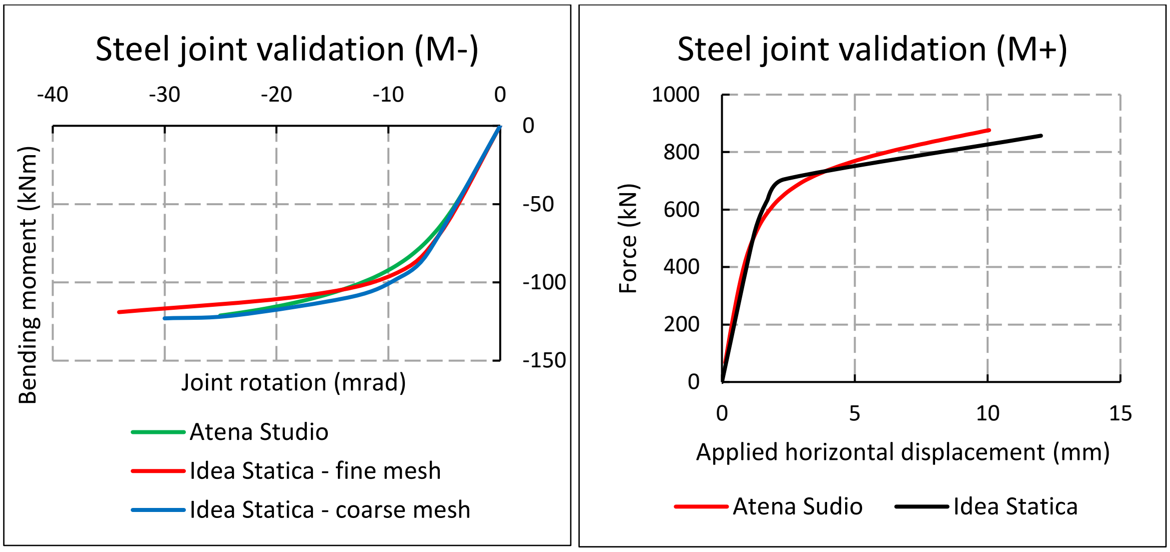

(a) (b)

Fig. 70. *Comparison of Atena results with Idea Statica results: bending moment-joint rotation diagram (a), force–applied displacement (b).*

For the connection loaded with a sagging moment, the position of the neutral axis in the experiment lay in the concrete slab according to the measured strain values on the strain gauge located on the top flange of the adjacent beam and strain gauges on the bottom surface of the slab. Thus, this connection was validated according to the Idea Statica model of a steel joint loaded with a normal force, Fig. 70 (the finite element mesh was 38 mm). The resulting material properties of the end-plate are on the sagging moment side: Young's modulus

E = 90 000 MPa, yield strength f_y = 275 MPa, hardening modulus HM = 400 MPa. The material properties of the bolt heads are the same as for the hogging moment loaded connection.

The initial stiffness and resistance of the models in Idea Statica and Atena are in good agreement with each other.

4.2.2 Concrete slab

The concrete slab was modelled using three finite element mesh elements along its thickness to well represent the actual bending behaviour. The thickness of the slab was 100 mm. The maximum aggregate size is the minimum mesh size of the finite element mesh to maintain the assumption of a heterogeneous material with smeared properties, as recommended by the Atena developers. The maximum aggregate size of the concrete used in the experiment was 16 mm. However, in [67], a minimum finite element mesh size of 40 mm is also given. On the other hand, to obtain realistic results for a bent structure, 4 to 6 elements of mesh along the height of the structure are recommended [68]. However, this is a composite concrete slab with a steel beam, so the slab is not fully bent as it is rather compressed or tensioned. Therefore, the choice of 33 mm element thickness along the height of the slab is a good compromise to maintain the assumption of heterogeneous material while obtaining a realistic bending behaviour of the concrete slab. In addition, computation time was saved and, according to the sensitivity analysis, refining the mesh changed the resulting joint moment-rotation behaviour negligibly.

The reinforcement bars were modelled as 1D (truss) elements.

The shear stiffness of the concrete slab was considered according to [53] with a reinforcement ratio of 1.5 % steel rebars. In the part of the concrete slab between the column flanges, a reinforcement ratio of 0.5 % was considered because there is only one reinforcement bar.

A longitudinal shear connection was created between the concrete slab and the top flange of the beam using an interface. Since the flange of the beam and the concrete slab have different finite element meshes, the interface was connected to the beam using a Master and Slave condition according to [68].

The connection between the concrete slab and the column was made using an interface. The column flange transferring the forces from the concrete slab by mechanism 1 was also connected to the concrete slab on the backside to prevent unrealistic deformation of the flanges by mechanism 1. No connection was made between the column flange and the slab at the connection loaded by the hogging bending moment, no connection was made even along the thickness of the column flanges. Because the column and the concrete slab have different finite element meshes, the Master and Slave conditions according to [68] were applied on one side of the interface.

4.2.3 Other steel elements and supports

Supporting plates were placed in the column supports and the loading plates were placed at the points of applied loads. These plates were made of elastic material (material model CC3DelastIsotropic, Young's modulus E = 210 000 MPa). Displacements were applied to the loading plates at the ends of the beams at 2 points. The loading plates were provided with supports to prevent the ends of the cantilevers from moving out of the plane of the frame (e.g. due to slight asymmetry in the finite element mesh). The outer surfaces (i.e. each node of the finite element mesh of these surfaces) of the supporting plates at the ends of the column were prevented from shifting in the transverse and vertical directions. In the longitudinal direction, displacements corresponding to the displacement of the column supports during the experiment were prescribed to them (another option was to set spring supports in the longitudinal direction). In this way, Sliding rigid column supports were created not to allow rotation and displacement in two directions but to allow the simulation of pushing of the supports in the longitudinal direction.

A fully rigid connection was created between the transverse stiffeners and the steel elements. The supplementary web plates were connected to the column web by joining the outer lines of the stiffeners to the adjacent lines of the column web. This simulated a fillet weld. However, the supplementary web plates were also connected to the column at the level of the concrete slab using connected surfaces to transfer the horizontal forces from mechanism 2 to the column. This prevents overloading of the supplementary web plates in bending due to these forces from the concrete slab acting on the column. This is consistent with [30], where the column web plate in shear is assumed to be infinitely rigid at the concrete slab level.

The root radii of the rolled sections between the flanges and the webs were simplistically modelled as square sections while maintaining the cross-sectional area of the original root radii, which simplifies the use of hexagonal mesh elements.

4.2.4 Comparison results of FEM to experiment

Monitors were placed in the model to investigate the behaviour of the structure under load. The following values were recorded: applied vertical displacements, reactions from applied displacements, longitudinal strain distribution in 3 sections of the concrete slab at the locations of the strain gauges during the experiment, 5 horizontal displacement monitors on both beams on the end-plate connection to detect the rotation of the connections, 2 horizontal displacement monitors on the column web above the concrete slab level and 2 below the concrete slab to evaluate column rotation, 2 horizontal displacement monitors on the column web panel to evaluate the rotation of the column web panel, principal stress monitors along the slab thickness to evaluate the minimum principal stress and its direction from mechanism 2 (the investigated section is shown in Fig. 82), longitudinal stress monitors at the interface between the column flange and the concrete slab to evaluate the force in mechanism 1, horizontal displacement monitors to determine the slip between the concrete slab and the beam at the end of the beams, and horizontal displacement monitors at the column supports.

Observed values from the numerical analysis are compared with the experimental results in the following graphs. Fig. 71 shows a graph of the force versus applied vertical displacement and sagging-hogging bending moment diagram. Fig. 72 shows a graph of the dependence of the bending moment on the joint rotation measured by the displacement sensors and inclinometers. All these graphs are compared with the results of the numerical analysis in Atena. On these graphs, the behaviour of the numerical model corresponds well to the behaviour of the tested steel-concrete joint.

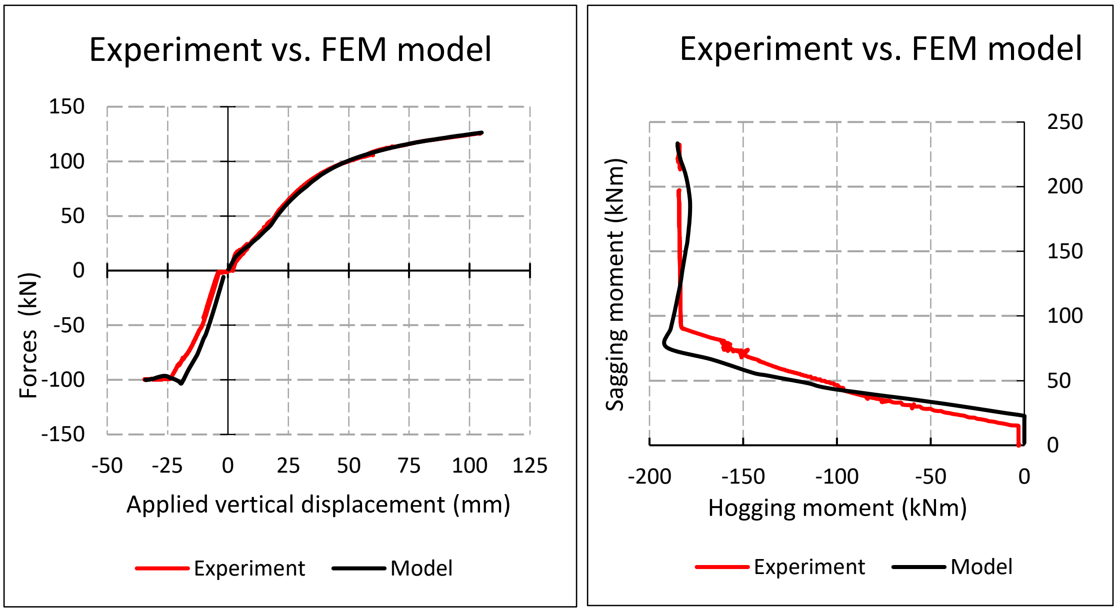

(a) *(b)*

Fig. 71. *Force-applied vertical displacement diagram (a), sagging-hogging bending moment diagram (b).*

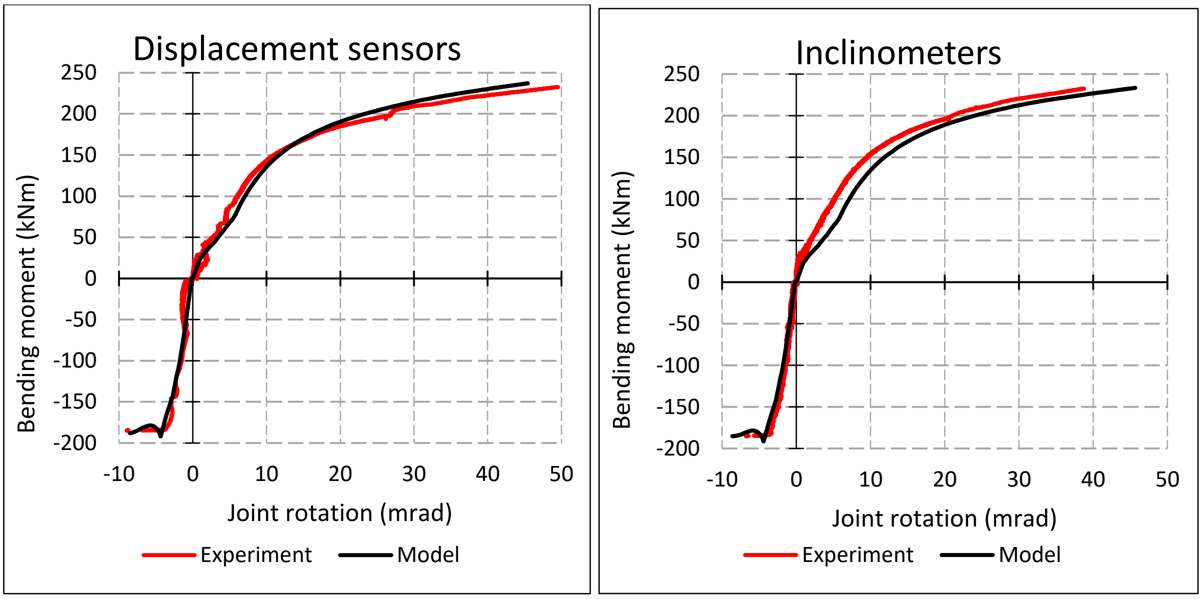

(a) *(b)*

Fig. 72. *The bending moment - joint rotation diagram measured by the displacement sensors (a) and inclinometers (b).*

The strain distribution on the top surface of the concrete slab in different cross-sections was compared with the results of the numerical analysis in Fig. 73. A better agreement in the 80 mm and 270 mm cross-sections was obtained for the concrete slab with a fine mesh (10 elements along the thickness) than with the coarse mesh (3 elements along the thickness), which was used in all other model and experimental comparisons. The fine mesh seems to better account for the triangular shape of the strain distribution along the thickness of the concrete slab (the neutral axis was inside the concrete slab during the experiment). However, the minimum finite element thickness is equal to the maximum aggregate size in the concrete of 16 mm (to maintain the assumption of a heterogeneous material with smeared properties, as recommended by the Atena developers), which is larger than that of the fine mesh model. Thus, the finer mesh slab model is used here only to illustrate the reason for the difference in strain distribution between the experiment and the finite element analysis and was not used in the other comparisons (where it also did not differ at all from the coarse mesh model).

In the section 80 mm away from the column, the strain gauge failed in the middle of the section during the experiment. Due to the crushing of the concrete in the area between the column and the strain gauges in the 80 mm section, the strain in the other strain gauges decreased. In the numerical analysis, this failure of the slab resulted in a high strain.

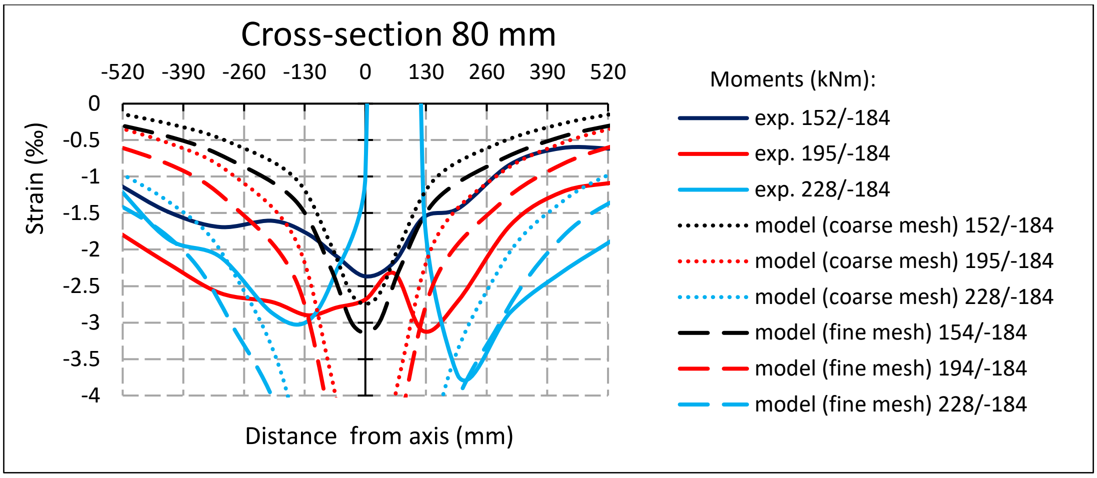

(a)

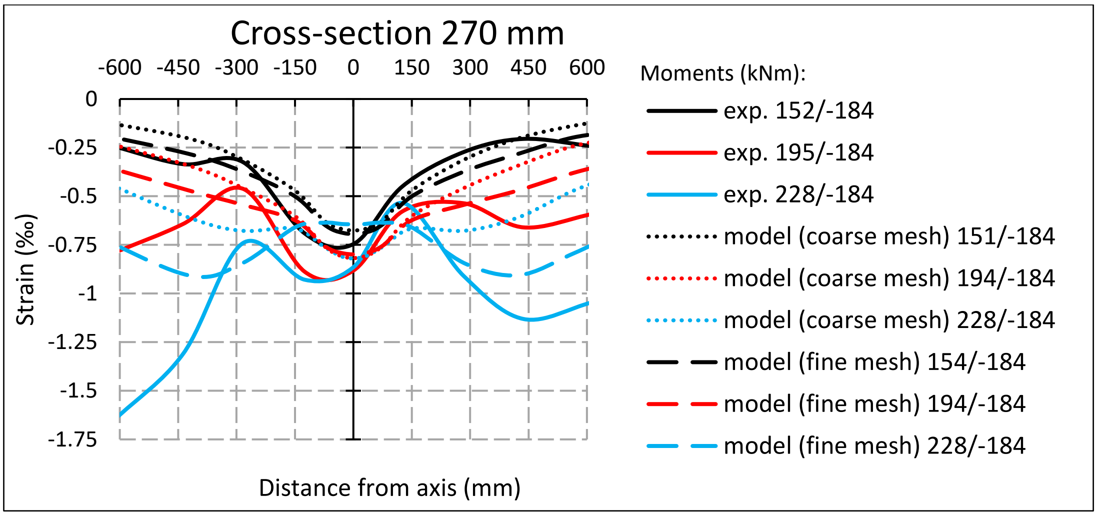

(b)

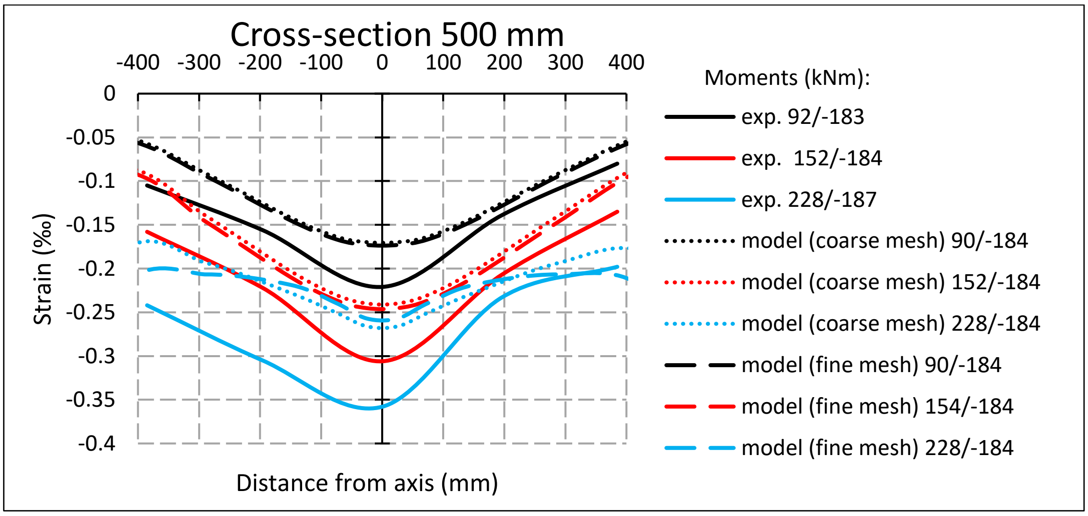

(c)

Fig. 73. *Strain distribution on the concrete slab top surface with coarse and fine mesh in cross-sections of 80 mm (a), 270 mm (b), and 500 mm (c) from the column.*

The other values measured in the experiment were compared with the results of the numerical analysis (e.g. reinforcement strain, the strain of steel elements) at critical loading phases and show acceptable agreement.

Fig. 74 shows the dependence of the slip (between the concrete slab and steel beam) on the bending moment. The stiffness of the interface simulating the longitudinal shear connection was chosen so that the slip on the sagging moment side corresponds to the slip value in the experiment, see Section 4.1.4. Fig. 74 also shows a graph of the moment versus the column web panel rotation, comparing the experimental results with the numerical model results.

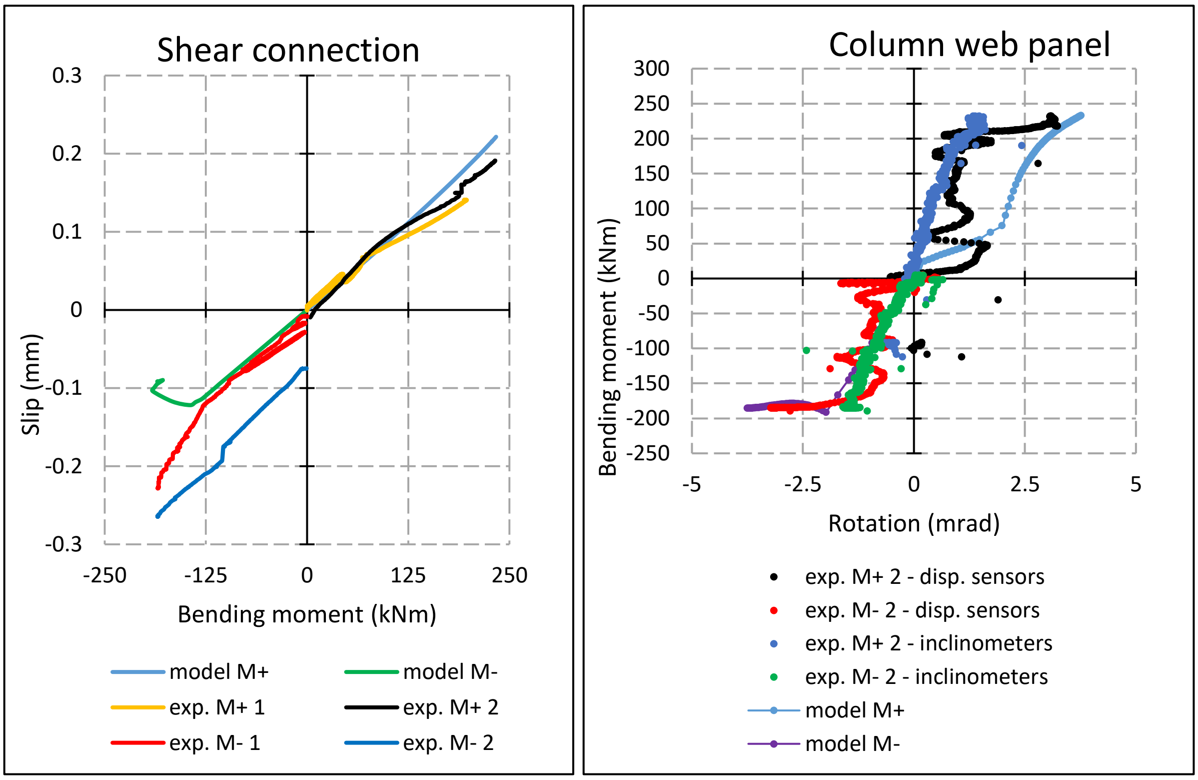

(a) *(b)*

Fig. 74. *Slip–bending moment diagram (a), the graph of the moment versus column web panel rotation during 2nd cycle (b).*

Demonstration of the model is shown in Fig. 75.

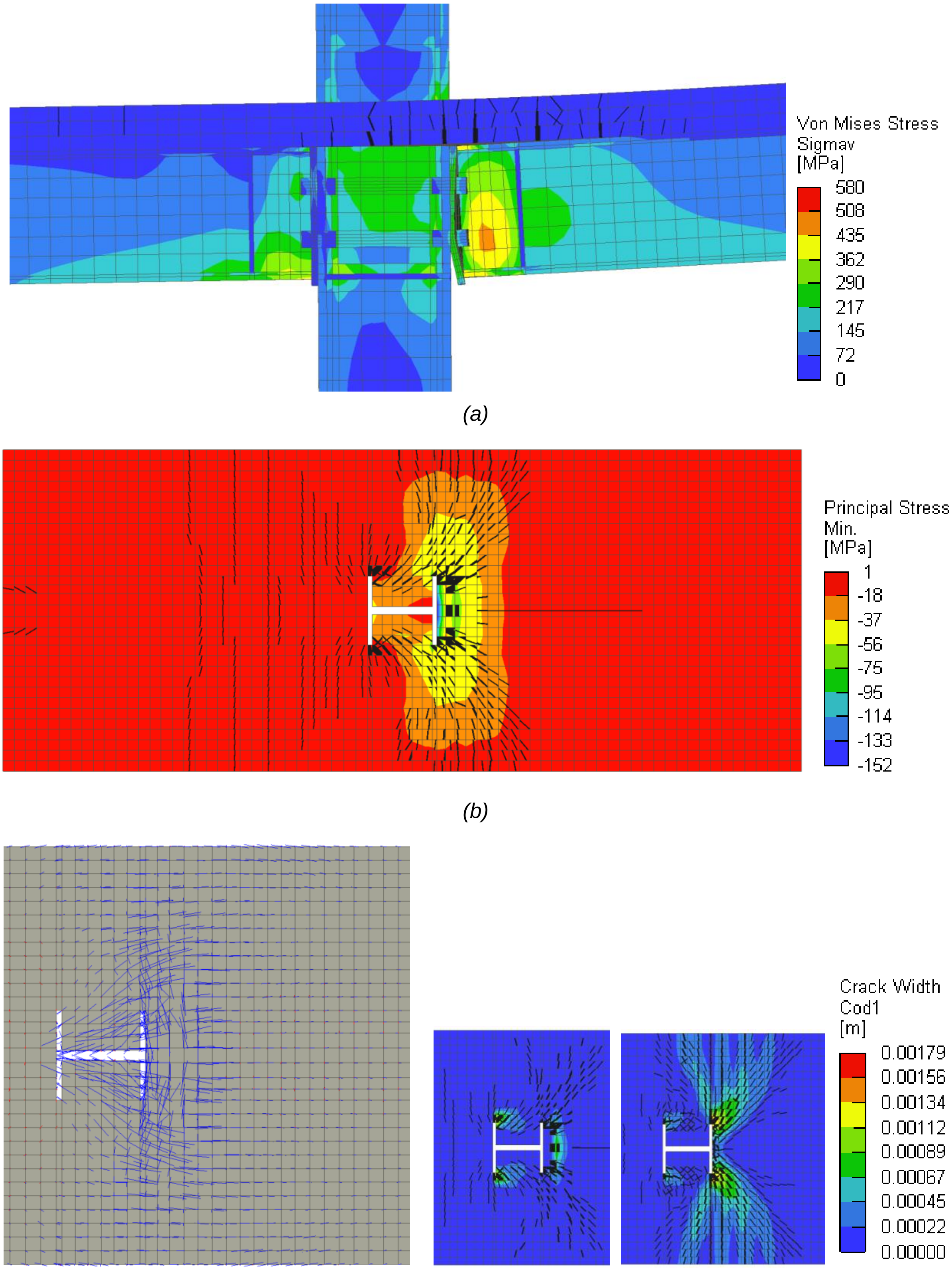

(a)

(b)

(c) (d) (e)

Fig. 75. *Model results in the last numerical analysis step: Von Mises stress on the steel components of the joint (a), the minimum principal stress and crack distribution (with a minimum width of 0.03 mm) on the top surface of the slab (b), the direction of the principal stress on part of the top surface of the slab (c), and crack width on the top (d) and bottom (e) concrete slab surfaces.*

The direction of the principal stress under the action of mechanism 2 was approximately 35 ° in Atena when the resistance was reached for the tested model of the bent steel-concrete composite joint, Fig. 76. This angle was determined as the weighted arithmetic mean of the angles of the individual mesh nodes in this section. This corresponds reasonably well with the experimental results, where the DIC method was used to estimate that the cracks in the concrete struts have an inclination of approximately 40 ° from the longitudinal axis of the slab, Fig. 57.

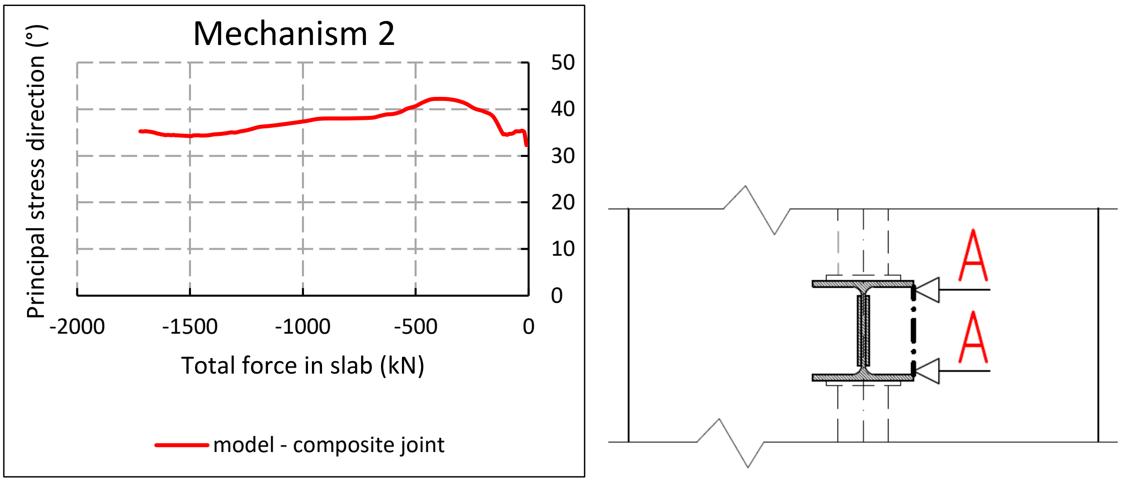

(a) *(b)*

Fig. 76. *Average principal stress direction - composite joint used in validation (a), investigated concrete slab section (b).*

4.3 Parametric study

Based on a preliminary analysis, dimensions of the structure and material properties of the steel-concrete joint components were chosen for the parametric study.

4.3.1 Model and sensitivity analysis

For the parametric study, a simplified model of a concrete slab in compression supported by a steel column was created, Fig. 77. These simplified models were loaded up to a failure of the slab to verify its resistance. The use of simplified models significantly saved computational time, and modelling time and enabled reliable determination of both the compressive resistance of the concrete slab and its stiffness.

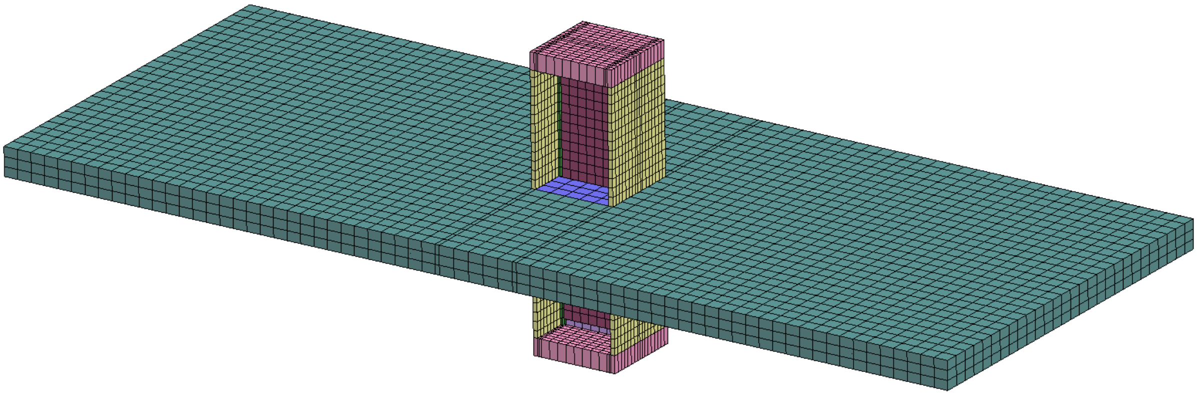

Fig. 77. *Simplified model of a compressed concrete slab supported by a column used in the parametric study.*

The displacement was introduced to one side of the slab, creating compressive stress in the concrete slab. Specifically, the displacement was applied on the one front face of the slab (Fig. 78) at each node of the finite element mesh of this surface. The model was supported only at the upper and lower ends of the column. There was two point pin supports on each of the support plates to prevent movement in all directions, Fig. 79. This allowed rotation in the plane of the original frame but prevented torsional rotation of the column in the case of finite element mesh asymmetry. The column was therefore supported by hinged supports and acted as a simple beam loaded in the middle of the span by a point load. This point support of the column allowed simple recording of the reactions.

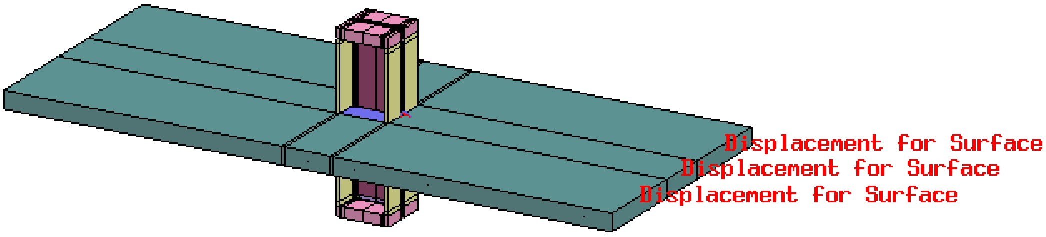

Fig. 78. *Applied displacement on the face of the slab.*

The finite element mesh was again created using hexahedral elements. A mesh size was generally chosen to be 50 mm for the concrete slab (range 16 to 75 mm, maximum aggregate size was 16 mm) and 10 to 50 mm for the steel elements. The concrete slab in front of the column was divided horizontally into a minimum of 6 mesh elements. The elements in bending should be divided into a minimum of 4 to 6 mesh elements to capture the bending behaviour [68].

Transverse and longitudinal reinforcement was modelled in the centre of gravity of the concrete slab. This avoided the additional bending moment caused by an eccentricity and the associated flexural deformation of the concrete slab. The intersecting transverse and longitudinal reinforcement were not connected at the intersection points. The reinforcement transferred both tensile and compressive forces.

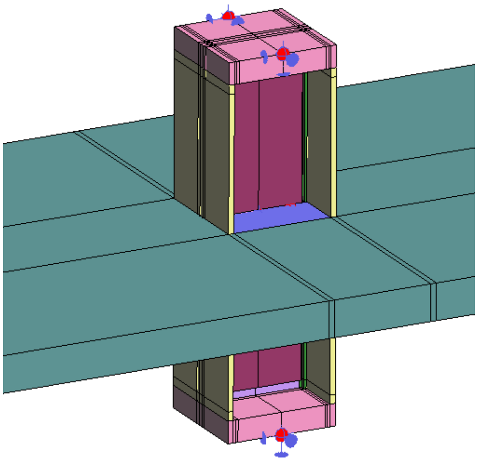

Fig. 79. Pin column supports

The height of the column was chosen to be approximate twice the height of the column profile.

In the parametric study, the supplementary web plates of the column were extended to the supporting plates. The supplementary web plates did not affect the resistance of the concrete slab at all.

The transverse reinforcement in the joint region was determined based on the minimum reinforcement requirements for the transmission of transverse tensile forces from mechanism 1 and mechanism 2 according to EN 1998-1 [3], Annex C. In other parts of the slab, the reinforcement was 14 mm in diameter, spaced at a distance equal to three times the slab thickness, which met the maximum spacing requirements for transverse reinforcement in EN 1992-1-1 [14].

The length of the concrete slab in the longitudinal direction was chosen based on the height of the column profile and the width of the slab. The distance between the face of the column flange and the face of the slab was the sum of the slab width and 200 mm.

Longitudinal reinforcement with a diameter of 14 mm was chosen at an axial distance of 200 mm (maximum axial distance for 200 mm thick slabs according to EN 1992-1-1 [14]). According to the sensitivity analysis, the longitudinal reinforcement did not affect the resulting compressive resistance of the concrete slab (Fig. 80), i.e. neither did the longitudinal reinforcement placed in front of the column flange.

The displacement of the component (Fig. 80, Fig. 81) was calculated as the difference between the horizontal displacement of the centre of the concrete slab in front of the column flange and the displacement of the concrete slab at its edge, which was no longer affected by the deformation of the component.

The amount of transverse reinforcement in front of the column also has a negligible effect on the compressive resistance of the slab, with a four times increase in the area of transverse reinforcement increasing the resistance of the slab by only 4 % compared to the resistance of the slab using the minimum transverse reinforcement according to EC8 [3], Fig. 80. However, the minimum reinforcement requirements must be met.

The width of the concrete slab was chosen to meet the geometric requirements for the formation of the strut and tie mechanism according to EN 1998-1 [3], Annex C. The larger concrete slab width did not increase the resistance of the slab according to the results of the sensitivity analysis, Fig. 80.

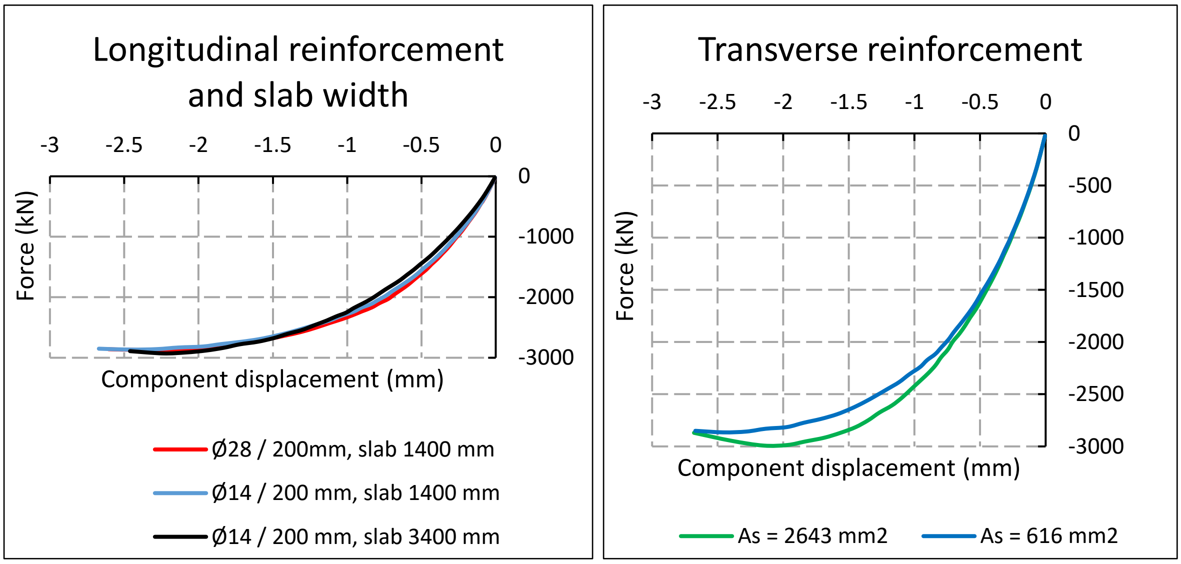

(a) *(b)*

Fig. 80. *Sensitivity analysis - longitudinal reinforcement of concrete slab and concrete slab width (a), transverse reinforcement in front of the column up to the column cross-section height (b).*

According to the sensitivity analysis, the combination of compressive stresses on one side (loads normally due to sagging bending moment) and tensile stresses (loads normally due to hogging bending moment) on the other side did not affect the resulting load resistance of the slab. Similarly, if only tension-inducing displacements were introduced into the slab, they affected the resulting slab resistance only negligibly, Fig. 81 (of course, the concrete slab had to be heavily reinforced with longitudinal reinforcement, so the resistance was determined by the concrete slab in compression at the column, not by the concrete slab cross-section in tension).

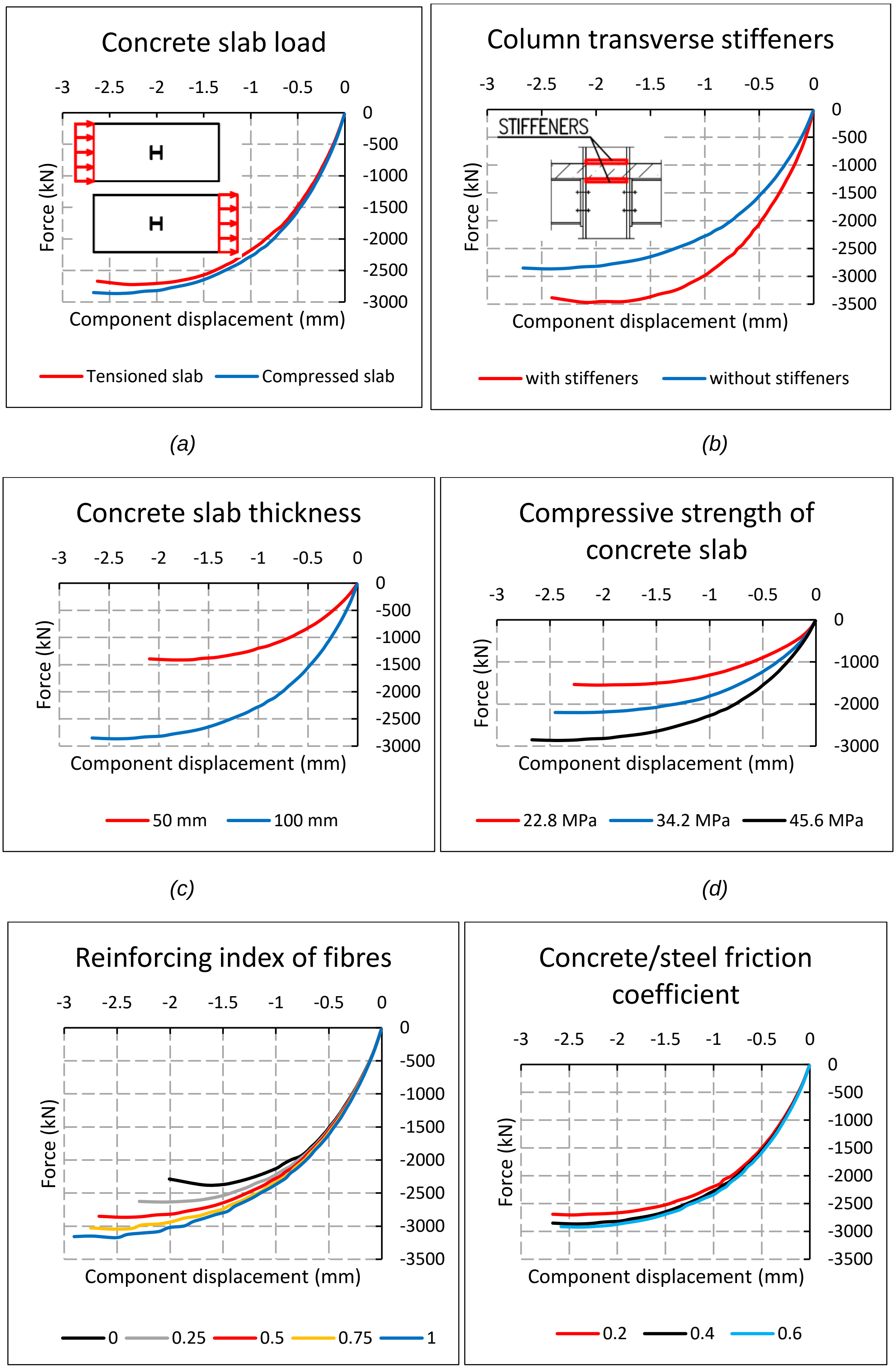

(a) *(b)*

(c) *(d)*

(e) *(f)*

Fig. 81. Sensitivity analysis.

If the column is provided with transverse stiffeners at the level of the top and bottom surface of the slab, the compressive resistance of the concrete slab significantly increases. It can therefore be assumed that the flexibility of the column flanges has a significant effect on the compressive resistance of the concrete slab, Fig. 81.

According to the sensitivity analysis, the variables affecting the resistance are mainly: column cross-section height h_c, column cross-section width b_c, concrete slab thickness d, concrete slab compressive strength f_c, reinforcing index of fibres by volume RI_v, and the concrete/steel friction coefficient μ.

On the other hand, the following parameters are not important for the resistance and stiffness: the way of loading (bending sagging moment or bending hogging moment and their combination), the amount of transverse and longitudinal rebars of the concrete slab (however, the minimum reinforcement requirements according to EN 1992-1-1 [14] and EN 1998-1 [3] must be met), and the width of the slab (however, the geometric requirements for the formation of the strut and tie mechanism according to EN 1998-1 [3] must be met).

In the simplified model of the compressed concrete slab, the direction of the principal stress in concrete struts under the action of mechanism 2 differed slightly from that in the full steel-concrete composite joint, Fig. 82. The maximum difference was approximately 5 °.

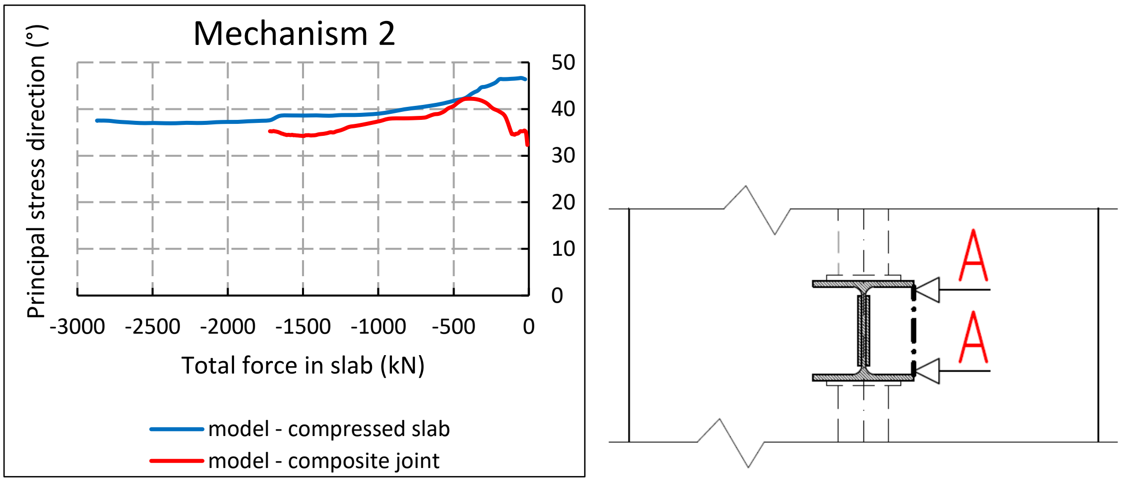

(a) *(b)*

Fig. 82. *Average principal stress direction - simplified compressed model used in parametric study vs. composite joint used in validation (a), investigated concrete slab section (b).*

4.3.2 Performing parametric study

Based on the sensitivity analysis, a parametric study was performed. The models differed in the parameters presented in section 4.3.1. These parameters are listed in Table 5 and Table 6 (n is the numerical designation of the model, E_c is the modulus of elasticity of the SFRC, t_f is the thickness of the column flange, and t_w is the thickness of the column web). The reference model corresponds in its geometry and basic material parameters to the experimental specimen (n is equal to 1). In other models (n is 2 to 51), these geometric and material parameters were varied for the parametric study.

Table 5. *Range of properties of FEM models.*

	RI_v	f_c	E_c	d	b_c	h_c	t_f	t_w	μ	t_f / (0.5b_c)
value	(-)	(MPa)	(MPa)	(mm)	(mm)	(mm)	(mm)	(mm)	(-)	(-)
max.	1.0	90	42700	200	600	1000	60	66	0.6	0.253
min.	0.0	20	27090	50	100	100	6	4	0.2	0.100

The results of the parametric study are presented in Table 6. The resistance has been determined as the maximum value of the transferred force and it is marked $F_{R,FEM}$. The initial stiffness factor $s_{ini,FEM}$ corresponds to reaching the level of 2/3 of the resistance and it was determined from the force-displacement ratio of the component. To obtain values in millimetres, this ratio is further divided by the modulus of elasticity of the steel according to EN 1993-1-8 [10]. In addition, the coefficient of secant stiffness corresponding to the resistance was determined, which is referred to as $s_{res,FEM}$.

Table 6. *Parametric study - specification of FEM models and their main results.*

n	RI_v	f_c	E_c	d	b_c	h_c	t_f	t_w	μ	$F_{R,FEM}$	$s_{ini,FEM}$	$s_{res,FEM}$
	(-)	(MPa)	(MPa)	(mm)	(mm)	(mm)	(mm)	(mm)	(-)	(kN)	(mm)	(mm)
1	0.5	44.4	34680	100	300	300	19	11	0.4	2865	13.0	5.55
2	0	44.4	34410	100	300	300	19	11	0.4	2376	14.1	6.70
3	0.25	44.4	34550	100	300	300	19	11	0.4	2635	13.5	6.03
4	0.75	44.4	34820	100	300	300	19	11	0.4	3043	12.8	5.71
5	1	44.4	34950	100	300	300	19	11	0.4	3174	12.7	6.02
6	0.5	21.6	28170	100	300	300	19	11	0.4	1551	7.73	3.57
7	0.5	33.0	31810	100	300	300	19	11	0.4	2203	10.4	4.63
8	0.5	44.4	34680	100	300	300	19	11	0.2	2704	12.7	5.22
9	0.5	44.4	34680	100	300	300	19	11	0.6	2922	13.2	5.85
10	0.5	58.0	37510	100	300	300	19	11	0.4	3553	15.4	6.58
11	0.5	44.4	34680	50	300	300	19	11	0.4	1413	7.29	2.96
12	0.5	58.0	37510	50	300	300	19	11	0.4	1771	8.47	4.24
13	0.5	44.4	34680	100	300	0	19	11	0.4	1800	8.24	3.53
14	0.5	44.4	34680	100	300	450	26	11	0.4	3663	14.7	6.10
15	0.5	58.0	37510	100	300	450	26	11	0.4	4530	17.7	8.02
16	0	20.0	27090	100	300	450	26	11	0.4	1524	9.05	5.29

Table 6. *(Continued).*

n	RI_v (-)	f_c (MPa)	E_c (MPa)	d (mm)	b_c (mm)	h_c (mm)	t_f (mm)	t_w (mm)	μ (-)	$F_{R,FEM}$ (kN)	$s_{ini,FEM}$ (mm)	$s_{res,\ FEM}$ (mm)
17	0.25	44.4	34550	100	300	450	26	11	0.2	3221	14.6	5.09
18	0.5	44.4	34680	100	300	600	30	11	0.4	4254	15.5	6.49
19	0.5	44.4	34680	200	300	600	30	11	0.4	8849	30.7	13.5
20	0	20.0	27090	100	300	600	30	11	0.4	1701	9.91	6.19
21	0.5	44.4	34680	100	300	1000	36	11	0.4	4774	17.6	7.84
22	0.5	58.0	37510	100	300	1000	36	11	0.4	5951	20.6	8.71
23	0.5	44.4	34680	50	100	100	10	3.7	0.4	668	5.42	2.39
24	0.5	44.4	34680	50	100	100	10	3.7	0.2	626	5.45	2.11
25	0.5	21.6	28170	50	100	100	10	3.7	0.4	369	3.47	1.57
26	0	20.0	27090	50	100	100	10	3.7	0.2	259	3.42	1.92
27	0.5	44.4	34680	100	300	100	19	11	0.4	2289	13.3	5.90
28	0	20.0	27090	100	300	100	19	11	0.2	875	8.43	4.99
29	0.5	44.4	34680	50	120	120	6	4.4	0.4	631	5.16	2.25
30	0.5	44.4	34680	100	240	240	12	8.8	0.4	2269	11.6	4.89
31	1	44.4	34950	100	240	240	12	8.8	0.4	2521	11.2	4.73
32	0.5	44.4	34680	100	240	480	24	8.8	0.4	3496	14.4	6.13
33	0.75	28.2	30590	70	192	360	18	7	0.5	1476	7.01	3.51
34	0.5	44.4	34680	100	150	300	19	11	0.4	2589	13.3	6.09
35	0.5	44.4	34680	100	150	300	8	11	0.4	1971	11.5	4.01
36	0.5	44.4	34680	50	160	160	13	5.9	0.4	911	6.19	2.99
37	0.5	21.6	28170	50	160	160	13	5.9	0.4	513	3.85	2.03
38	0	20.0	27090	50	160	160	13	5.9	0.2	359	3.87	2.26
39	0.5	58.0	37510	50	160	160	13	5.9	0.4	1118	7.49	3.33
40	0	25.0	28960	50	100	100	10	3.7	0.4	342	3.97	2.02
41	0	25.0	28960	50	160	160	13	5.9	0.4	472	4.39	2.40
42	0	30.0	30590	50	160	160	13	5.9	0.4	552	5.07	2.87
43	0	30.0	27090	100	300	450	26	11	0.4	2062	12.2	7.38
44	0.5	90.0	42700	50	300	300	19	11	0.4	2534	10.0	4.54
45	0.5	44.4	34680	100	450	450	26	16.5	0.4	3882	14.1	6.26
46	0	30.0	30590	100	300	600	30	11	0.4	2322	13.5	9.01
47	0.5	44.4	34680	100	600	600	60	22	0.4	5794	18.3	9.63
48	0.5	44.4	34680	100	600	600	30	22	0.4	4768	14.9	7.32
49	0.5	44.4	34680	100	450	450	52	16.5	0.4	4594	18.4	8.59
50	0.5	44.4	34680	100	300	300	19	22	0.4	2891	13.1	5.54
51	0.5	44.4	34680	100	300	300	19	66	0.4	3001	13.6	6.29

5 Analytical solution

The analytical solution was derived using multiple linear regression for the compressive resistance of the concrete slab, its initial stiffness coefficient, and also the secant stiffness coefficient at reaching resistance.

During the sensitivity analysis and derivation of analytical solutions, the input parameters were sequentially generated and the results were tested. This process then resulted in the final input parameters used in the analytical solutions.

The results of the 49 models (n = 1 to 49) were used to derive an analytical relationship for calculating the resistance. The results of all models (1 to 51) were used to derive stiffness coefficients.

5.1 Validity limits of derived relations

The parametric study was performed with input parameters with values in the range shown in Table 5 for the joint not located on the uppermost floor. Other validity limits of derivation relations are based on standard requirements, in particular:

- minimum transverse reinforcement by the requirements of EN 1998 -1, Annex C [3],
- the width of the concrete slab shall comply with the geometric requirements for the formation of struts and tie mechanism by EN 1998-1, Annex C [3].

5.2 Concrete slab resistance in compression

Multiple linear regression was performed (Table 7 and Table 8) to obtain a relationship for calculating the compressive resistance of the SFRC slab in the composite frame joint. The material properties of the SFRC and the dimensions of the structure given in Table 7 were used as input parameters.

The 2.5 % upper quantile $t_{0.025}$ of a distribution with 43 degrees of freedom [69], [70] has a value of 2.014. The values of the t-statistic are higher than the upper quantile for all parameters, so F_R depends on all these input parameters.

The coefficient of determination is 0.96 and the adjusted coefficient of determination is 0.95. Thus, the values are close to 1.00, which means that the regression model is of good quality and explains a significant part of the variability of the dependent variable.

Table 7. *Multiple linear regression to determine the resistance.*

Multiple correlation coefficient	Coefficient of determination	Adjusted coefficient of determination	Standard Error	Significance *F*	Observations
0.978	0.956	0.952	238.7	3.01E-29	49

Table 8. *Analysis of variance.*

	Coefficient	Standard error	*t*-statistic	*P*-value	Lower limit (95 %)	Upper limit (95 %)
Intercept	-173.3	143.6	-1.207	0.23	-462.7	116.2
RI_v (-)	634.4	139.6	4.546	4.3E-05	353.2	915.7
b_c (mm)	5.966	0.4167	14.32	3.6E-18	5.127	6.806
h_c - 2t_f (mm)	2.412	0.2569	9.389	4.5E-12	1.894	2.930
(t_f / (0,5b_c))^2 (-)	16320	3169	5.148	5.9E-06	9929	22700

A relationship was derived to calculate the compressive resistance of a concrete slab in a steel-concrete composite joint.

$$F_{R,an} = \begin{pmatrix} 634.4\,RI_v + 5.966\,b_c + 2.412\,\left(h_c - 2t_f\right) + \\ +16320\left(\dfrac{t_f}{0{,}5\,b_c}\right)^2 - 173.3 \end{pmatrix} \frac{d}{100}\,\frac{f_c}{44.4} \tag{38}$$

where		
	$F_{R,an}$	the resistance of the concrete slab in compression (kN),
	RI_v	reinforcing index of fibres by volume (-),
	b_c	column cross-sectional width (mm),
	h_c	column cross-sectional height (mm),
	t_f	column flange thickness (mm),
	d	concrete slab thickness (mm),
	f_c	compressive strength of the concrete (MPa).

The cylindrical compressive strength of concrete f_c is an average value, so $F_{R,an}$ is an average value of the resistance. To obtain a characteristic value of the resistance, it is necessary to take into account the characteristic value of the concrete strength f_{ck}. Similarly, to obtain the design value of the resistance, it is necessary to consider the design value of the strength of the concrete f_{cd}.

The value of the dependent (i.e. predicted) variable is the resistance, which was recalculated in the regression analysis to be valid for a reference concrete slab of 100 mm thickness d by multiplying by 100 / d (d in mm) and a reference concrete compressive strength f_c of the of 44.4 MPa by multiplying by 44.4 / f_c (f_c in MPa). In the derived analytical formula for calculating the resistance, the resistance is recalculated back to the actual thickness by multiplying by d / 100 and to the actual concrete compressive strength by multiplying by f_c / 44.4. The dependence of resistance on slab thickness and concrete compressive strength is approximately linear, Fig. 81

5.3 Initial stiffness

Multiple linear regression was performed (Table 9 and Table 10) to obtain a relationship for calculating the initial compressive stiffness coefficient of the SFRC slab in a composite frame joint. The initial stiffness coefficient $s_{ini,FEM}$ corresponds to 2 / 3 of the resistance. The material properties of the SFRC and the dimensions of the structure given in Table 9 were used as input parameters. The 2.5 % upper quantile $t_{0.025}$ of a distribution with 47 degrees of freedom [69], [70] has a value of 2.012. The values of the t-statistic are higher than the upper quantile for all parameters, so $s_{ini,an}$ depends on all these input parameters. The coefficient of determination is 0.94 and the adjusted coefficient of determination is 0.93. Thus, the values are again close to 1.00.

***Table 9**. Multiple linear regression to determine the initial stiffness coefficient.*

Multiple correlation coefficient	Coefficient of determination	Adjusted coefficient of determination	Standard Error	Significance *F*	Observations
0.969	0.938	0.934	1.289	2.13E-28	51

***Table 10.** Analysis of variance.*

	Coefficient	Standard error	*t*-statistic	*P*-value	Lower limit (95 %)	Upper limit (95 %)
Intercept	-3.046	0.6094	-4.998	8.5E-06	-4.272	-1.820
d (mm)	0.005223	0.001371	3.811	4.0E-04	0.002466	0.007981
t_f (mm)	0.1144	0.02596	4.406	6.1E-05	0.06216	0.1666
$h_c - 2t_f$ (mm)	0.1241	0.007743	16.03	1.1E-20	0.1085	0.1397

A relationship was derived to calculate the coefficient of initial stiffness of a concrete slab in compression in a steel-concrete composite joint:

$$s_{ini,an} = \left(0.1241\, d + 0.1144\, t_f + 0.005223\, (h_c - 2t_f) - 3.046\right) \frac{E_c}{34680} \tag{39}$$

where $s_{ini,an}$ the coefficient of initial stiffness (mm),

d concrete slab thickness (mm),

t_f column flange thickness (mm),

h_c column cross-sectional height (mm),

E_c modulus of elasticity of concrete (MPa).

The value of the dependent (i.e. predicted) variable is the initial stiffness coefficient, which was recalculated in the regression analysis to be valid for a reference modulus of elasticity of concrete E_c of 34 680 MPa by multiplying by 34 680 / E_c (E_c in MPa). In the derived analytical formula for calculating the initial stiffness coefficient, the initial stiffness coefficient is recalculated back to the actual modulus of elasticity of concrete by multiplying by E_c / 34 680.

5.4 Secant stiffness

Multiple linear regression was performed (Table 11 and Table 12) to obtain a relationship for the calculation of the secant stiffness coefficient. The secant stiffness coefficient $s_{res,FEM}$ corresponds to the achievement of the resistance. The material properties of the SFRC and the dimensions of the structure given in Table 11 were used as input parameters. The 2.5 % upper quantile $t_{0.025}$ of a distribution with 48 degrees of freedom [69], [70] has a value of 2.011. The values of the t-statistic are higher than the upper quantile for all parameters listed in Table 11, so $s_{res,an}$ depends on all these input parameters. The coefficient of determination is 0.92 and the adjusted coefficient of determination is 0.91.

Table 11. *Multiple linear regression to determine the secant stiffness coefficient.*

Multiple correlation coefficient	Coefficient of determination	Adjusted coefficient of determination	Standard Error	Significance *F*	Observations
0.959	0.920	0.911	0.708	1.50E-23	51

Table 12. *Analysis of variance.*

	Coefficient	Standard error	*t*-statistic	*P*-value	Lower limit (95 %)	Upper limit (95 %)
Intercept	-5.976	1.132	-5.281	3.6E-06	-8.255	-3.697
d (mm)	0.05012	4.321E-03	11.60	4.1E-15	0.04141	0.05882
t_f (mm)	0.08040	1.432E-02	5.615	1.2E-06	0.05156	0.1092
h_c - $2t_f$ (mm)	0.001778	7.586E-04	2.344	2.4E-02	2.499E-04	3.306E-03
E_c (MPa)	0.0001583	3.666E-05	4.320	8.5E-05	8.451E-05	2.322E-04
RI_v (-)	-1.457	0.5107	-2.853	6.5E-03	-2.485	-0.4285

A relationship was derived for the calculation of the secant stiffness coefficient of a concrete slab in compression in a steel-concrete composite joint:

$$\begin{aligned} s_{res,an} = 0.05012\,d + 0.08040\,t_f + 0.001778\,(h_c - 2t_f) + \\ + 0.0001583\,E_c - 1.457\,RI_v - 5.976 \end{aligned} \tag{40}$$

where		
	$s_{ini,an}$	the coefficient of secant stiffness (mm),
	d	concrete slab thickness (mm),
	t_f	column flange thickness (mm),
	h_c	column cross-sectional height (mm),
	E_c	modulus of elasticity of concrete (MPa),
	RI_v	reinforcing index of fibres by volume (-).

6 Comparison of analytical solution with FEM model results, Eurocodes, and literature

6.1 Comparison of analytical solution with FEM model results

Fig. 83 and Table 13 compare the results of the finite element analysis and the analytical solutions. The graphs in Fig. 83 are supplemented with intervals of ± 15 %. For clarity, the results of the model with $n = 19$ with higher resistance and stiffness coefficients are not shown in Fig. 83 ($F_{R,an} = 8849$ kN, $F_{R,an}$ / $F_{R,FEM} = 0.88$, $s_{ini,an}$ / $s_{ini,FEM} = 0.91$, $s_{res,an}$ / $s_{res,FEM} = 0.90$). Further comparisons are given in the following section 6.2.

Table 13. *Comparison of the analytical solution with the results of the FEM models and with the results calculated by EC8 [3], EC3 [10], and Bennacer et al. [20].*

n	$F_{R,an}$ (kN)	$\frac{F_{R,an}}{F_{R,FEM}}$ (-)	$s_{ini,an}$ (mm)	$\frac{s_{ini,an}}{s_{ini,FEM}}$ (-)	$s_{res,an}$ (mm)	$\frac{s_{res,an}}{s_{res,FEM}}$ (-)	$\frac{s_{ini,an}}{s_{ini,EC3}}$ (-)	$\frac{F_{R,an}}{F_{R,EC8}}$ (-)	$\frac{F_{R,an}}{F_{R,BENN}}$ (-)
1	2828	0.99	12.9	1.00	5.79	1.04	1.30	1.25	1.17
2	2510	1.06	12.8	0.91	6.48	0.97	1.30	1.11	1.04
3	2669	1.01	12.9	0.95	6.14	1.02	1.30	1.18	1.10
4	2986	0.98	13.0	1.01	5.45	0.95	1.30	1.32	1.23
5	3145	0.99	13.0	1.03	5.11	0.85	1.30	1.39	1.30
6	1376	0.89	10.5	1.36	4.76	1.34	1.30	1.25	1.17
7	2102	0.95	11.8	1.14	5.34	1.15	1.30	1.25	1.17
8	2828	1.05	12.9	1.02	5.79	1.11	1.30	1.25	1.17
9	2828	0.97	12.9	0.98	5.79	0.99	1.30	1.25	1.17
10	3694	1.04	14.0	0.91	6.24	0.95	1.41	1.25	1.17
11	1414	1.00	6.70	0.92	3.29	1.11	0.96	1.25	1.17
12	1847	1.04	7.25	0.86	3.73	0.88	1.03	1.25	1.17
13	2196	1.22	11.5	1.40	5.33	1.51	1.16	1.65	1.27
14	3384	0.92	14.4	0.98	6.60	1.08	1.28	1.24	1.22
15	4421	0.98	15.6	0.88	7.04	0.88	1.28	1.24	1.22
16	1381	0.91	11.3	1.24	6.12	1.16	1.28	1.12	1.11
17	3226	1.00	14.4	0.98	6.94	1.36	1.28	1.18	1.16
18	3889	0.91	15.6	1.01	7.17	1.10	1.30	1.22	1.25
19	7778	0.88	28.0	0.91	12.2	0.90	1.65	1.22	1.25
20	1609	0.95	12.2	1.23	6.70	1.08	1.30	1.12	1.15

Table 13*. (Continued).*

n	$F_{R,an}$	$\frac{F_{R,an}}{F_{R,FEM}}$	$s_{ini,an}$	$\frac{s_{ini,an}}{s_{ini,FEM}}$	$s_{res,an}$	$\frac{s_{res,an}}{s_{res,FEM}}$	$\frac{s_{ini,an}}{s_{ini,EC3}}$	$\frac{F_{R,an}}{F_{R,EC8}}$	$\frac{F_{R,an}}{F_{R,BENN}}$
	(kN)	(-)	(mm)	(-)	(mm)	(-)	(-)	(-)	(-)
21	5112	1.07	18.3	1.04	8.34	1.06	1.41	1.15	1.27
22	6678	1.12	19.8	0.96	8.79	1.01	1.41	1.15	1.27
23	793	1.19	4.72	0.87	2.24	0.94	0.96	2.10	1.96
24	793	1.27	4.72	0.87	2.24	1.06	0.96	2.10	1.96
25	386	1.05	3.83	1.11	1.21	0.77	0.96	2.10	1.96
26	286	1.10	3.69	1.08	1.77	0.92	0.96	1.68	1.57
27	2345	1.02	11.9	0.89	5.44	0.92	1.20	1.43	1.20
28	914	1.04	9.27	1.10	4.96	0.99	1.20	1.23	1.03
29	642	1.02	4.41	0.85	1.97	0.87	1.09	1.42	1.32
30	2260	1.00	11.9	1.02	5.15	1.05	1.47	1.25	1.17
31	2577	1.02	12.0	1.07	4.46	0.94	1.47	1.42	1.33
32	3271	0.94	14.4	1.00	6.50	1.06	1.34	1.28	1.31
33	1246	0.84	8.28	1.18	3.31	0.94	1.20	1.42	1.45
34	2718	1.05	12.9	0.97	5.79	0.95	1.30	1.70	1.74
35	1910	0.97	11.8	1.02	4.95	1.23	1.63	1.19	1.23
36	926	1.02	5.35	0.86	2.58	0.86	0.94	1.53	1.43
37	451	0.88	4.34	1.13	1.55	0.76	0.94	1.53	1.43
38	346	0.96	4.18	1.08	2.10	0.93	0.94	1.27	1.19
39	1210	1.08	5.78	0.77	3.02	0.91	0.94	1.53	1.43
40	357	1.04	3.94	0.99	2.06	1.02	0.96	1.68	1.57
41	432	0.92	4.46	1.02	2.40	1.00	0.94	1.27	1.19
42	519	0.94	4.72	0.93	2.66	0.93	0.94	1.27	1.19
43	2072	1.01	11.3	0.92	6.12	0.83	1.13	1.12	1.11
44	2866	1.13	8.25	0.82	4.56	1.00	0.96	1.25	1.17
45	4007	1.03	14.4	1.02	6.60	1.05	1.23	1.18	1.10
46	2413	1.04	13.8	1.02	7.25	0.80	1.30	1.12	1.15
47	5534	0.96	18.7	1.02	9.48	0.98	1.10	1.22	1.14
48	5190	1.09	15.6	1.05	7.17	0.98	1.22	1.15	1.07
49	4535	0.99	17.1	0.93	8.59	1.00	1.09	1.34	1.25
50	-	-	12.9	0.99	5.79	1.05	1.20	-	-
51	-	-	12.9	0.95	5.79	0.92	0.94	-	-

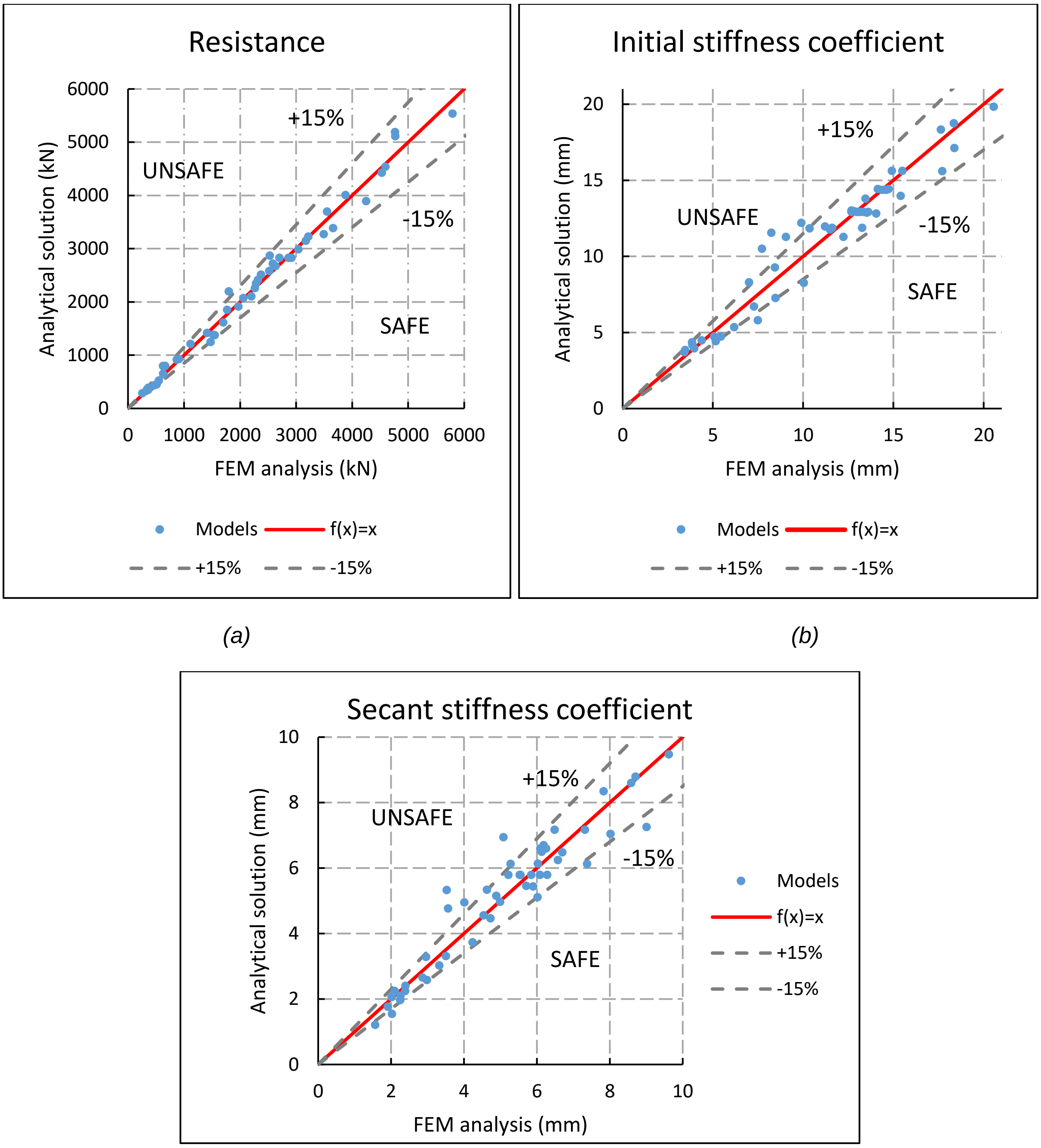

(a) *(b)*

(c)

Fig. 83. *Comparison of analytical solutions with FEM model results.*

Table 14 shows the maximum and minimum ratios of the analytical solution results to the FEM model results, the average values of these ratios, the median values of the ratios and their sample standard deviations, the mean absolute deviation, the average deviation from 1.0, and the maximum and minimum value of the ratios, and number of ratios greater and less than 1.0. The average values of the ratios and their medians are close to 1.00.

Table 14. *Comparison of analytical solution results with FEM model results.*

	$\frac{F_{R,an}}{F_{R,FEM}}$ (-)	$\frac{s_{ini,an}}{s_{ini,FEM}}$ (-)	$\frac{s_{res,an}}{s_{res,FEM}}$ (-)
Average	1.01	1.00	1.00
Median	1.01	1.00	0.99
Sample standard deviation	0.09	0.12	0.14
Mean absolute deviation	0.06	0.09	0.10
Average deviation[3] from 1.0	0.06	0.09	0.10
Max.	1.27	1.40	1.51
Min.	0.84	0.77	0.76
Number of ratios > 1.0	27	24	23
Number of ratios < 1.0	22	27	28

6.2 Comparison of analytical solution with Eurocodes and literature

Fig. 84 and Table 13 compare the resistance calculated according to the proposed analytical relationship with the resistance calculated according to Annex C of EN 1998-1 [3] and with the resistance calculated according to Bennacer et al. [20]. Furthermore, the proposed initial stiffness coefficient is compared with the initial stiffness coefficient calculated according to EN 1993-1-8 [10]. The graphs are supplemented with intervals of ± 15 %. For clarity, the results of the model with $n = 19$ with higher resistance and stiffness coefficients are not shown in Fig. 84 ($F_{R,an}$ / $F_{R,EC8}$ = 1.22, $F_{R,an}$ / $F_{R,BENN}$ = 1.25, $s_{ini,an}$ / $s_{ini,EC3}$ = 1.65).

---

[3] for resistance: $\left(\sum_{n=1}^{49} |\, 1 - \frac{F_{R,an}}{F_{R,FEM}} \,|\right)\frac{1}{n}$, for stiffness coefficients: $\left(\sum_{n=1}^{51} |\, 1 - \frac{s_{an}}{s_{FEM}} \,|\right)\frac{1}{n}$

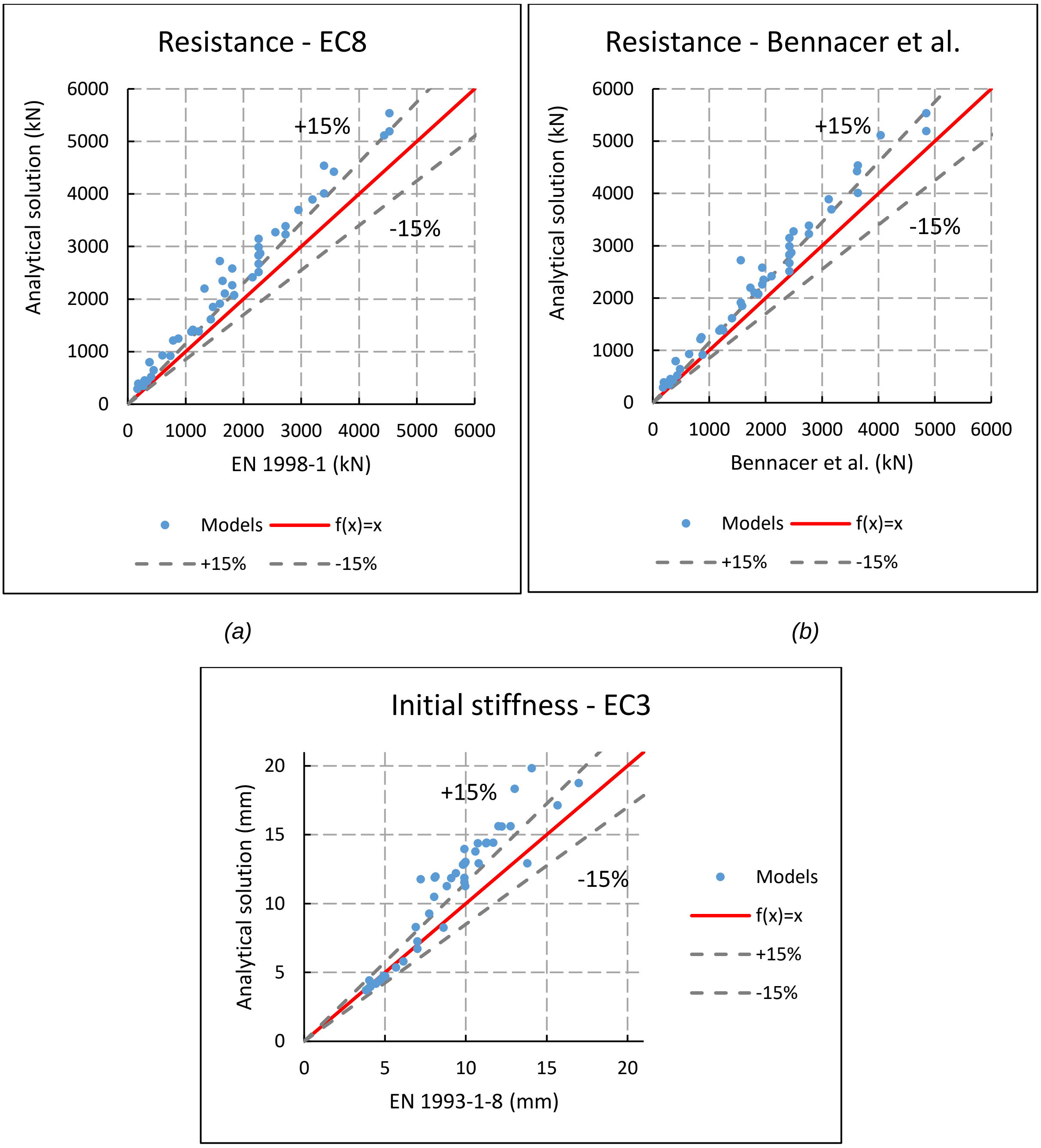

(a) *(b)*

(c)

***Fig. 84**. Comparison of analytical solutions with existing solutions.*

Table 15 shows the maximum and minimum ratios of the analytical solution results to those calculated according to EN 1998-1 [3], EN 1993-1-8 [10], and Bennacer et al. [20], the mean values of these ratios, the median values of the ratios and their sample standard deviations, the mean absolute deviation, the average deviation from 1.0, and the maximum and minimum value of the ratios, and the number of ratios greater and less than 1.0. The average values of the ratios and their median values are close to 1.20, i.e. the proposed analytical solutions provide higher values of the resistance and initial stiffness coefficient by approximately 20 %.

Table 15. *Comparison of analytical solution results with results calculated by EC8 [3], EC3 [10], and Bennacer et al. [20].*

	$\frac{F_{R,an}}{F_{R,EC8}}$ (-)	$\frac{F_{R,an}}{F_{R,BENN}}$ (-)	$\frac{s_{ini,an}}{s_{ini,EC3}}$ (-)
Average	1.35	1.28	1.20
Median	1.25	1.20	1.23
Sample standard deviation	0.25	0.22	0.19
Mean absolute deviation	0.18	0.16	0.16
Average deviation[4] from 1.0	0.35	0.28	0.22
Max.	2.10	1.96	1.65
Min.	1.11	1.03	0.94
Number of ratios > 1.0	49	49	37
Number of ratios < 1.0	0	0	14

---

[4] for resistance: $\left(\sum_{n=1}^{49} \mid 1-\frac{F_{R,an}}{F_{R,FEM}} \mid\right)\frac{1}{n}$, for stiffness coefficients: $\left(\sum_{n=1}^{51} \mid 1-\frac{s_{an}}{s_{FEM}} \mid\right)\frac{1}{n}$

7 Conclusions

7.1 Research summary

This thesis deals with steel fibre-reinforced concrete slab in compression as a component of a composite steel-concrete frame joint. Based on the results of the experiments with a realistic-sized steel-concrete specimen, a numerical model has been validated in Atena Science. Based on a parametric study with simplified models, an analytical relationship for the resistance, initial stiffness, and secant stiffness of the steel fibre-reinforced concrete slab in compression component was derived using multiple linear regression.

The parametric study was carried out with input parameters in the range shown in Table 5 for a joint not located on the topmost floor.

The direction of the principal stress under the action of mechanism 2 was evaluated in FEM models in the range of 35 ° – 40 °. The actual direction is accounted for in the resistances and stiffness coefficients calculated in the finite element models but was not quantified for each of the models because it was not needed as an input parameter for the analytical solution.

The way of loading (sagging bending moment only, hogging bending moment only, and the combination of a sagging bending moment on one side of the joint with a hogging bending moment on the other side of the joint) does not have a significant effect on the resistance and stiffness of the concrete slab.

The resistance of the concrete slab in the proposed analytical relationship depends mainly on the following parameters: reinforcing index of fibres, compressive strength of the concrete slab, width and height of the column cross-section, the thickness of the concrete slab, and the square of the column flange thickness divided by half of the column cross-section width. The analytical relationship for calculating the resistance, therefore, takes into account the effect of the inverse of the column flange slenderness on the resistance of the concrete slab. The flexibility of the column flange, therefore, influences significantly the resistance of this component of the composite joint. The resistance can be significantly increased by transverse column stiffeners at the level of the top and bottom slab surfaces.

Contrary to what was expected [5], the resistance of the concrete slab depends only negligibly on the amount of transverse reinforcement in front of the column and on the coefficient of friction between the column and the concrete slab.

The initial stiffness coefficient in the proposed analytical relationship depends on the modulus of elasticity of the SFRC, the thickness of the concrete slab, the height of the column cross-section, and the column flange thickness.

The secant stiffness coefficient in the proposed analytical relationship depends on the modulus of elasticity of the SFRC, the thickness of the concrete slab, the thickness of the column flange, the height of the column cross-section, and the reinforcing index of fibres.

The proposed analytical solutions give approximately 20 % higher values of the resistance and initial stiffness factor than the results calculated according to EN 1998-1 [3], EN 1993-1-8 [10], and Bennacer et al. [20].

7.2 Future research

The experiment with the bent steel-concrete composite joint was very time-consuming and costly. It is more advantageous to perform numerous simple experiments, e.g. similar to the simplified model used in the parametric study in this work. Further research could be aimed at verifying the obtained analytical relationships based on the results of more experiments with a wider range of input parameters such as concrete strength, different column profiles, etc.

References

[1] European committee for standardization. (2005). EN 1994-1-1: Eurocode 4: Design of composite steel and concrete structures. General rules and rules for buildings.

[2] European Commission, Directorate-General for Research and Innovation. J. Jaspart, U. Kuhlmann, L. Rölle et al. (2009). Robust structures by joint ductility. Publications Office. https://data.europa.eu/doi/10.2777/29746

[3] European committee for standardization. (2004). EN 1998-1: Eurocode 8: Design of structures for earthquake resistance - Part 1: General rules, seismic actions and rules for buildings.

[4] A. Y. Elghazouli. (2015). Seismic Code Developments for Steel and Composite Structures. Geotechnical, Geological and Earthquake Engineering. 39. 129-151. https://doi.org/10.1007/978-3-319-16964-4_5

[5] A. Plumier, C. Doneux, L. Sanchez-Ricart, R. Agatino, C. Plumier, A.S. Elnashai, M. Tsujii, R. Pinho, J. Bouwkamp, H. Parung, B. Broderick, A. Elghazouli, E. Cosenza, G. Manfredi. (2001). Seismic Behaviour and Design of Composite Steel Concrete Structures. ICONS Report 4. Publisher: LNEC Edition, Lisbon. Editor: A. Plumier & C. Doneux. https://doi.org/10.13140/2.1.1951.1361

[6] European Commission, Directorate-General for Research and Innovation, D. Anderson. (1997). *COST C1 : Composite steel-concrete joints in braced frames for buildings*, Publications Office. ISBN 92-827-9573-x

[7] ENV 1994-1-1: Eurocode 4: Design of composite steel and concrete structures. General rules and rules for buildings. European committee for standardization. 1994.

[8] A. Braconi, A. Elamary, W. Salvatore. (2010). Seismic behaviour of beam-to-column partial-strength joints for steel–concrete composite frames. Journal of Constructional Steel Research. 66(12). 1431-1444. https://doi.org/10.1016/j.jcsr.2010.05.004

[9] W. Salvatore, O.S. Bursi, D. Lucchesi. (2005). Design, testing and analysis of high ductile partial-strength steel–concrete composite beam-to-column joints. Computers & Structures. Vol. 83. 2334-2352. https://doi.org/10.1016/j.compstruc.2005.03.028

[10] European committee for standardization. (2005). EN 1993-1-8: Eurocode 3: Design of steel structures - Part 1-8: Design of joints.

[11] European committee for standardization. (2005). EN 1993-1-1: Eurocode 3: Design of steel structures - Part 1-1: General rules and rules for buildings.

[12] A. Braconi, S. Caprili, H. Degee, M. Guendel, M. Hjiaj, B. Hoffmeister, S.A. Karamanos, V. Rinaldi, W. Salvatore, H. Somja. (2015). Efficiency of Eurocode 8 design rules for steel and steel-concrete composite structures. Journal of Constructional Steel Research. Volume 112. 108-129. https://doi.org/10.1016/j.jcsr.2015.04.021

[13] L. S. da Silva, R. D. Simões, P.J.S. Cruz. (2001). Experimental behaviour of end-plate beam-to-column composite joints under monotonical loading. Engineering Structures. Vol. 23(11). 1383-1409. https://doi.org/10.1016/S0141-0296(01)00054-2

[14] European committee for standardization. (2006). EN 1992-1-1: Eurocode 2: Design of concrete structures - Part 1-1: General rules. Rules for buildings, bridges and civil engineering structures.

[15] J.Y.Richard Liew, T.H Teo, N.E Shanmugam. (2004). Composite joints subject to reversal of loading-Part 2: Analytical assessments. Journal of Constructional Steel Research. 60(2). 247-268. https://doi.org/10.1016/j.jcsr.2003.08.011

[16] J.-F. Demonceau. (2008). Steel and composite frames: sway response under conventional loading and development of membrane effects in beams further to an exceptional action. Doctor of philosophy thesis, Civil and Environmental Engineering, University of Liège.

[17] D.P. du Plessis, J.H. Daniels. (1973). Strength of Composite Beam-to-Column Connections. Fritz Engineering Laboratory Report 374.3. Department of Civil Engineering, Lehigh University, Bethlehem, Pennsylvania.

[18] B. Kato, Y. Tagawa. (1985). Strength of composite beams under seismic loading. Composite and Mixed Construction, Proceedings of the U.S./Japan Joint Seminar. ASCE. ISBN 0872624765, ISBN 9780872624764

[19] Y. Tagawa, B. Kato, A. Hirohumi. (1989). Behavior of composite beam in steel frames under hysteretic loading. Journal of Structural Engineering. 115(8). 2029-2045. https://doi.org/10.1061/(ASCE)0733-9445(1989)115:8(2029)

[20] M.A. Bennacer, A. Beroual, A. Kriker, J.F. Demonceau. (2015). Analytical model for composite joints under sagging moment. Engineering Structures. 101. 399-411. https://doi.org/10.1016/j.engstruct.2015.07.024

[21] G.A. Macrae, M. Hobbs, D.K. Bull, T. Chaudhari, R. Leon, G.Ch. Clifton, J.G. Chase. (2013). Slab Effects on Beam-Column Subassemblies—Beam Strength and Elongation Issues. International Conference on Composite Construction in Steel and Concrete 2013. 77-92. https://doi.org/10.1061/9780784479735.007

[22] HERA. (1989).The HERA Report: R4-49. New Zealand Steel Work Design Guide volume 2.

[23] T.P. Green, R. Leon, G.A. Rassati. (2004). Bidirectional tests on partially-restrained, composite beam-to-column connections. Journal of Structural Engineering. 130(2). 320-327. https://doi.org/10.1061/(ASCE)0733-944592004)130:2(320)

[24] American Institute of Steel Construction (AISC). (2002). Seismic provisions for structural steel buildings: Part 2.

[25] H. Somja, F. Marie. (2017). Concrete Structures Reinforced by Steel Profiles. SMARTCOCO Project. RFCS GRANT AGREEMENT N° RFSR-CT-2012-00031. Deliverable D8.3 Strut-and-tie models for shear keys. Contribution to the calibration report. INSA Rennes, Internal Report.

[26] S.A. Civjan, M.D. Engelhardt, J.L. Gross. (2001). Slab Effects in SMRF Retrofit Connection Tests. Journal of Structural Engineering-ASCE. 127(3). 230-237. https://doi.org/10.1061/(ASCE)0733-9445(2001)127:3(230)

[27] A. Braconi, O.S. Bursi, G. Fabbrocino, W. Salvatore, R. Tremblay. (2008). Seismic performance of a 3D full-scale high-ductility steel–concrete composite moment-resisting structure—Part I: Design and testing procedure. Earthquake Engineering & Structural Dynamics 37(14). 1609 - 1634. https://doi.org/10.1002/eqe.829

[28] F. Ferrario. (2004). Analysis and modelling of the seismic behaviour of high ductility steel-concrete composite structures. Doctor of philosophy thesis, University of Trento.

[29] European Commission, Directorate-General for Research and Innovation, D. Bitar, Y. Ryan, S. Caramelli, W. Salvatore, F. Taucer, J.-P. Jaspart, J.-F. Demonceau, M. Haller, J. Grijalvo, F.-J. Heise, R. Kindmann, M. Kraus, B. Hoffmeister, M. Oppe, H. Stangenberg. (2006). Applicability of composite structures to sway frames. Publications Office. ISBN: 92-79-00813-7

[30] A. Braconi, W. Salvatore, R. Tremblay, O.S. Bursi. (2007). Behaviour and modelling of partial-strength beam-to-column composite joints for seismic applications. Earthquake Engineering & Structural Dynamics. 36(1). 142 - 161. https://doi.org/10.1002/eqe.629

[31] European Commission, Directorate-General for Research and Innovation, O. Bursi, M. Haller, F. Ferrario et al. (2009). Prefabricated composite beam-to-concrete filled tube or partially reinforced-concrete-encased column connections for severe seismic and fire loadings. Publications Office. https://doi.org/10.2777/62963

[32] C. Amadio, C. Bedon, M. Fasan. (2017). Numerical assessment of slab-interaction effects on the behaviour of steel-concrete composite joints. Journal of Constructional Steel Research. 139. 397-410. https://doi.org/10.1016/j.jcsr.2017.10.003

[33] J.Y.R. Liew, T.H. Teo, N.E. Shanmugam. (2004). Composite joints subject to reversal of loading-Part 1: Experimental study. Journal of Constructional Steel Research. 60(2). 221-246. https://doi.org/10.1016/j.jcsr.2003.08.010

[34] Scia Engineer 16. Nemetschek Group. Downloaded 10/2016.

[35] COP AM 2.1.2. Feldmann + Weynand GmbH. Downloaded 1/2018.

[36] H. Zhu, Ch. Li, D. Gao, L. Yang, S. Cheng. (2019). Study on mechanical properties and strength relation between cube and cylinder specimens of steel fiber reinforced concrete. Advances in Mechanical Engineering. 11(4). https://doi.org/10.1177/1687814019842423

[37] J.P Jaspart, R. Marquoi. (1992). Investigation by testing of the structural response of semi-rigid joints. Testing of metals for structures. Edited by F.M. Mazzolani.

[38] Y.Ch. Ou, M.-S. Tsai, K.-Y. Liu, K.-Ch. Chang. (2012). Compressive Behavior of Steel-Fiber-Reinforced Concrete with a High Reinforcing Index. Journal of Materials in Civil Engineering. 24(2). 207-215. https://doi.org/10.1061/(ASCE)MT.1943-5533.0000372

[39] VIC-3D. Correlated Solutions, Inc.

[40] Atena Studio 5.6.1. Cervenka Consulting s.r.o. Downloaded 7/2019.

[41] GID 12.0.10. International centre for numerical methods in engineering (CIMNE). Downloaded 7/2019.

[42] T. Sajdlova. (22.8.2016). ATENA Program Documentation, Part 4-7, ATENA Science – GiD FRC Tutorial. Cervenka Consulting. [Online]. Available: https://www.cervenka.cz/assets/files/atena-pdf/ATENA-Science-GiD_Tutorial_FRC.pdf [Accessed 24 June 2019]..

[43] Z.P. Bazant, B.H. Oh. (1983). Crack Band Theory for Fracture of Concrete. Matériaux et Constructions. 16(3). 155-177. https://doi.org/10.1007/BF02486267

[44] J. Cervenka, V. Cervenka, S. Laserna. (2014). On finite element modeling of compressive failure in brittle materials. Computational Modelling of Concrete Structures - Proceedings of EURO-C 2014. 1. 273-281.

[45] V. Cervenka, J. Margoldova. (1995). Tension Stiffening Effectin Smeared Crack Model. Engineering Mechanics, Proc. 10th Conf., Boulder, Colorado. 655-658.

[46] V. Cervenka, L. Jendele, J. Cervenka. (26.1.2018). Program Documentation, Part 1, Theory. Cervenka Consulting. [Online]. Available: https://www.cervenka.cz/assets/files/atena-pdf/ATENA_Theory.pdf [Accessed 24 June 2019].

[47] P. Menetrey, K. Willam. (1995). Triaxial failure criterion for concrete and its generalization. ACI Structural Journal. 92(3). 311-318.

[48] J. Cervenka, V. Cervenka, S. Laserna. (2018). On Crack Band Model in Finite Element Analysis of Concrete Fracture in Engineering Practice. Engineering Fracture Mechanics. 197. 27–47. https://doi.org/10.1016/j.engfracmech.2018.04.010

[49] V. Cervenka. (1985). Constitutive Model for Cracked Reinforced Concrete. Journal ACI. 82(6). 877-882.

[50] D. Darwin, D.A.W. Pecknold. (1974). Inelastic Model for Cyclic Biaxial Loading of Reinforced Concrete. Civil Engineering Studies, University of Illinois.

[51] F.J. Vecchio, M.P. Collins. (1986). Modified Compression-Field Theory for Reinforced Concrete Beams Subjected to Shear. ACI JOURNAL, Proceedings V. 83, No. 2. 19(17). 219-231.

[52] M.A. Crisfield, J. Wills. (1989). The Analysis of Reinforced Concrete Panels Using Different Concrete Models. Journal of Engineering Mechanics, ASCE. 115(3). 578-597. https://doi.org/10.1061/(ASCE)0733-9399(1989)115:3(578)

[53] W. Kolmar. (1986). Beschreibung der Kraftuebertragung uber Risse in nichtlinearen Finite-Element-Berechnungen von Stahlbetontragwerken, Dissertation. Technical University of Darmstadt (in German).

[54] H. Kupfer, H.K. Hilsdorf, H. Rusch. (1969). Behavior of Concrete under Biaxial Stress. ACI Materials Journal. Vol. 66(8). 656-666.

[55] V.-K. Papanikolaou, A. Kappos. (2007). Confinement-sensitive plasticity constitutive model for concrete in triaxial compression. International Journal of Solids and Structures. 44. 7021-7048. https://doi.org/10.1016/j.ijsolstr.2007.03.022

[56] P.E.C. Seow, S. Swaddiwudhipong. (2005). Failure Surface for Concrete under Multiaxial Load—a Unified Approach. Journal of Materials in Civil Engineering. 17(2). 219-228. https://doi.org/10.1061/(ASCE)0899-1561(2005)17:2(219)

[57] D. Pryl, J. Cervenka. (26.4.2018). ATENA Program Documentation, Part 11, Troubleshooting Manual. Cervenka Consulting. [Online]. Available: https://www.cervenka.cz/assets/files/atena-pdf/ATENA-Troubleshooting.pdf [Accessed 24 June 2019].

[58] B. Xu, H.S. Shi. (2009). Correlations among mechanical properties of steel fiber reinforced concrete. Construction and Building Materials. 23(12). 3468-3474. https://doi.org/10.1016/j.conbuildmat.2009.08.017

[59] J.A.O. Barros, J. Figueiras. (1999). Flexural Behavior of SFRC: Testing and Modeling. Journal of Materials in Civil Engineering. 11 (4). 331-339. https://doi.org/10.1061/(ASCE)0899-1561(1999)11:4(331)

[60] S.-Ch. Lee, J.-Y. Cho, F.J. Vecchio. (2013). Simplified Diverse Embedment Model for Steel Fiber-Reinforced Concrete Elements in Tension. Aci Materials Journal. 110(4). 403-412.

[61] S.-W. Choi, J. Choi, S.-Ch. Lee. (2019). Probabilistic Analysis for Strain-Hardening Behavior of High-Performance Fiber-Reinforced Concrete. Materials (Basel, Switzerland). 12(15). https://doi.org/10.3390/ma12152399

[62] Z. Khalil, A.M. El-Shennawy. (2019). Design of SFRC according to FIB model code 2010 using simplified diverse embedment model (SDEM) as a design input. Conference: fib Symposium 2019: Concrete - Innovations in Materials, Design and Structures. At: Krakow, Poland.

[63] F.J. Vecchio, M.P. Collins. (1986). The Modified Compression-Field Theory for Reinforced Concrete Elements Subjected to Shear. ACI Journal. 83 (2). 219-231.

[64] J. Kollegger, G. Mehlhorn. (1990). Material model for the analysis of reinforced concrete surface structures. Computational Mechanics. 6. 341–357. https://doi.org/10.1007/BF00350417

[65] CEB-FIP Model Code 1990, First Draft, Comittee Euro-International du Beton, Bulletin d'information No. 195,196.

[66] Idea Statica 10.1 - Connection. Idea Statica. Downloaded 10/2019.

[67] J. Červenka, V. Červenka, M. Sýkora, J. Mlčoch. (2018). Evaluation of Safety Formats for Structural Assessment Based on Nonlinear Analysis. Proceedings of the Conference on Computational Modelling of Concrete and Concrete Structures (EURO-C 2018), February 26 - March 1, 2018, Bad Hofgastein, Austria. 669-678. https://doi.org/10.1201/9781315182964

[68] V. Cervenka, J. Cervenka, Z. Janda, D. Pryl. (6.10.2017). ATENA Program Documentation, Part 8, User’s Manual for ATENA-GiD Interface. Cervenka Consulting. [Online]. Available: https://www.cervenka.cz/assets/files/atena-pdf/ATENA-Science-GiD_Users_Manual.pdf [Accessed 24 June 2019].

[69] D. Jaruskova. (2002). Pravdepodobnost a matematicka statistika 12. Czech Technical University in Prague, Faculty of Civil Engineering (in Czech). ISBN 80-01-02253-6.

[70] M. Meloun, J. Militky. (1994). Statistické zpracování experimentálních dat. Plus (in Czech). ISBN 80-85297-56-6.

[71] Úřad pro technickou normalizaci, metrologii a státní zkušebnictví. (2015). ČSN P 73 2452: Vláknobeton - Zkoušení ztvrdlého vláknobetonu.

[72] P. Reiterman. (2019). Stanovení mechanických parametrů drátkobetonu. Czech Technical University in Prague, Faculty of Civil Engineering (in Czech).

[73] ČSN EN ISO 6892-1. (2021). Kovové materiály - Zkoušení tahem - Část 1: Zkušební metoda za pokojové teploty.

Annexes

A Determination of mechanical properties of SFRC

The protocol was drafted and the material parameters were determined by Reiterman [72].

Table 20 shows the results of the four-point bending test of FRC beams (dimensions 150 mm x 150 mm x 700 mm) according to ČSN P 732452 [71]. The spacing of the supports is 600 mm, the distance of the points of applied displacement is 200 mm, and the deflection is measured in the middle of the beam span. According to the results obtained, the fibre-reinforced concrete can be classified as **L1.6/1.1**.

Table 16. *Determination of the cubic compressive strength.*

Specimen	Height (mm)	Width 1 (mm)	Width 2 (mm)	Weight (g)	Density (kg/m^3)	Max. force (kN)	Compressive strength (MPa)
1	151.3	150.0	150.0	8070	2371	1420	62.6
2	152.2	150.0	150.0	7040	2056	1460	64.0
3	151.8	149.9	150.0	7830	2294	1340	58.9
Average					2240		61.8

Table 17. *Determination of the splitting tensile strength.*

Specimen	Height (mm)	Width 1 (mm)	Width 2 (mm)	Weight (g)	Density (kg/m^3)	Max. force (kN)	Splitting tensile strength (MPa)
4	151.0	150.0	149.9	8020	2362	235	6.6
5	151.2	150.0	149.9	8070	2374	188	5.3
6	149.4	149.0	149.8	7970	2390	188	5.4
Average					2375		5.8

Table 18. *Determination of modulus of elasticity.*

Specimen	Height (mm)	Width 1 (mm)	Length (mm)	Weight (g)	Density (kg/m^3)	Modulus of elasticity (GPa)
1	100.9	99.9	400	9510	2359	36.4
2	99	99.9	400	9315	2355	35.9
3	98	99.9	400	9260	2365	35.1
Average					2375	35.8

Table 19. *Determination of the flexural tensile strength.*

Specimen	Height (mm)	Width 1 (mm)	Length (mm)	Weight (g)	Density (kg/m^3)	Max. force (kN)	Flexural tensile strength (MPa)
4	99.0	99.9	400	9450	2389	27.42	8.3
5	101.8	99.9	400	9700	2385	27.04	8.0
6	99.8	99.9	400	9270	2324	27.44	8.3
Average					2363		8.2

Table 20. *Mechanical properties of SFRC.*

Specimen	T1	T2	T3
Max. force (kN)	28.29	25.66	37.36
Flexural tensile strength (MPa)	5.0	4.6	6.6
Average value		5.4	
Characteristic average values			
$F_{Rk,0,5}$ (kN)		19.71	
$f_{fc,tk,0,5}$ (MPa)		1.6	
$F_{Rk,3,5}$ (kN)		17.29	
$f_{fc,tk,3,5}$ (MPa)		1.1	

B Static scheme of the test set-up

The test set-up is shown in Fig. 36 and its static scheme is shown below in Fig. 85.

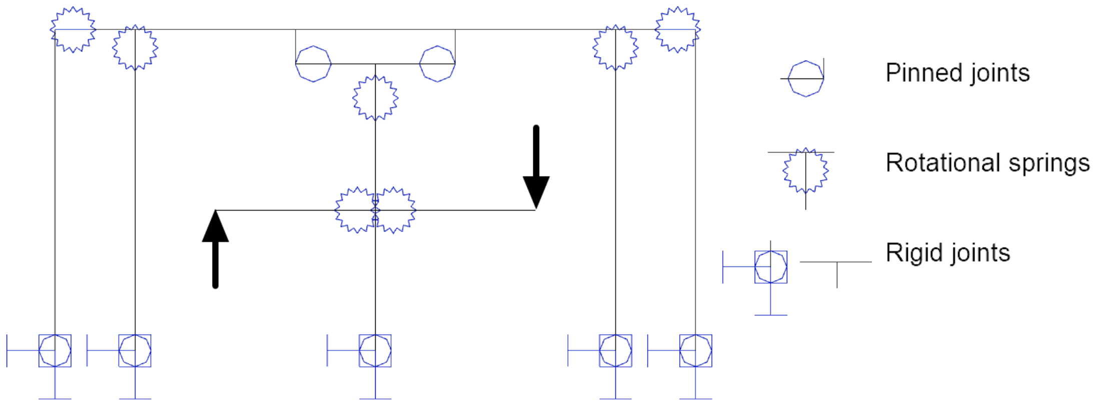

Fig. 85. *Static scheme of the test set-up [34].*

C Coupon tests with steel member and rebar specimens

Fig. 86 shows the results of coupon tests with steel member and slab reinforcement specimens. Coupon tests were performed and evaluated according to [73].

Table 21 shows the measured dimensions of specimen members. The column cross-section had an imperfection shape, as illustrated in Fig. 55.

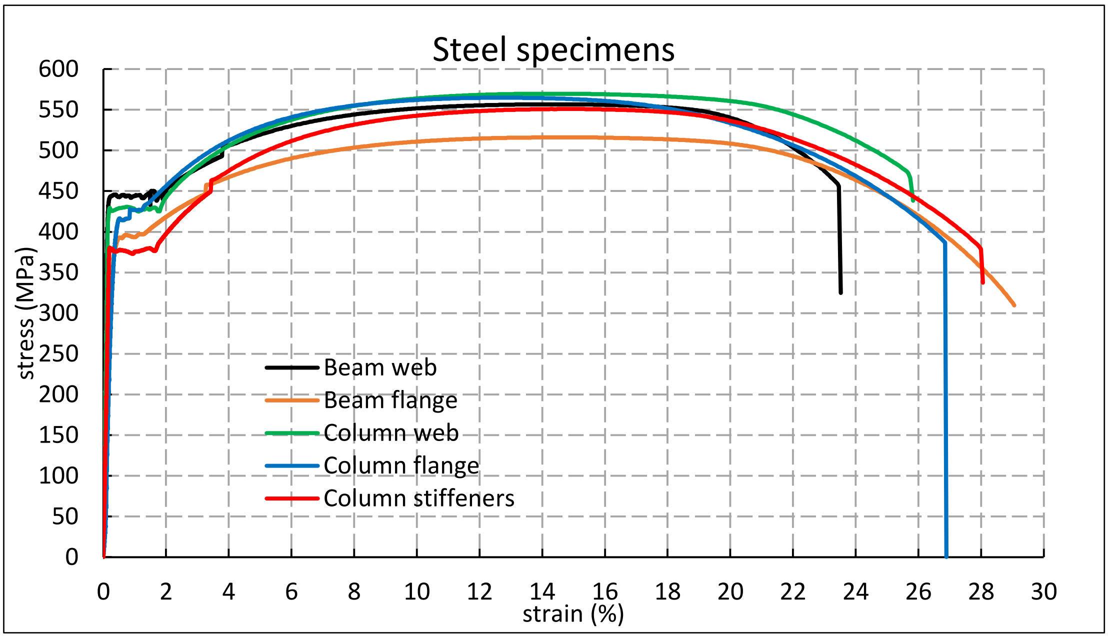

(a)

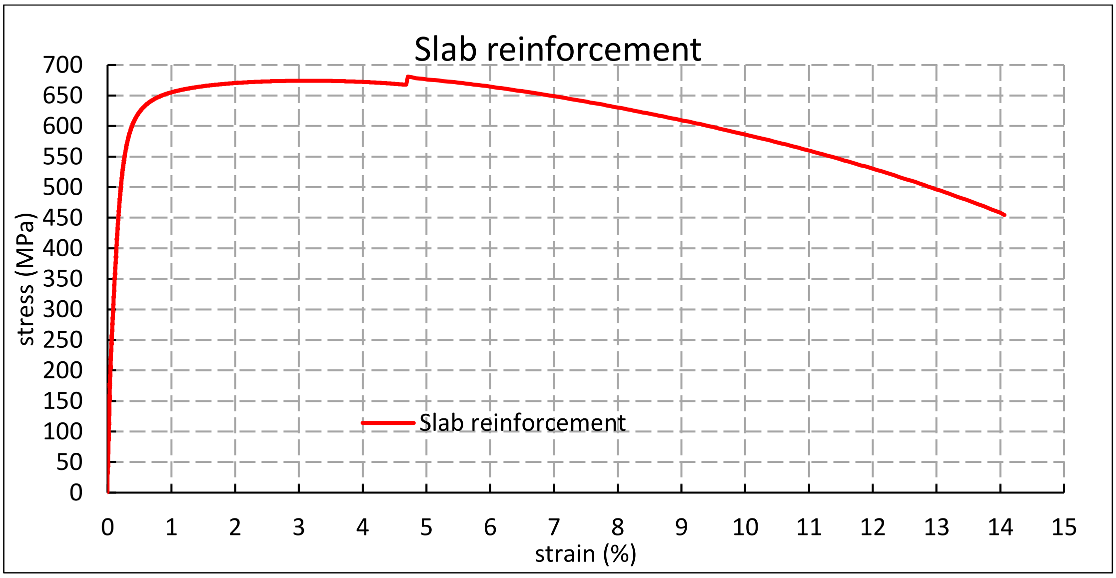

(b)

Fig. 86. *Results of coupon tests with steel member specimens (a) and reinforcement (b) specimen.*

Table 21. *Measured dimensions of specimen members in units of mm.*

	$t_{f,top}$	$t_{f,bottom}$	b_{top}	b_{bottom}	t_w	h_{middle}	h_{left}	h_{right}
beam (IPE 300)	11.2	11.3	151	151	6.9	303	303	303
column (HEB 300)	19.2	19.2	297	297	11.2	301	299	303

D Other experimental results

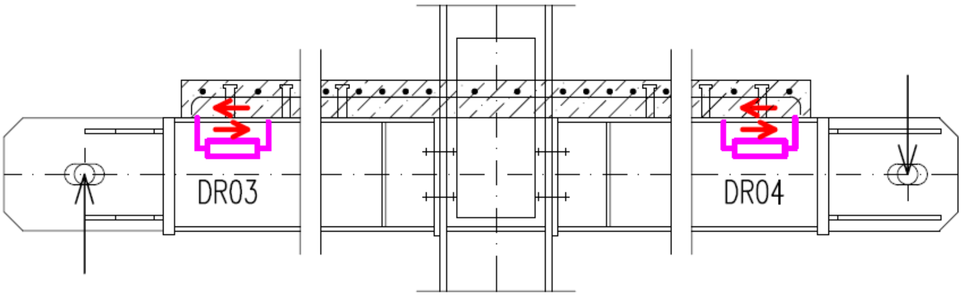

Fig. 87. *The actual direction of the measured slips, which are plotted in Fig. 74.*

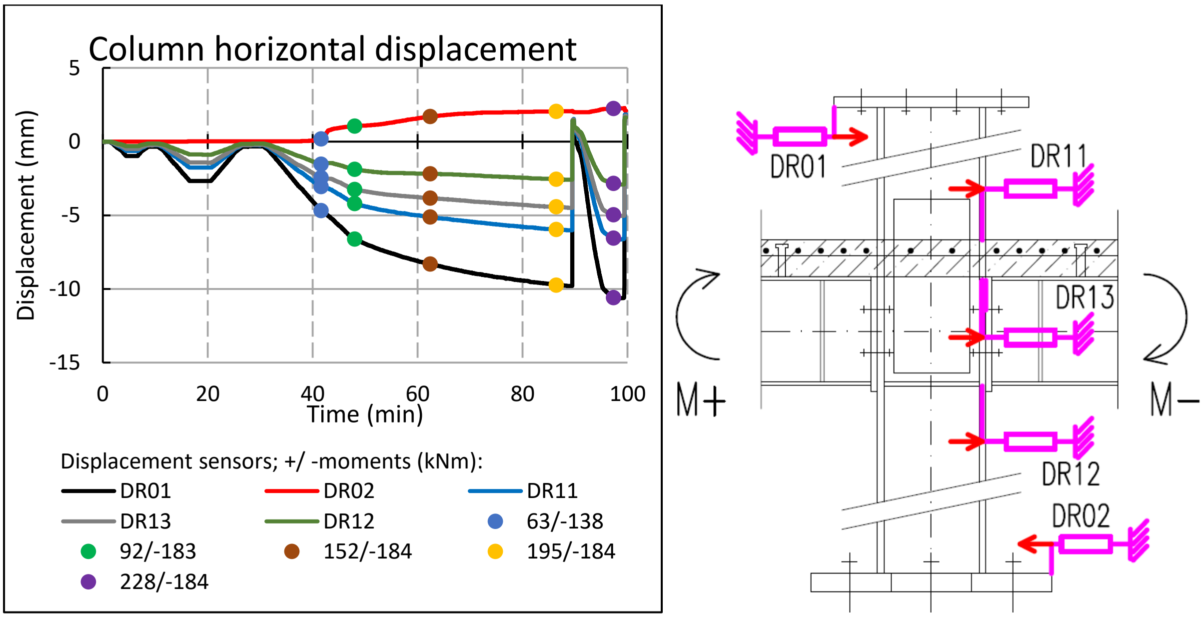

(a) *(b)*

Fig. 88. *Horizontal displacement of the column in the area of the supports and the joint depending on the test duration with the values of the sagging and hogging moments for the selected times marked (a), location of the displacement sensors with the actual direction of displacement marked (b).*

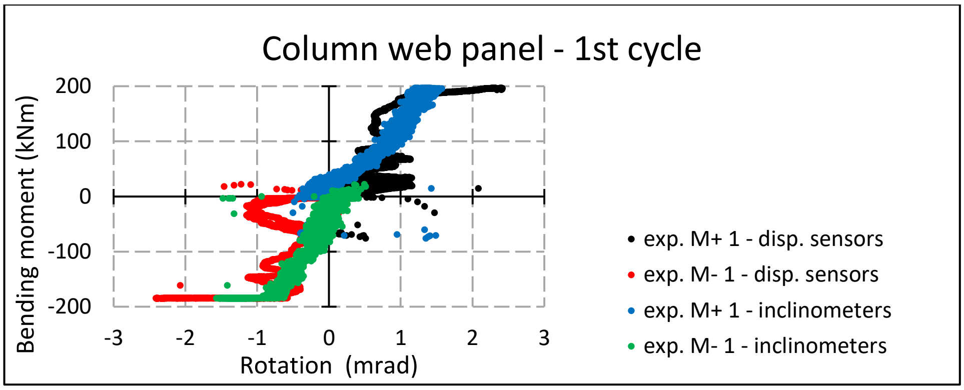

Fig. 89. *Graph of the moment versus column web panel rotation in shear for 1st cycle (results for 2nd cycle in Fig. 74).*

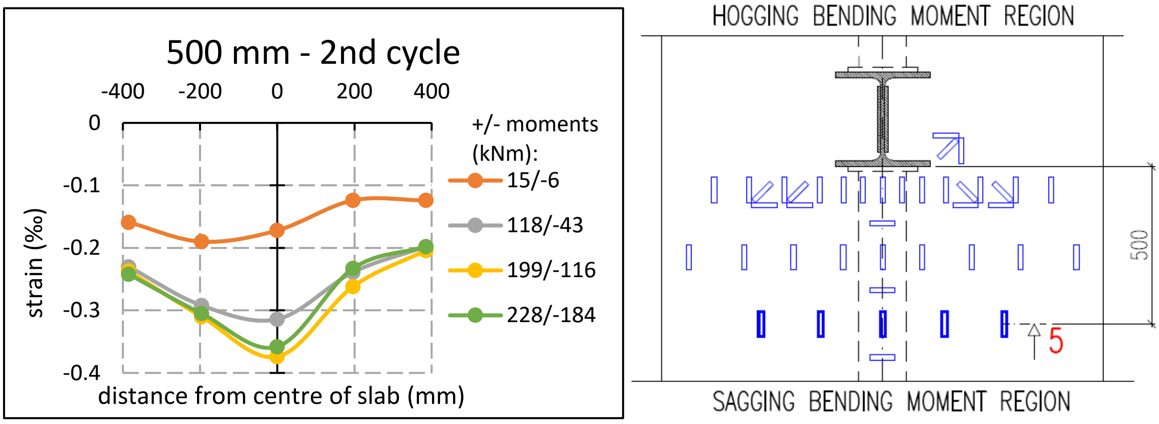

(a) *(b)*

Fig. 90. *Strain distribution on the top surface of the slab at a distance of 500 mm from the face of the column flange as a function of bending moments for 2nd cycle (a) (for 1st cycle in Fig. 56), investigated cross-section (b).*

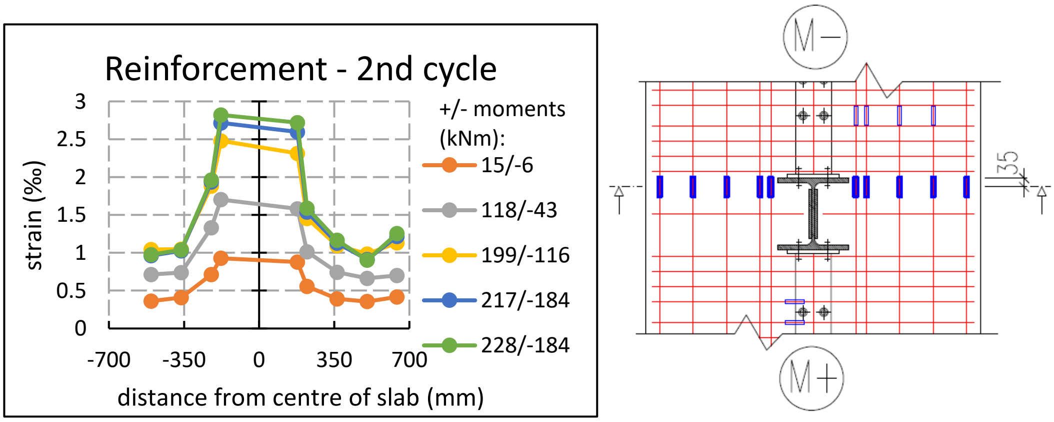

(a) *(b)*

Fig. 91. *Strain distribution of the reinforcement at the connection as a function of the bending moments for the 2nd cycle (a) (results for the 1st cycle in Fig. 58), investigated cross-section (b).*

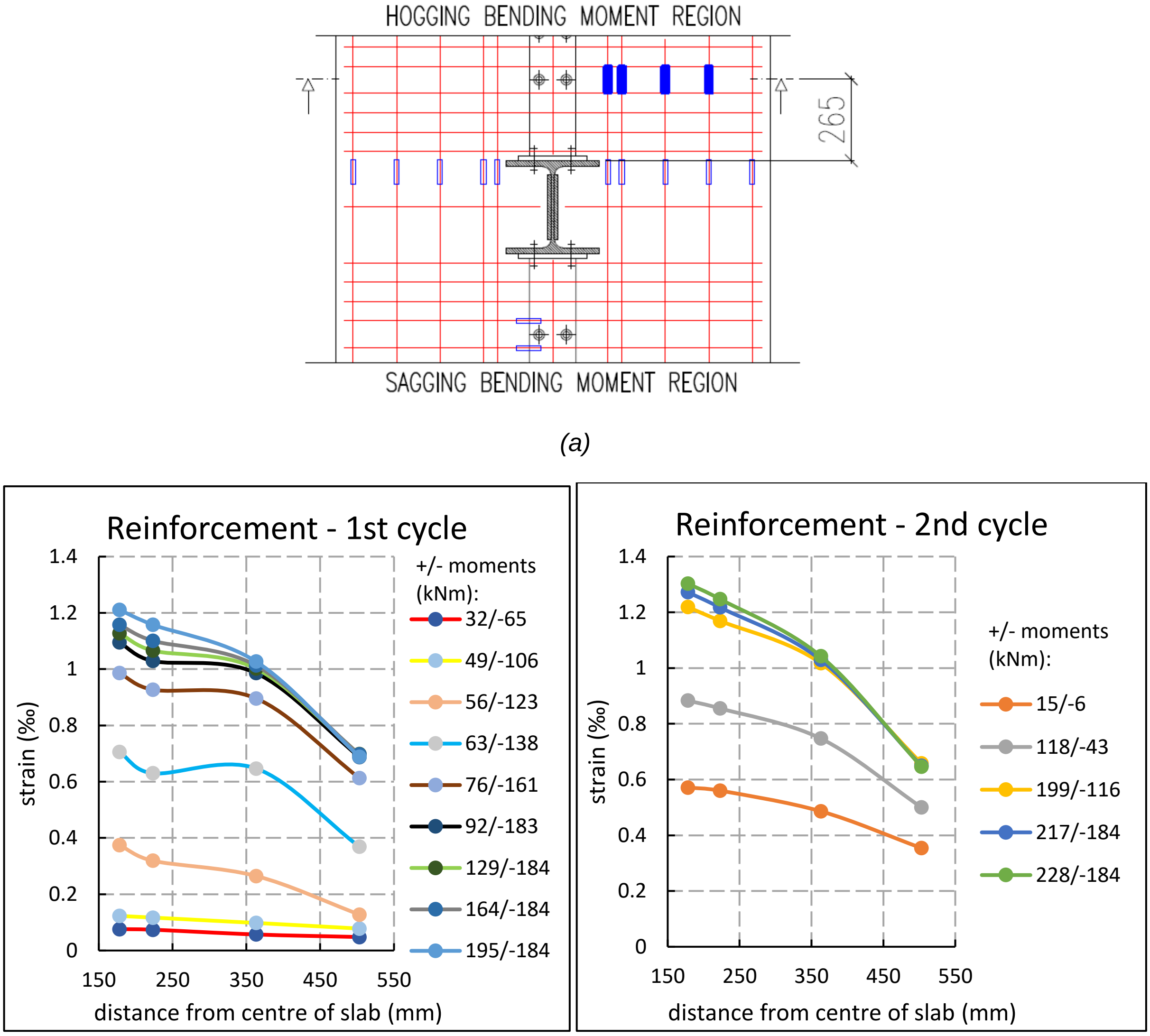

(a)

(b)

(c)

Fig. 92. *Strain distribution of the reinforcement in the cross-section at a distance of 265 mm from the connection (a) depending on the bending moments - for the 1st cycle (b), for the 2nd cycle (c).*

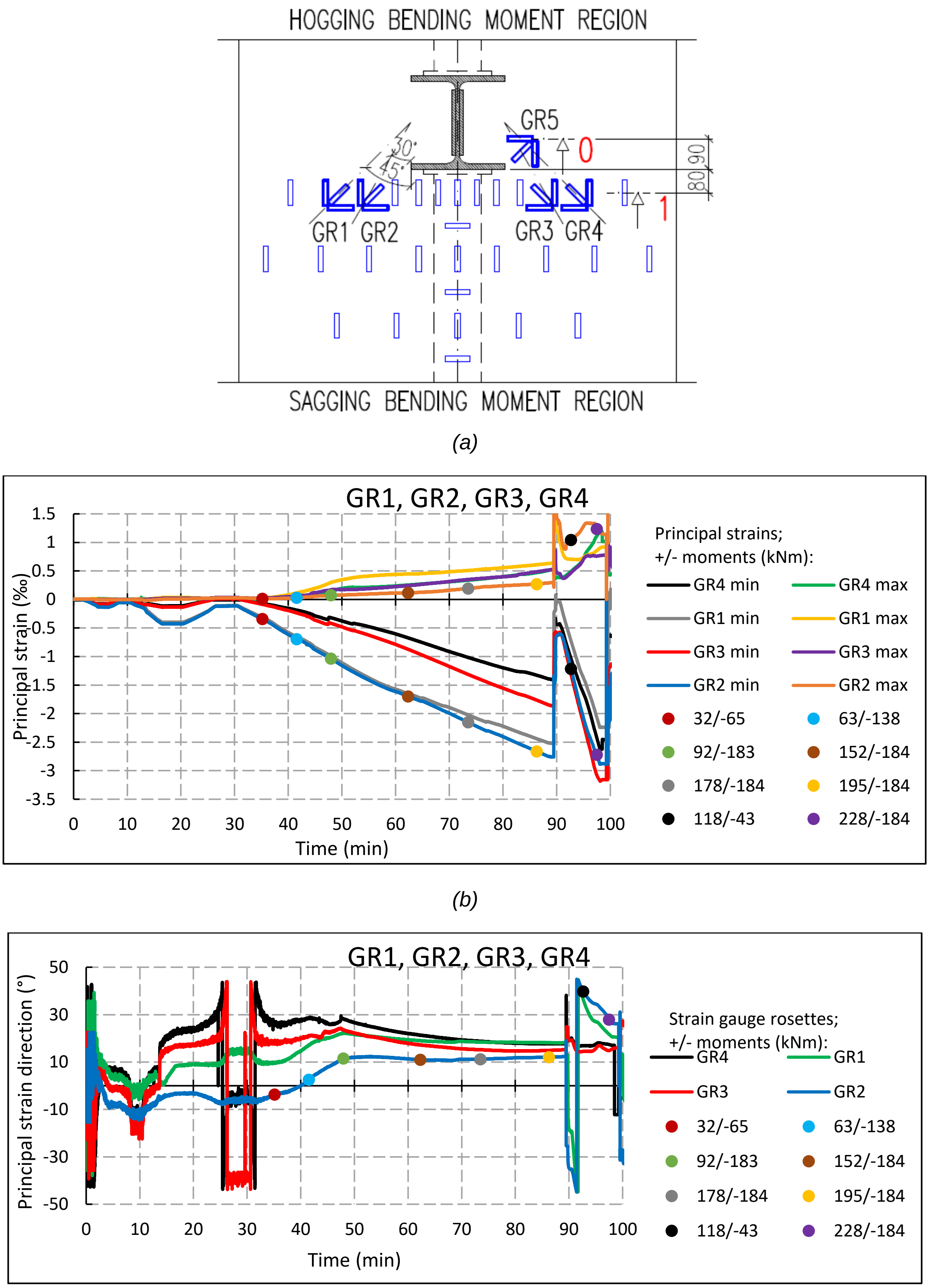

(a)

(b)

(c)

Fig. 93. *Strain gauge rosettes No. 1 - 4 on the top surface of the concrete slab - individual strains (a), principal strains (b), and directions of principal strains (c) as a function of test duration. The values of the sagging and hogging moments for the selected times are given*

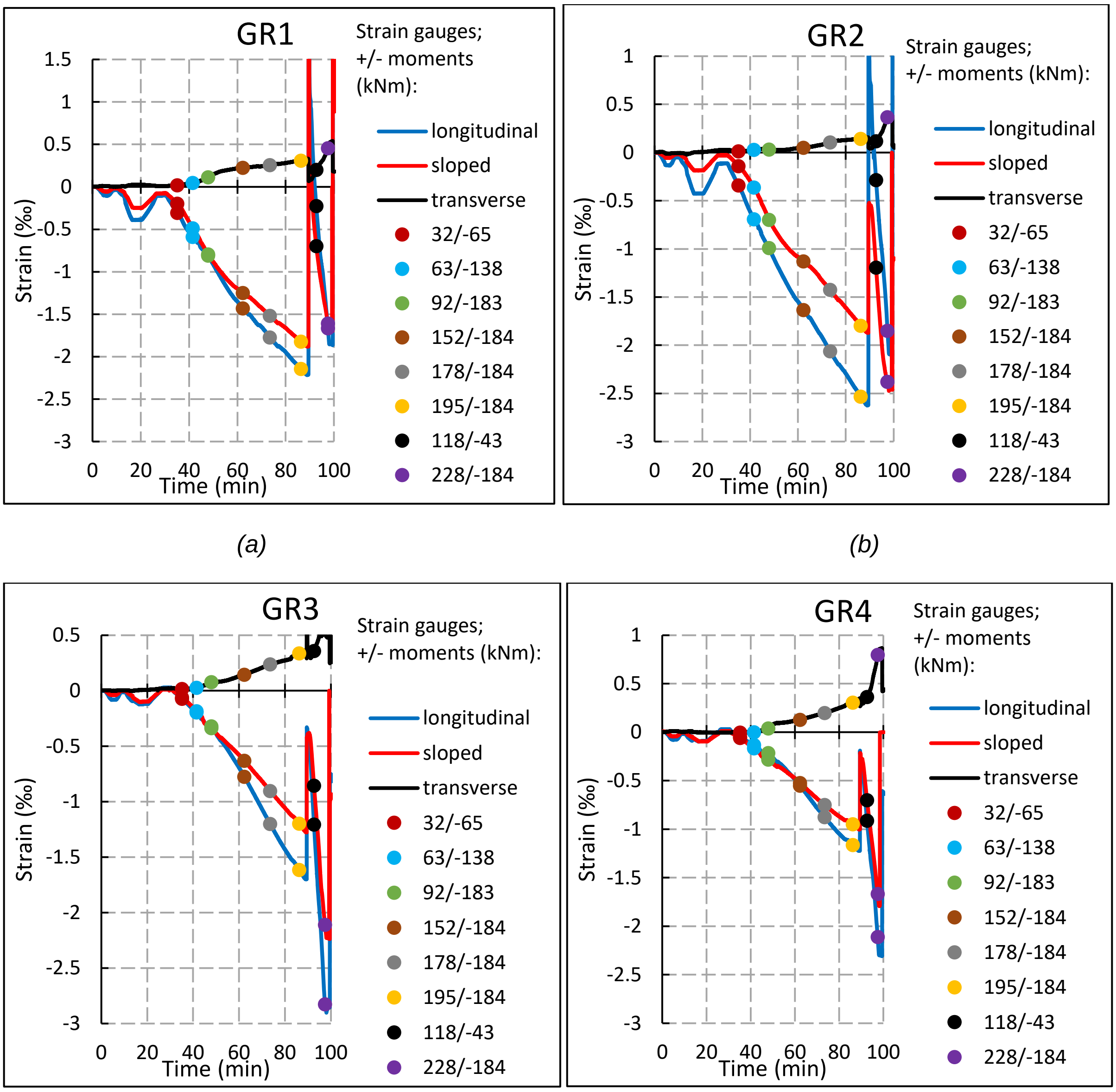

(a) *(b)*

(c) *(d)*

Fig. 94. *Individual strains versus test duration for strain gauge rosettes No. 1 - 4 on the concrete slab. The values of the sagging and hogging moments for the selected times are given.*

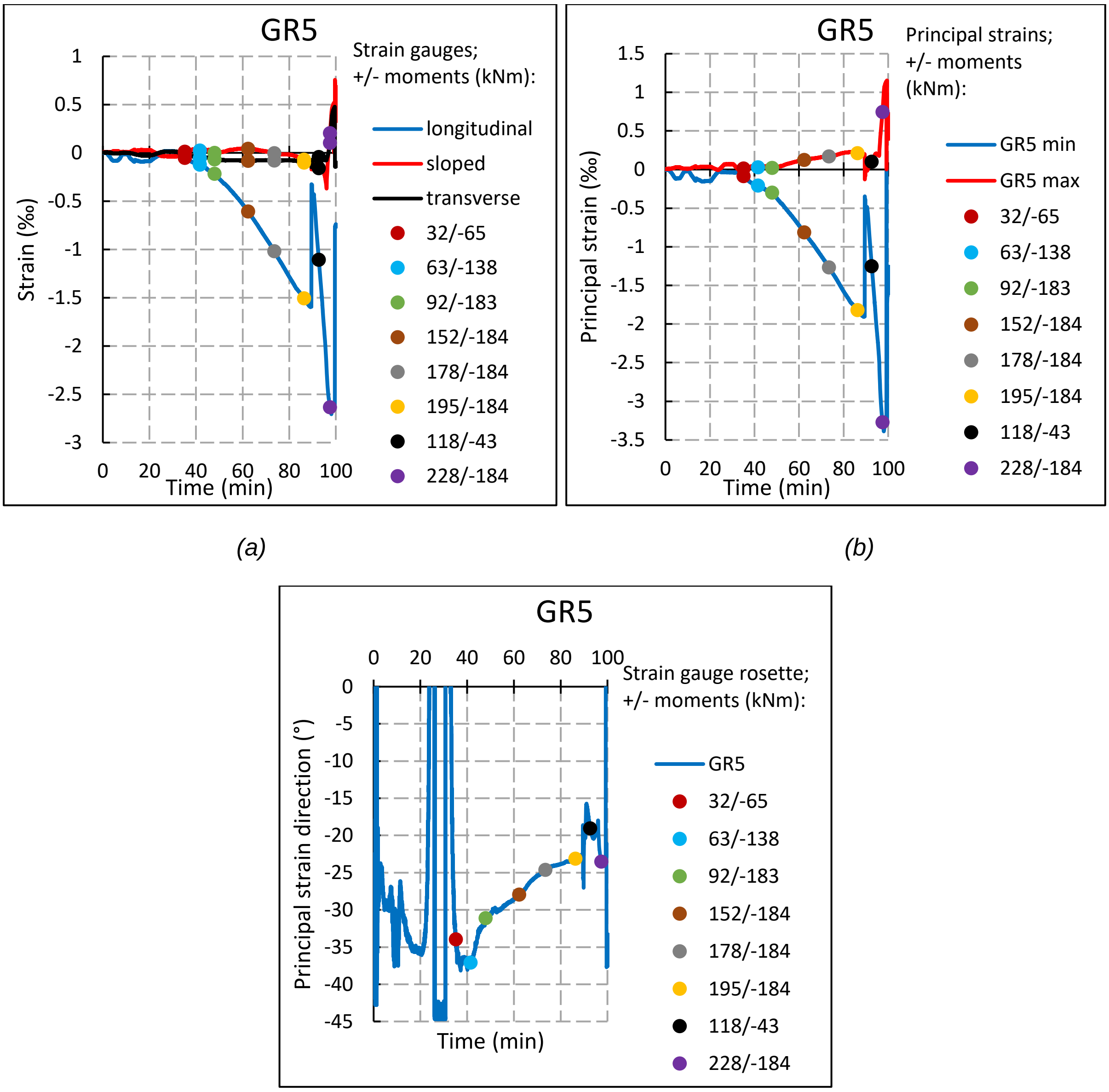

(a)

(b)

(c)

Fig. 95. *Strain gauge rosette No. 5 on the top surface of the concrete slab (location of the rosette shown in Fig. 93) - individual strains (a), principal strains (b), and direction of principal strains (c) as a function of test duration. The values of the sagging and hogging moments for the selected times are given.*

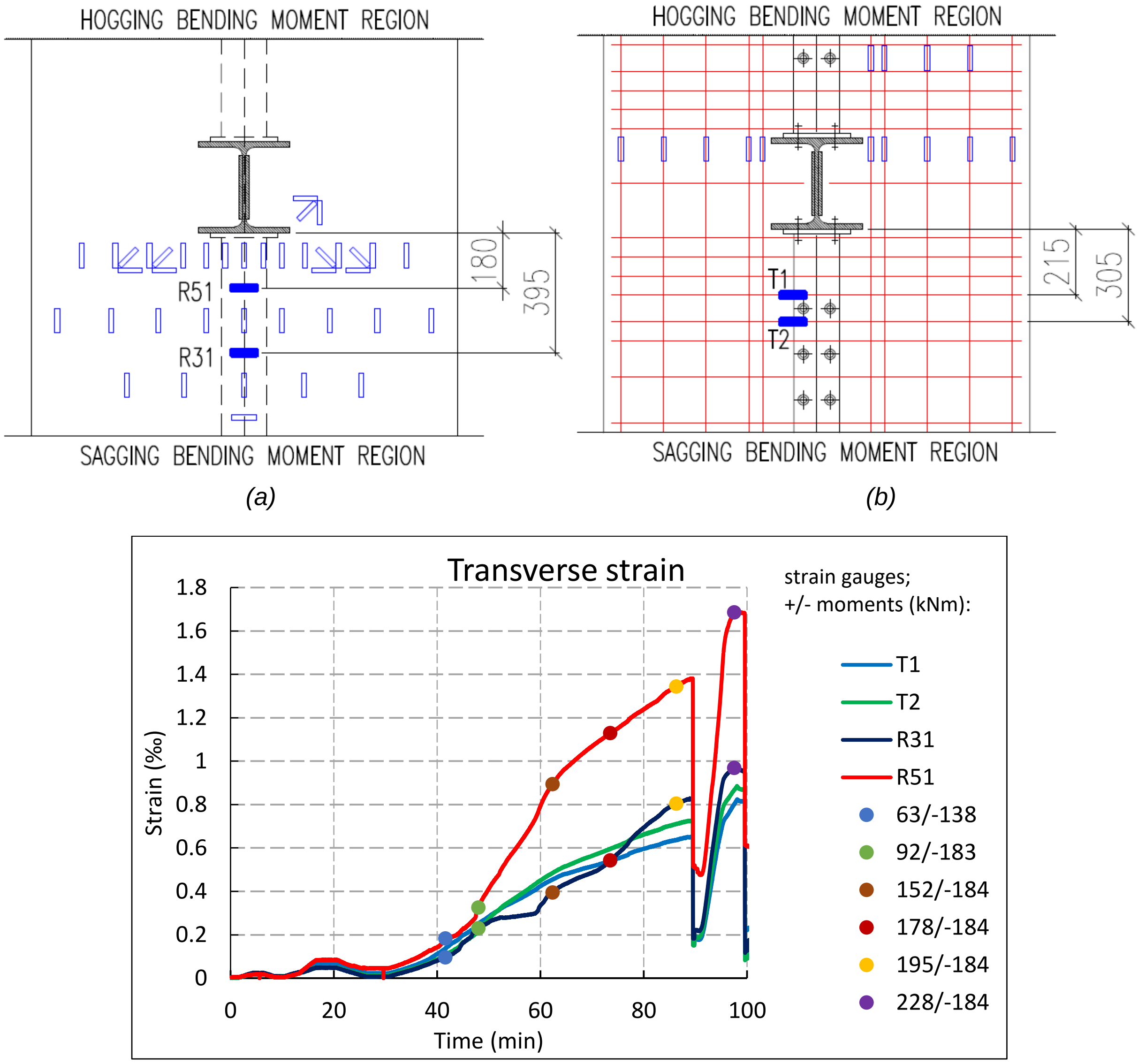

(a)

(b)

(c)

Fig. 96. *Dependence of strain on test duration for transverse reinforcement and the top surface of the concrete slab. The values of the sagging and hogging moments for the selected times are given.*

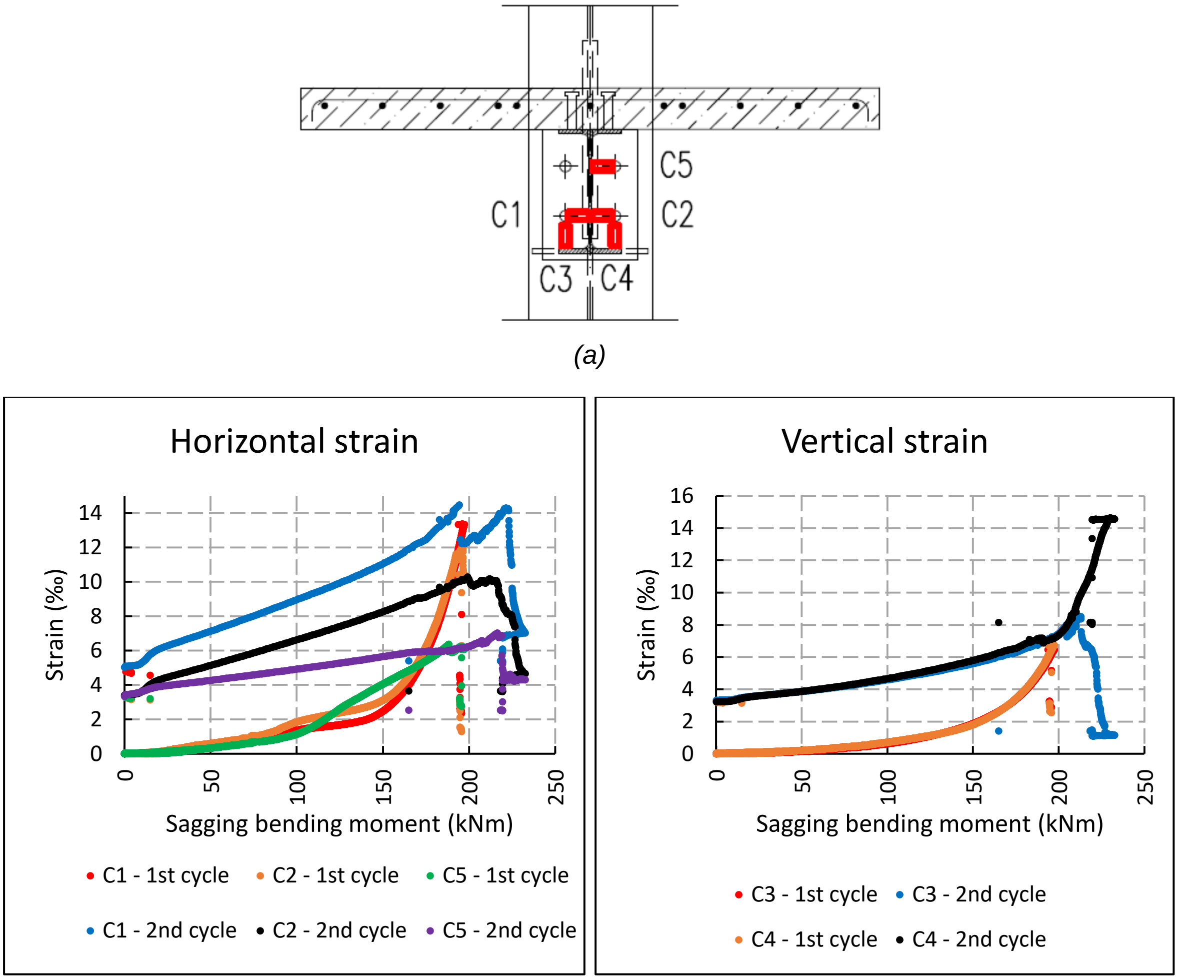

(a)

(b)

(c)

Fig. 97. *Strain gauges on the end-plate on the sagging moment side (a), horizontal strain (b), and vertical strain (c). Strain gauge C3 failed at a strain of 8 ‰.*

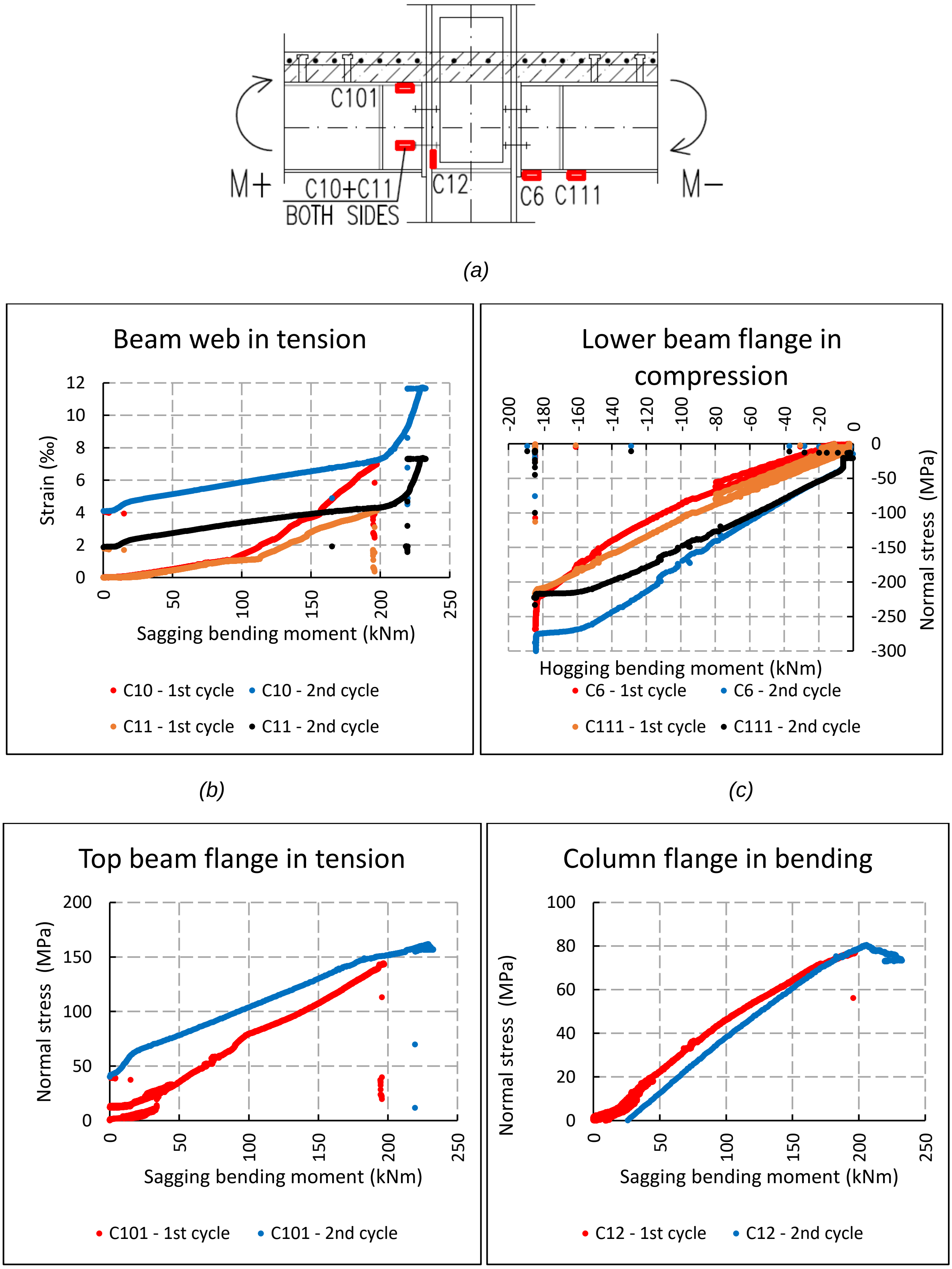

(a)

(b)

(c)

(d)

(e)

***Fig. 98**. Other strain gauges on the steel part of the joint: location of strain gauges (a), the strain of the beam web in tension (b); normal stress ($\sigma = E\ \varepsilon_{measured}$) of the bottom beam flange on the hogging moment side (c), of the top beam flange on the sagging moment side (d), of the column flange in bending (e).*

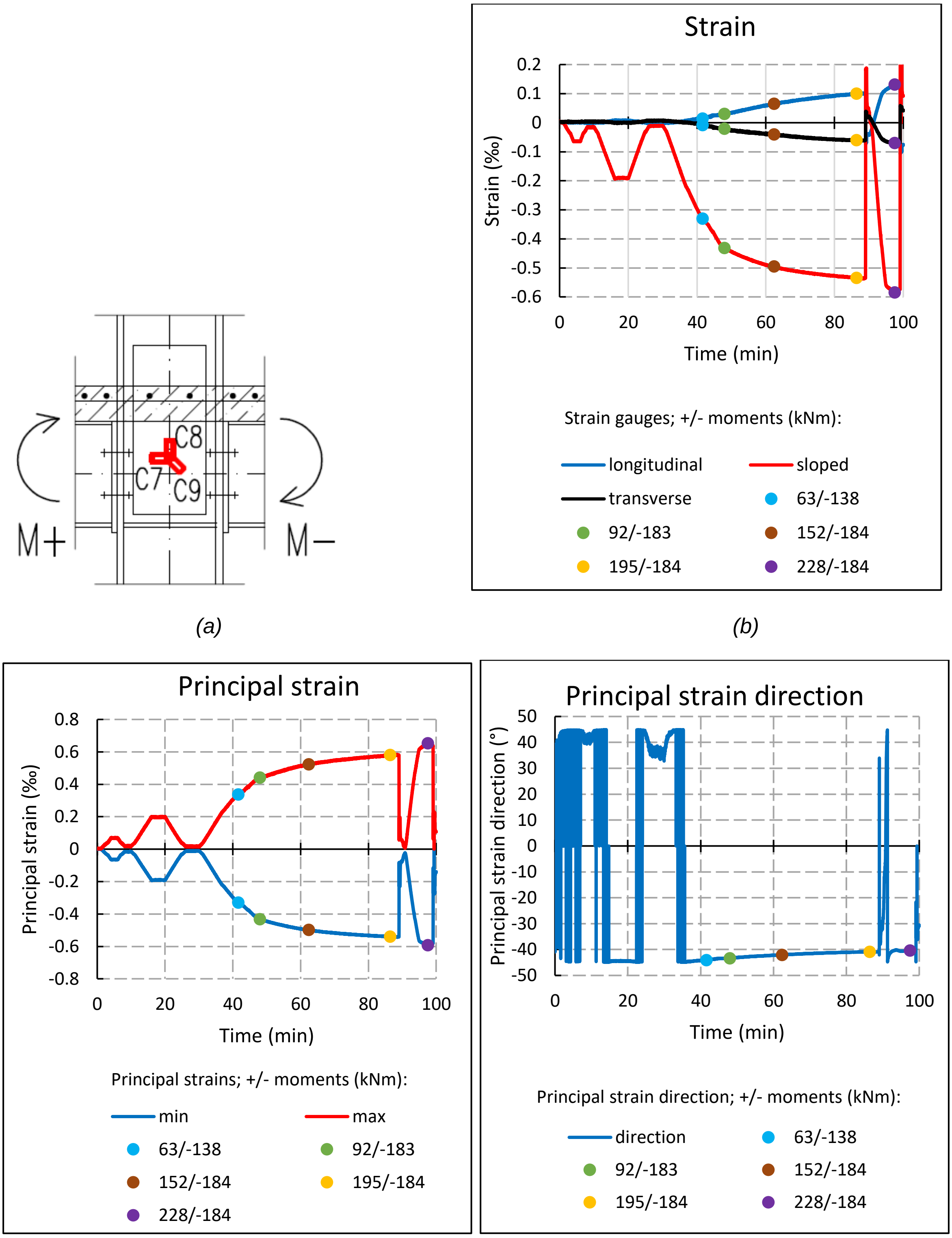

(a) *(b)*

(c) *(d)*

Fig. 99. *Strain gauge rosette on the column web panel in shear.*